Synthesis and Structural-Electrical Properties Correlation of Hybrid Polyaniline-CNT Nanocomposites

Ph.D. Thesis

Anil Kumar
(2012RMT9020)

**Department of Metallurgical and Materials Engineering
Malaviya National Institute of Technology Jaipur, India**

September, 2017

Synthesis and Structural-Electrical Properties Correlation of Hybrid Polyaniline-CNT Nanocomposites

This thesis is submitted as a partial fulfilment
of the Ph.D. programme in Engineering

Anil Kumar
(2012RMT9020)

Department of Metallurgical and Materials Engineering
Malaviya National Institute of Technology Jaipur, India

September, 2017

IN THE NAME OF GURU, THE MOST MERCIFUL, THE MOST GRACIOUS

This thesis is dedicated to

My Parents: Sh. Mohinder Singh & Smt. Susheela Rani

My Wife: Minakshi

My Son: Arsh Joria

For their unconditional love, motivation and especially never ending patience

CERTIFICATE

This is to certify that the thesis entitled **"Synthesis and Structural-Electrical Properties Correlation of Hybrid Polyaniline-CNT Nanocomposites"** is being submitted by me to the award of the degree of **Doctor of Philosophy** in **Metallurgical and Materials Engineering**, **Malaviya National Institute of Technology Jaipur**, is an original research work carried out by me. The content of the thesis has been checked using plagiarism detector software.

I have incorporated all the suggestions/queries/changes raised by the examiner in the thesis evaluation report.

(Anil Kumar)

This is to certify that the above statement made by the candidate is true to my knowledge.

Vinod Kumar	**Dr. Kamlendra Awasthi**
(Supervisor)	**(Supervisor)**
Assistant Professor	Assistant Professor
Discipline of Metallurgy Engineering and	Department of Physics
Materials Science, IIT, Indore, India	MNIT, Jaipur, India

Ph.D. viva-voce examination of Mr. Anil Kumar, research scholar was held on 02.09.2017 in the seminar hall of department of Metallurgical and Materials Engineering MNIT Jaipur. The candidate defended the viva-voce successfully to the satisfaction of oral defence committee. The committee recommends for the award of Ph.D. degree.

(Signature of external examiner)

ACKNOWLEDGEMENTS

(Anil Kumar)

ABSTRACT

Two types of polyaniline were prepared with (PANI 1) and without (PANI 2) solvent using ammonium peroxodisulfate oxidant via chemical oxidative polymerization and solid state oxidative polymerization method respectively. These PANIs were vacuum dried and designated as PANI 1VD and PANI 2VD. PANI 1VD was selected as matrix for the developing hybrid nanocomposites. MWCNTs were selected as filler material. A facile and easy solution mixing method was used to prepare the hybrid nanocomposites. By covalent functionalization, MWCNTs have been functionalized to improve the dispersion in PANI matrix. PANI 1VD was also processed through solution casting method for the development of self-standing film. The prepared film further protonated with hydrochloric acid. X-ray diffractometry (XRD), Fourier-transform infrared spectroscopy, Raman spectroscopy, scanning electron microscopy (SEM), transmission electron microscopy (TEM), thermogravimetric analysis and ultraviolet-visible spectroscopy were used to characterize the matrix, filler, and nanocomposites. The electrical properties were evaluated using electrometer. X-ray diffractometry analysis confirmed the high crystallinity of PANI prepared with solvent. The high electrical conductivity of PANI (prepared with solvent) was due to the mixed (granular and fibrillar) morphology. SEM and TEM analysis revealed the formation of PANI nanofibers and dispersion of f-MWCNTs in PANI matrix. The percolation threshold was found to occur at 0.1 vol. % of f-MWCNTs. At 3.3 vol. %, the f-MWCNTs/PANI nanocomposite was fully percolated and maximum achieved conductivity was 1.8×10^{-1} S/cm with 13.9 vol. % of f-MWCNTs. The achieved electrical conductivity of nanocomposites is in the range which is required for ESD and EMI applications. In addition, the selected pure PANI (in powder form) for nanocomposites also processed for the development of self-standing film. SEM study revealed that the prepared film have very dense structure without any void. The non-protonated film (PANI A) have short fibers only. However, protonated (PANI B) also have long fibers or bunch of fibers along with short fibers. Though, a detail study is still going over the film part.

Contents

List of Figures

List of Tables

Abbreviations and Symbols

PF	Polyfluorene
PTh	Polythiophene
PPP	Poly(p-phenylene
PTV	Poly (thienylene vinylene)
PPy	Polypyrrole
ICPs	Intrinsically conducting polymers
ECPs	Extrinsically conducting polymers
PA	Polyacetylene
2MA	2-Methylaziridine
AZ	Azetidine
PY	Pyrrolidine
PP	Piperidine
HXMI	Hexamethyleneimine
HPMI	Heptamethyleneimine
DMPU	1,3-Dimethyl-3,4,5,6-tetrahydro-2(1H)-pyrimidinone
NMP	1-methyl-2-pyrrolidinone
PANI	Polyaniline
MWCNT	Multiwall carbon nanotube
SWCNT	Singlewall carbon nanotube
PMCs	Polymer matrix composites
EMI SE	Electromagnetic interference shielding effectiveness
ESD	Electrostatic dissipation
APS	Ammonium peroxodisulfate
VD	Vacuum dried
PMC	Polymer matrix composites
f-MWCNT	Carboxylic-functionalized MWCNT
ρ_c	Percolation threshold
σ	Electrical conductivity

Z_0 Free space impedance

X_c Degree of crystallinity

CHAPTER ONE

Introduction

In this chapter, general introduction about conducting polymer and the work carried out in the Ph.D. thesis has been dealt. The importance of the conducting polymers, conducting polymer composites/nanocomposites, their advantages, and applications have given introduced in this chapter.Especially, discussion on the PANI and its nanocomposites has mainly focused. In the end, motivation, objective for the work undertaken, the methodology adopted, and the results given in brief.

==

The interest in electrically conducting polymers continues to rise rapidly, with the wide range of applications. The motivating force for ongoing research in this field is the potential for a variety of electrical properties combined with advantages of polymers, for instance, light weight, the relative ease in processing and chemical resistance. Conducting polymers are widely used for various applications, including actuators, sensors, electromagnetic interference (EMI) shielding, electronic nanodevices, fuel cell, supercapacitors, etc. [1]. Great efforts have been made during the past two decades in the understanding of the structural, electrical, chemical and optical phenomenon of these polymers, such as polypyrrole (PPy), polythiophene (PT), polyaniline (PANI), polyphenylene (PPh) and their derivatives. Among these polymers, PANI has been the center of focus during the last decade due to the presence of reactive NH- groups in its polymer chains, interesting redox properties, low-cost monomer, facile synthesis and good electrical conductivity. PANI has been center of attraction among the researchers because of their unique electrical properties; however, the PANI has the tendency of agglomeration in the organic solvent which limits its processability. Various gel-inhibitors like 2-Methylaziridine (2MA), azetidine (AZ) and heptamethyleneimine (HPMI), etc. are used to avoid the agglomeration or to improve the processability of PANI [2]. Among these gel inhibitors, 2MA is a toxic compound and the film having AZ is too brittle. But, HPMI additive has found as an excellent gel inhibitor for a polymeric solution with non-toxic and environmental favorable characteristics.

Various fillers like metals (or their oxides like iron oxide (Fe_3O_4) and barium titanium oxides ($BaTiO_3$), graphite, dielectric/magnetic, etc. are extensively used in PANI matrix to increase the level of electrical conductivity and especially for electromagnetic interference (EMI) applications [3]. However, the heavyweight, corrosion nature, high density and uneconomic processing of metals make them unsuitable for composites. Likewise, graphite has two-dimensional structure, high percolation threshold, and poor dispensability. Carbon nanotubes have also been used as filler for improving the electrical conductivity of matrix component. However, the cost of single-wall carbon nanotubes (SWCNTs) is higher than that of multi-wall carbon nanotubes (MWCNTs) and hence cost limits the application of SWCNTs. In addition, MWCNTs have higher permittivity as compare to SWCNTs due to

presence of more number of defects. Agglomeration of CNTs is the major problem which limits its dispersion in the matrix material. These problems can be rectified via functionalization process through which functional group created on the surface of CNTs. Various routes like covalent functionalization, defect functionalization, and non-covalent exohedral functionalization has been used for the functionalization of CNTs. Defect functionalization breaks the CNTs in short segment of the tube with a length of 100-300 nm. Covalent functionalization has an advantage over other because it improves the dispersion of CNTs in solvent and polymer matrix [1].

In the light of the above, the present research work is an attempt to prepare a PANI-based hybrid system with improved electrical properties. As per literature reported so far, two types of morphologies (either granular or fibrillar) are possible in the PANIs, when prepared with different routes. Hence, for the selection of PANI matrix, it has been prepared with two different routes, e.g., via chemical oxidative polymerization (PANI 1) and solid state oxidative polymerization method (PANI 2). These PANIs were vacuum dried and designated as PANI 1VD (having granular and fibrillar morphology) and PANI 2VD (mostly having granular morphology). PANI 1VD was selected as a matrix for developing hybrid nanocomposite, as it has relatively low moisture content and dual morphology which resulted in the better electrical conductivity. MWCNTs were selected as filler material, as MWCNTs are cheaper than SWCNTs which makes it commercially suitable. A facile and easy solution mixing method was adopted to prepare the hybrid nanocomposite. By covalent functionalization, MWCNTs were functionalized to improve the dispersion in PANI matrix. Self-standing films were prepared with PANI 1VD through solution casting method. These films were further protonated with hydrochloric acid to enhance the conductivity.

Matrix, filler, and prepared nanocomposites were characterized using X-ray diffractometry (XRD), Fourier transforms infrared (FTIR) spectroscopy, Raman spectroscopy, transmission electron microscopy (TEM), scanning electron microscopy (SEM), and thermogravimetric analysis (TGA) techniques. Electrical properties were measured/evaluated using electrometer. In MWCNTs/PANI nanocomposites, the percolation threshold found at 0.1 vol. % of the MWCNTs and the maximum electrical conductivity was found to be 0.1 S/cm at 13.9 vol. %. Based on the results obtained so far, the hybrid MWCNTs/PANI nanocomposites, beyond percolation, could be a potential candidate for EMI shielding and electrostatic dissipation (ESD) applications.

1.1 Objectives of the Research Work and Motivation

The main objectives of present work have outlined as follows:

- Synthesis of PANI powder with and without solvent via chemical oxidative polymerization and solid state oxidative polymerization methods, respectively.
- Synthesis of hybrid MWCNTs / PANI nanocomposites with aim to improve the electrical conductivity
- Synthesis of self-standing film of PANI via solution casting method and their characterizations.
- Materials-Structure-Electrical Properties correlation of hybrid polyaniline-CNT nanocomposites.

CHAPTER TWO

Literature Review

This chapter covers the literature review for the conducting polymers, conducting polymer matrix composites/nanocomposites, methods adopted for the synthesis of pure polyaniline and hybrid CNT/PANI composites/nanocomposites. Various routes were used to functionalize the CNT for better dispersion is PANI matrix also explained in detail with suitable figures. Emphasis has given on the structure of the PANI obtained via various route and correlated it with the electrical properties. The possible applications of hybrid CNT/PANI nanocomposites in the area of actuators, sensors, EMI shielding, electronic nanodevices, fuel cell and supercapacitors also described in detail.

==
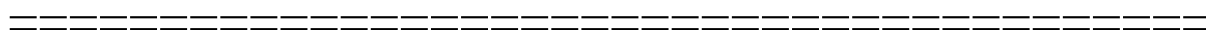
2.1 Brief Introduction

Conducting polymers usually refers to a class of organic conjugated polymers having electrical conductivity. There are many examples of conducting polymers like polyfluorene (PF), polythiophene (PTh), poly(p-phenylene) (PPP), poly (thienylenevinylene) (PTV), polypyrrole (PPy) [4-6], etc. These conducting polymers are different from the normal organic polymer. The organic polymers typically described by sigma (σ) and pi (π) bonds. The σ -bonds are fixed and motionless due to covalent bonds between the carbon atoms. On the other hand, π-electrons in a conjugated polymer are relatively localized, unlike the sigma electrons.

Conducting polymers can be broadly divided into two types, i.e., intrinsically conducting polymers (ICPs) and extrinsically conducting polymers (ECPs). ICPs have electrical conductivity in their pure form (without the addition of foreign constituent), or doped form. On the other hand, ECPs, are made conducting through a blend of ICPs with organic polymers or metal oxides, etc. In 1960, the discovery of ICPs, become an interesting area of research because of their excellent properties. The impact of this field in science was recognized in the year 2000, when MacDiarmid, Heeger, and Shirakawa awarded with the noble prize in chemistry for developing polyacetylene (PA) as a conducting polymer. This polymer was referred as "synthetic metals" having a π-conjugated system in the polymeric chains and showed a higher level of electrical conductivity when processed with oxidative and reductive polymerization [7]. They exploited π-bond of the conjugated system as it is weak due to sidewise overlapping of p-orbital. Similarly, the structure of polymers mentioned above can exploit for wide use in numerous commercial applications such as electronic, electrical, electrochemical, chemical, electro-luminescence, electromechanical, thermoelectric, membrane, electromagnetic, electro-rheological and sensors [8, 9]. The intrinsic conducting polymers like polyaniline (PANI), PPy, and PTh in their doped form, susceptible de-doping processes. These ICPs are most promising for the applications mentioned above, mainly for stability reasons. The processing of these polymers into fibers and film shapes presents an additional challenge. In general, the processing of conducting

polymers is less energy intensive as compared to the conventional electronic materials but it still somewhat problematic about conventional polymers. Among various ICPs, PANI is a comparatively well-investigated conjugated polymer, taking the subject of wide-range research for over many years. PANI offerings itself is well-matched for a multiplicity of applications because of its low-cost monomer, ease of synthesis, the presence of reactive NH-groups in its polymer chains, better stability, tuneable properties and most important is its redox characteristics [10, 11]. The processability of PANI is very limited because of its very high glass transition temperature (T_g) and even higher melting temperature mainly in its doped state. The T_g of PANI range ranges from 220-250 °C [12]. In the early 1980s, conducting properties of PANI
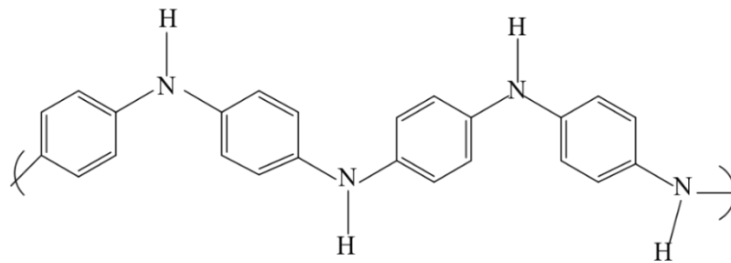
Leucoemeraldine (fully reduced, clear)
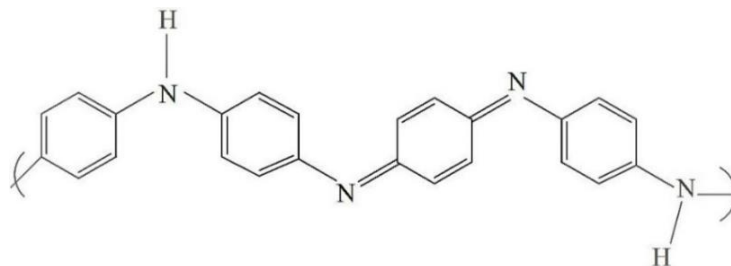
Emeraldine Base (partially oxidized, blue)
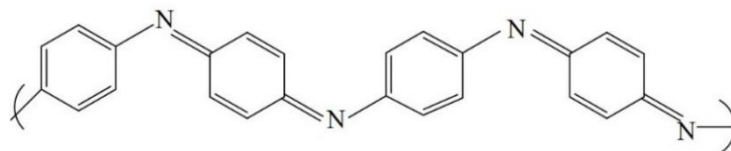
Pernigraniline (fully oxidized, violet)

Figure 2.1: Chemical structures of polyaniline.

were rediscovered and tailored for various potential applications like anticorrosion coatings [13, 14], electromagnetic shielding devices [15], and lightweight battery electrodes, etc. [16].

PANI has three idealized oxidation states: the fully oxidized state (pernigraniline), the fully reduced state (leucoemeraldine), and the partially oxidized state (emeraldine base or emeraldine salt) (**figure 2.1**).

The conducting emeraldine salt (**figure 2.2**) (green color) form of PANI is limited to soluble in most of the organic solvent.The de-doping of emeraldine salt to emeraldine base (blue color) form in ammonium hydroxide [17] or suitable basic solution make it soluble in a solvent like DMPU, m-cresol, and NMP, etc. PANI also has a tendency to agglomerate in the solvent because of which its processability is limited to casting. Various gel-inhibitors like 2-

Emeraldine Base

Doped with protonic acid   De-dope with strong base

Electronic rearrangement

Emeraldine salt (conducting)
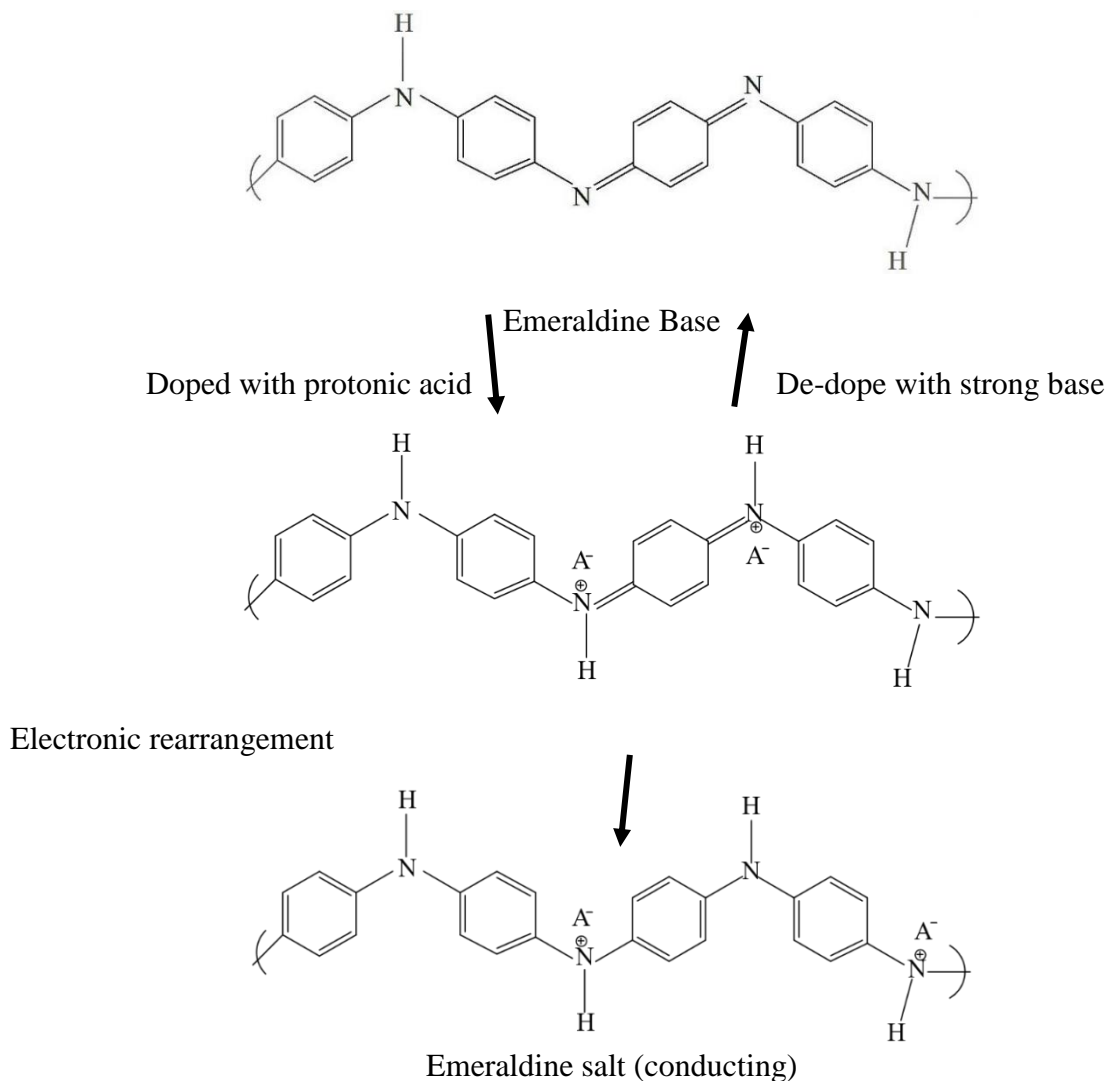
Figure 2.2: Chemical structures of the emeraldine base, its acid-doped intermediate, and final doped form, emeraldine salt.

Methylaziridine (2MA), azetidine (AZ), pyrrolidine (PY), piperidine (PP),hexamethyleneimine (HXMI) and heptamethyleneimine (HPMI) are used to avoid the

agglomeration of PANI. These secondary amine inhibitors inhibit the gelation and also provide strength to the film. The electrical conductivity of PANI can be tuned using various dopants like HCl, H_2SO_4, HCOOH, I_2, camphor sulfonic acid (CSA) and methylene blue. [18]. The chemical treatment taken for doping and de-doping process affects the electrical conductivity as well as the morphology of the PANI polymer [19]. PANI conductivity in emeraldine salt form is close to the value of common semiconductors (conductivity ~10^2S/cm) and it exceeds in common polymers (conductivity <10^{-12} S/cm).

Various polymerization methods are available for the synthesis of PANI like electrochemical polymerization, template polymerization, enzymatic polymerization, photo-polymerization, plasma polymerization, chemical polymerization, and some other special methods. Among these methods, chemical polymerization is most attractive due to easy handling, very simple, and large mass production point of view. The typical chemical oxidative polymerization methods of aniline include emulsion, solution blending, dispersion, interfacial, heterophase, self-assembling, metathesis, sonochemical and seeding polymerizations. The development of PANI-based hybrid nanocomposites acquired the excellent properties that individual components can never attain. PANI has been used both as a filler and matrix material to achieve the desired properties of the multi-phase component. The processability of PANI makes it suitable for the fabrication of PMCs by incorporating conducting carbon nanotube (CNT) as filler. In recent time, unidirectional nanostructure CNT (having sp^2 hybridized carbon structures) widely used in the matrix of PANI. The unique nanoscale morphology of CNT has a great impact on its mechanical, electrical, optical, and chemical properties [20]. The semiconducting and metallic nature of CNT depends upon the arrangement of the hexagon rings along with tubular surface. Single-wall carbon nanotubes (SWCNT) having closed ends at both sides with a semi-fullerene molecule consist of a single graphite sheet. Multi-wall carbon nanotubes (MWCNTs) consisting of up to dozens of concentric tubes comprise a central tube of nanometric diameter surrounded by graphitic layers with an intertube spacing roughly equal to the van der Waals graphite interplanar distance, 0.34 nm [21]. However, the difficult manipulation of CNT in any solvents, lack of solubility and dispersion (due to the existence of weak van der Wall force) have imposed great limitations for its use. These van der Wall forces can minimize with the surface modification of one-dimensional structures are grouped into three categories.

(a) Wrapping of functional groups or non-covalent adsorption at the surface of nanotubes

(b) Endohedral filling of their empty inner cavity.

(c) Reactions onto the π-conjugated skeleton of CNT for covalent attachment of chemical groups.

CNT can form supramolecular complexes after interaction with different classes of compounds [22-28]. In the current scenario, the incorporation of CNT in PANI nanostructures (nanofibers, nanorods, nanotubes, and nanowires) develop a new functional material. The attention of scientific society toward hybrid CNT/PANI system paid at the end of 20th century. The expected applications of hybrid CNT/PANI nanocomposite include diodes, solar cells, supercapacitors, sensors, electrochemical energy storage devices, EMI shielding or EM absorbers and supercapacitors. These applications directly linked to mechanical, thermal, morphological, electrical, and electrochemical properties of hybrid CNT/PANI nanocomposite. The incorporation of CNT in PANI approves a change in electronic and physical structure which leads to generating many novel properties [29]. The individual chemical properties of filler and matrix material may alter the developed hybrid CNT/PANI nanocomposites. In hybrid CNT/PANI nanocomposite, the filler might be covalently bonded to the matrix or with filler-matrix interaction. As of morphological point of view, PANI can attach to the CNT surface at different selective sites. There are more ways to prepare the hybrid CNT/PANI nanocomposites, out of which chemical and electrochemical polymerization are most utilized techniques. Research on the subject of the development and properties of hybrid CNT/PANI nanocomposite has been carried out in dissimilar fields. As believed CNT/PANI is a donor–acceptor system where photo-induced charge transfer occurred between PANI and CNT for photovoltaic effect [30].

2.2 Methods for Synthesis of Polyaniline

2.2.1 Electrochemical Polymerization

Nowadays, the electrochemical approach used significantly for the synthesis of polyaniline films deposited on the working electrode. Electrochemical polymerization (ECP) technique is interesting because of the following two reasons.

(1) ECP method provides better polymerization with a fine control of the initiation and termination steps.

(2) It has a degree of technological potential.

The reactions carried out by this method is often much cleaner which results to form relatively pure form of PANI compared to obtained through chemical polymerization. This method is clean because no additional chemicals such as oxidant, surfactant, and so on are not used here. So, this method controls the pollution problem. The polymerization cell design is of equal importance, and the same versatility in the form of assembly is attained to prepare polyaniline. EC route used for the polymerization of aniline under constant current (galvanostatic), constant potential and a potential scanning/cycling or sweeping. The galvanostatic route comprises of two-electrode assembly dipped in an electrolyte solution (containing monomer), and a constant current is supplied to form PANI film on the surface of a platinum foil electrode. Diaz *et al.* [31] reported that polymerization of aniline monomer at constant potential produces polymer powder which observed weakly on the electrode. Genies *et al.* [32] demonstrated that electro-oxidation of aniline monomer by uninterrupted cycling amid predetermined potentials produces an even polymeric film which confidently sticks to the electrode surface. Gupta *et al.* [33] reported the PANI nanowires via the electrochemical route; these nanowires deposited on stainless steel electrode at the potential of 0.75 V vs. SCE **(figure 2.3a and 2.3b).**They found the long-standing cyclic stability of the PANI nanowires which confirmed its implications for the high-performance supercapacitors. PANI nanofibers prepared by Karami *et al.* [34] by using pulsed galvanostatic electropolymerization
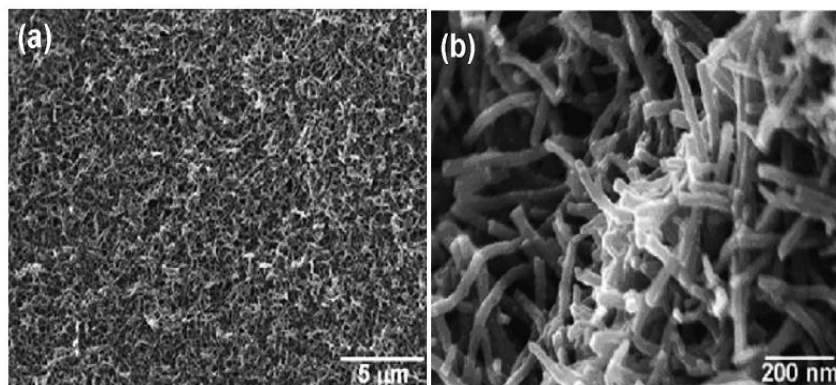
Figure 2.3: SEM images (a and b) of the PANI nanowires at different magnifications [33].

of aniline at different conditions. To produce the uniform morphology of PANI nanofibers, the effect of such variables as bath temperature, relaxation time (t_{off}), pulse height (current amplitude), pulse time (t_{on}), $HClO_4$ and aniline concentrations were studied. The optimum

conditions used to prepare the PANI leads to develop the uniform morphology of PANI nanofibers on an average length of 4 m and an average diameter of 80 nm.

2.2.2 Photo-Induced Polymerization of Aniline

The photochemically initiated polymerization of aniline involves the photo-excitation of monomer for the synthesis of polyaniline. In this method, synthesis is done by irradiating gold electrode with a Nd: YAG laser in a solution containing aniline monomer under an applied external bias. [35]. Visible argon laser irradiation also forms polymer on the electrode. However, the thorough polymerization mechanism is not yet known. Photopolymerization is a direct way to make PANI in which photons and metallic ions replace conventional oxidants to support polymerization of aniline. With photo-catalytically route PANI was also achieved by Teshima *et al.* [36] in the double layer structure composed of ruthenium complex-incorporated Nafion and viologen-pendant-poly(siloxane) in acidic aqueous solutions. It explained that N-phenyl-p-phenylenediamine (PPD, head-to-tail coupling dimer of aniline) along with aniline monomer also essential to induce photopolymerization [35]. In this process PPD worked as an initiator for photopolymerization, the assumed photopolymerization mechanism shown in **figure 2.4.**
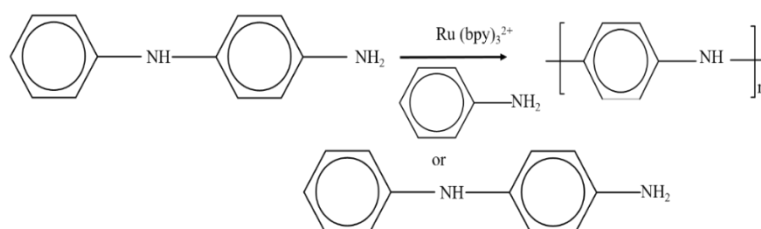
Figure 2.4: Schematic representation of the photo-polymerization of aniline derivatives with ruthenium complex

Barros *et al.* [37] reported that the morphology of the resulting polymer intensely depends on the excitation wavelength. Photo-polymerization approach yields a composite material where Ag nanowires and microwires made along with PANI. They observed the globular morphology for the UV synthesis, and a fibrillar observed for visible light excitation **(figure 2.5).** These results revealed the granular morphology for PANI, while nano and micro Ag wire growth were also observed **(figure 2.5a).** Besides, when wavelength changes to the visible region, simply fibrillar morphology was observed for PANI, and there is a no

appearance of Ag wire with the polymer **(figure 2.5b)**. From these results, it concluded that the polymerization strongly depends upon the excitation energy. The time required for
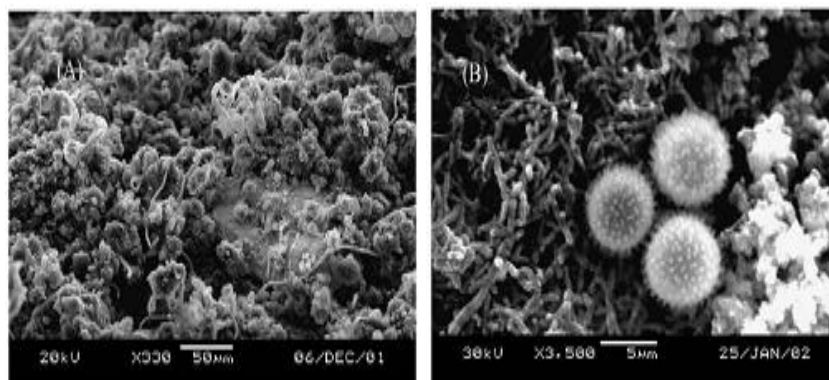
Figure 2.5: SEM images of PANI composite (a) with UV synthesis and (b) with visible light synthesis [37]

polymerization with visible excitation was more than that of UV excitation. The delay in time was due to the change in structure.

2.2.3 Template Synthesis of Polyaniline Nanostructures

Template synthesis is very simple and effective method used to obtain the nanostructure of polymeric material [38, 39]. With this route, the desired shape of material can be acquired in the pores of a template. This route has been widely used in electrochemical and chemical polymerization to develop conducting polymer nanostructure [40]. The self-templating electrochemical synthesis of PANI nanowires using aluminum as a template illustrated in **figure 2.6.** The chemical etching is used to remove the aluminum oxide from the aluminum substrate which arises the pre-structured aluminum. After that, constant current density supplied on pre-structured aluminum. The nanowires of PANI fabricated in porous alumina by disappearing the barrier in phosphoric acid (H_3PO_4). The anodization process is the key factor to obtain the morphology of the shape of the pores [41]. Template method is most interesting and useful due to its effectiveness in the preparation of one-dimensional nanostructured or microstructured PANI with a controllable length, diameter, and orientation [42]. Wu *et al.* reported the PANI filaments (diameters of 3 nm) in the hexagonal channels of a mesoporous aluminosilicate [43]. However, some shortcomings of this method are as follows:

(a) This method forms the unwanted aggregates, or nanostructured polymers may destroy after released from the templates

(b) To remove the templates very tedious post-synthesis process is required.
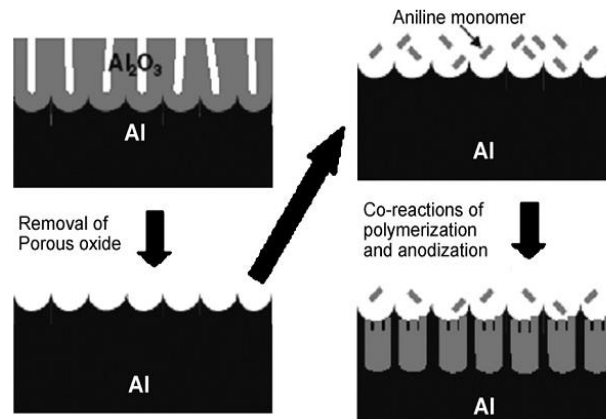
Figure 2.6: Self-templating production of PANI nanowires on the pre-structured aluminum via electrochemical reaction [41]
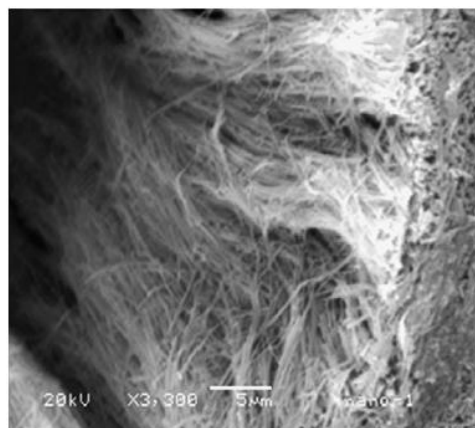
Figure 2.7: SEM image of a template synthesized PANI nanofibril membrane after dissolving in alumina template partly [42]

The uniform and aligned PANI nanofibers can also prepare via template polymerization using AAO as a template [42]. The mechanism of nanofibers formation depends upon the molar ratio of monomer/oxidant reagents, structure of AAO and polymerization temperature. The SEM image of aligned fibers shows the brush like morphology (**figure 2.7**) of PANI formed after the immersion of membrane in 6 mol/l aqueous NaOH for 20 min [42]. The extremely oriented uniform PANI fibers have a length of about 60 μm and a fibril density of 5.3 X 10^8 cm^{-2}. Zheng *et al*. [44] prepared an array of

PANI coaxial nanowires using an anodic aluminum oxide (AAO) membrane as the template. The nanotubule array of PANI in an AAO membrane depicted in **figure 2.8** The SEM image with a top view (**figure 2.8a**) shows the diameter of the pores in AAO membrane is about 60 nm. The TEM image shows that PANI nanotubules were not in contact with the walls of the
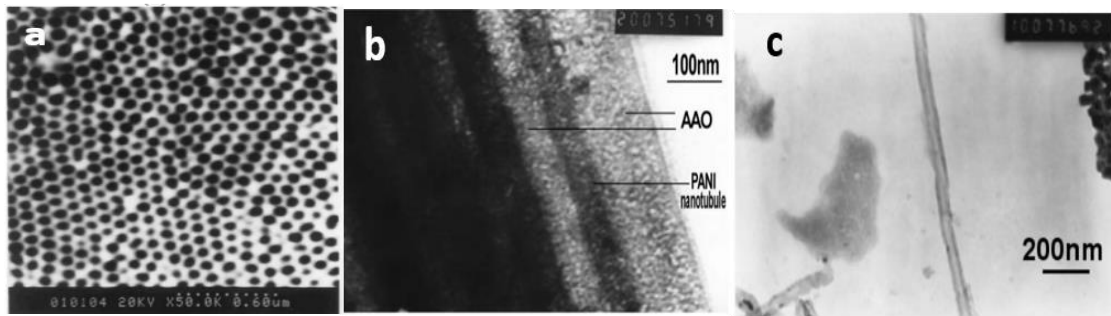
Figure 2.8: SEM top view(a), TEM cross-section view of PANI nanotubules array in AAO membrane(b) and, TEM image of a PANI nanotubules (c) [44]

pores in an AAO membrane **(figure 2.8b).** The TEM image of one PANI nanotubule shown in **figure 2.8c.** It illustrates that the inner diameter of PANI nanotubule is less than 10 nm and the outer diameter less than 30 nm which is inconsistent with the diameter of PANI nanotubules in AAO membrane exposed in **figure 2.8b**.

2.2.4 Enzymatic Polymerization

During the last decade, conducting polymers are extensively used in many enzymatic displays [45]. The most studied system based on glucose oxidase (GOD) enzyme which is very interesting because of its cheapness, naturally robust and sugar analysis silently active in the field of research. Conducting polymers like PTh, PANI, and PPy [46, 47], or other derivatives are extensively used to develop ECP-GOD devices. The synthesis of PANI via enzymatic polymerization of aniline takes place under milder conditions compared to chemical polymerization. The biological molecules like Urease [48], uricase [49], tyrosinase [50], horseradish peroxidase (HRP) and soybean peroxidase (SBP) widely used in combination of conducting polymers [51]. Mejias *et al.* [52] reported that soybean peroxidase (SBP) and horseradish peroxidase (HRP) are oxidoreductase enzymes, has the ability to oxidize aromatic amines in the presence of hydrogen peroxide (H_2O_2). HRP and SBP enzymes have high reaction selectivity toward aromatic compounds. They cut down the oxidation by-products to water because of which peroxidase catalyzed polymerization of

aniline to PANI is considered to be an environmentally friendly route. McEldoon *et al.* [53] explain that the melting temperature of SBP is 90.5 °C at the pH of 8.0 (in the presence of 1mMCaCl$_2$) because of which this enzyme is thermodynamically more stable than that of HRP enzyme. From early studies, it was found that low molecular weight branched PANI prepared via enzymatic polymerization. To avoid this issues, enzymatic polymerization of aniline takes place with polyelectrolyte templates such as polystyrene sulfonate (PSS).Some other templates like poly(vinylphosphonic acid) and deoxyribonucleic acid (DNA) also used for the polymerization of aniline monomer [54]. In this approach PSS, release the counter ions for doping emeraldine base form of PANI to its conducting emeraldine salt. It also plays a vital role in imparting the water-soluble complex of emeraldine salt form of PANI with a well-defined structure at pH > 4.3 [55]. The high degree of complex formation makes it difficult to obtain PANI in bulk form; especially for fibers and free-standing films. Peroxidase-catalyzed polymerization of aniline monomer is an eco-friendly method to acquire PANI because this enzyme is derived from non-pollutant renewable sources and had extraordinary reaction selectivity to aromatic compounds. It was reported that bulk emeraldine salt form of PANI could be prepared using HRP enzyme at pH 3.0. However, enzyme drives through denaturing process at these reaction conditions. This issue can solve by carrying the reaction at high pH (above 6.0). When the reaction is taking place at higher pH without an anionic template, the obtained product possess some structural defects like ring coupling and cross-linked chain. These defects affect the conjugation of PANI backbone which leads to the decline in the conductivity of PANI [56]. On the other hand, soybean peroxidase (SBP) possess well catalytic activity in an acidic
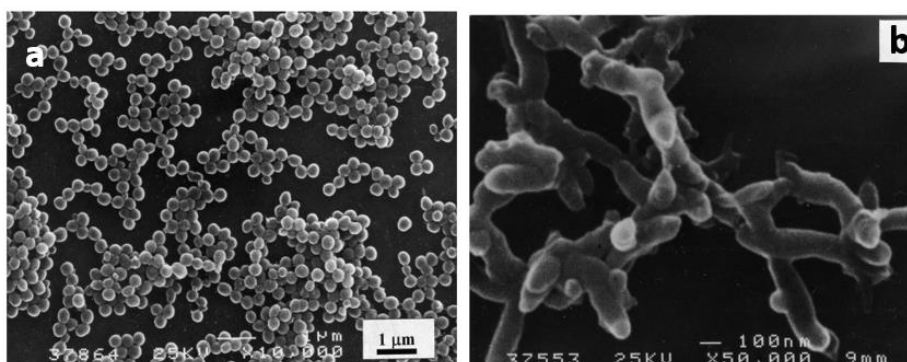
Figure 2.9: Polyaniline dispersion particles stabilized by hydroxypropyl cellulose prepared at 0 °C (a) and 40 °C (b) [57].

environment and advanced thermodynamic stability than HRP. These properties of SBP enzyme may be useful in producing conducting PANI at the same condition. Stejskal *et al.* [57] reported the dispersion of PANI in the presence of hydroxypropyl cellulose. They obtained the uniform particle of PANI in sub micrometer at 0 °C (**figure 2.9a**), and core like cylindrical morphology at 40 °C (**figure 2.9b**).

2.2.5 Plasma Polymerization

Plasma polymerization of aniline monomer is a low-cost and reliable method for the synthesis of polyaniline without using any oxidizing agent and solvent [58]. Cruz *et al.* [59] prepared the PANI film via plasma polymerization using RF glow discharges with resistive coupling between stainless-steel electrodes. They acquired the polymer at a pressure in the range (2–8) x 10^{-2} Torr and a frequency of 13.5 MHz. The PANI film doped with I_2 was adhere to metal and glass surface. The morphology of PANI film at 350 X (**figure 2.10a**) shows the layers stacked over the substrate with different thickness. While removing the film from the surface, its edges get disturbed and look like sharp edges. **Figure 2.10b** shows the morphology of film at 2500 X having two regions with different appearances (plain film and distribution of bubble on the surface). The normal surface is the homogeneous growth of polymer. However, bubbles ascribed to drops of oligomers or monomer trapped between the layers that vaporize. Plasma polymerization also used to deposit the thin films of PANI-nano carbon on a silicon substrate with functional gradient properties and electronic transport with charge accumulation [60]. Nastase *et al.* [61] explore the possibility to deposit
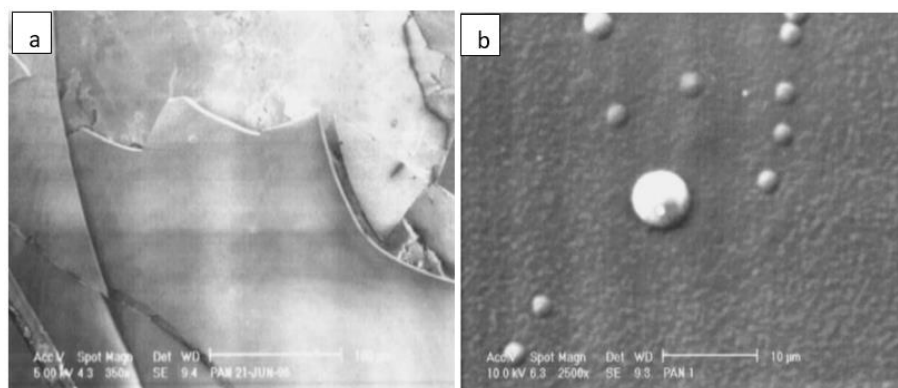
Figure 2.10: Microphotograph of PANI film at 350X (a) and 2500X (b) [59]

polythiophene-silicon dioxide (PTh-SiO$_2$) and polyaniline-silicon dioxide (PAni-SiO$_2$) nanocomposites via plasma polymerization method. They produced the film by spraying of mixtures of silica nanoparticles dispersed in the liquid monomer into a plasma stream of the DC-plasma discharge reactor. It was observed that the silica in polymer matrix alter the mechanism of conduction from ohmic to ballistic and traps inducing the space charged limited currents (SCLC). It was also seen that the filler material varies the composition of deposited films and the morphology. This method is used for the preparation of hybrid PANI nanocomposite with various nanofiller materials. For preparing hybrid CNT/PANI nanocomposites, the surface of CNT is activated using N$_2$ plasma afterward; plasma induces the polymerization of aniline monomer.

2.2.6 Chemical Polymerization

Chemical polymerization is a facile and efficient method having the capability of generating bulk quantities of conducting polymers [62]. It is cost-effective for commercial mass production, comparatively less time consuming and some companies generating bulk powders, dispersions, and coated products. The synthesis of PANI via a chemical polymerization involves the mixing of the monomer with an oxidizing agent in acidic, aqueous and non-aqueous media. Sapurina and Stejskal used a silver nitrate oxidant [63] to polymerize aniline via chemical polymerization. It revealed that the product contained non-conducting aniline oligomers or conducting PANI with a high molecular weight. Liu and his co-workers [64, 65] synthesized hydrochloric acid (HCl) doped PANI with ammonium peroxidisulfate [(NH$_4$)$_2$S$_2$O$_8$ or APS] as an oxidant and observed a beltlike morphology stacked by spherical particles. The morphology of the polymer depends on the dopant and could be altered by suitable dopants and further tuned by the drying conditions. The oxidizing agent APS was used because of its high oxidation potential (2.01V) [63]; this, in turn, accelerated the polymerization mechanism. This oxidizing agent is very prominent to the incorporation of HSO$_4^-$/SO$_4^{2-}$ as the dopant anions (A$^-$) in the PANI.HA product. These reactions take place in an acidic media with pH <3; to assist the solubilization of the aniline monomer in aqua and prevent the massive formation of undesired branched products. The oxidant to aniline monomer ratio of <1.2 is employed because of S$_2$O$_8^{2-}$ anion is a two-electron oxidizer (acceptor) which remove two electrons from each aniline monomer during polymerization. Kumar *et al*. used APS as an oxidant for the synthesis of PANI in air and vacuum dried condition with (PANI 1 and PANI 1VD) and without (PANI 2 and PANI 2 VD) solvent via chemical oxidation polymerization method [66]. They obtained dual

(granular and fibrillar) morphology of PANI prepared with solvent and only granular morphology without solvent. The clear view of nanofibers was also shown with the TEM image of PANI 1. A. Kumar and his group explained that growth mechanism of PANI nanofibers and conversion of one-dimensional morphology shape to granular shape depends upon the rate of addition of aniline monomer (one drop every 10 seconds for nanofibers). The electrical conductivity of PANI 1, PANI 1VD, PANI 2 and PANI 2VD were reported as 3.3 x 10^{-2} S/cm, 0.3 x 10^{-2} S/cm, 0.1 x 10^{-2} S/cm and 0.3 x 10^{-3} S/cm, respectively.

PMCs using carbon nanotube (CNT) as a filler are more popular because they are light-weight, easy to process, corrosion resistance and having a high level of electrical conductivity due to the generation of conductive paths in the polymer. Experimental studies revealed possible improvements in the electrical and mechanical properties of PANI by efficient incorporation of CNT [67].The intriguing properties of CNT like chemical stability, electrical and thermal properties are exploiting in the field of materials chemistry and polymer matrix nanocomposites. However, the issues which limit the reinforcing efficiency of CNT in a polymer matrix is its poor dispersion and contamination. These problems can solve by the surface treatment of CNT.

2.3 Functionalization of CNTs

CNTs are tremendously resistant to wetting, hard to disperse and dissolve in aquatic and non-aquatic media. The carbon nanotube has low mass density, large aspect ratio (typically ca. 300-1000) and high flexibility [68]. The preparation of hybrid composites/nanocomposites using insoluble nanotubes as a filler is a huge problem in generating, aligned assemblies, which is important for the construction of electronic devices. An appropriate functionalization of the carbon nanotubes represents a strategy for overpowering these obstacles and become an attractive mark for materials scientists. The functionalization of CNT can improve processability, solubility and permit the combination of the exceptional properties of nanotubes with those of other types of materials. Chemical bonds are responsible for the interaction of the nanotube with other entities, such as a polymer, biopolymer matrices, and solvent, etc. It is believed that functionalized nanotube have good electrical and mechanical properties than that of the un-functionalized nanotube, and thus may exploit in the field of material chemistry. There are numerous methods for functionalization of CNTs including covalent functionalization, defect functionalization, and non-covalent functionalization [24].

2.3.1 Covalent Functionalization

Covalent functionalization of CNTs is a very promising approach for nanotubes modification and derivatization [69]. Though, it is hard to achieve control over the chemo- and regioselectivity with the addition of halogens, carbenes, arynes, and drastic reaction conditions. The reactivity of CNT is very high due to the presence of sp^2 hybridized (π-orbital) carbon atom in their structure. These orbitals have more tendency to covalently bond with the chemical species having sp^2 and sp^3 hybridization of carbon atom [70]. The change in hybridization from sp^2 to sp^3 affects the translational symmetry of CNT which further influences it's electronic and transport properties. Covalent functionalization of CNT enhances its dispersion in solvent and polymer matrix either by direct reagents to the sidewalls of nanotubes or by modification of surface-bound carboxylic acid groups on the nanotubes. The oxidation of CNT is possible in the presence of air, oxygen, concentrated sulfuric acid, nitric acid, aqueous hydrogen peroxide, and acid mixture which generates the functional groups like –COOH or –OH on the surface of CNT. The pristine MWCNTs has a very smooth surface, and after surface treatment, its surface gets rough which shows the defects in the carbon-carbon bonding along with carboxylic acid groups. The required parameter to increase the number of –COOH groups on the surface of CNTs are acid treatment, time and temperature. With increasing time and temperature number of –COOH groups also increases [71, 72]. The –COOH group on the surface of CNT is an appropriate
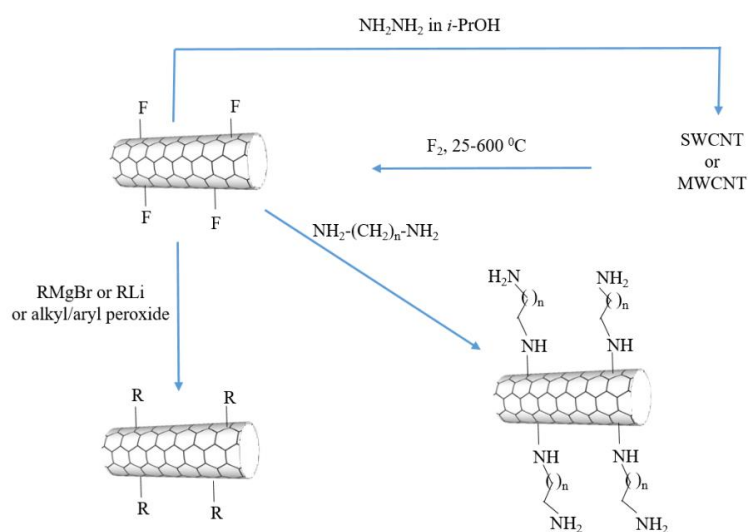
Figure 2.11: Scheme for fluorination of nanotubes, defunctionalization, and further derivatization.
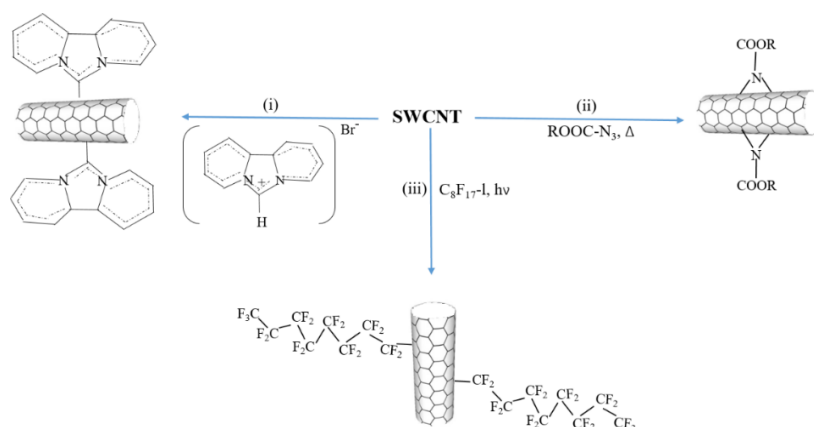
Figure 2.12: Derivatization reactions: (i) carbene addition; (ii) functionalization by nitrenes; and (iii) photoinduced addition of fluoroalkyl radicals
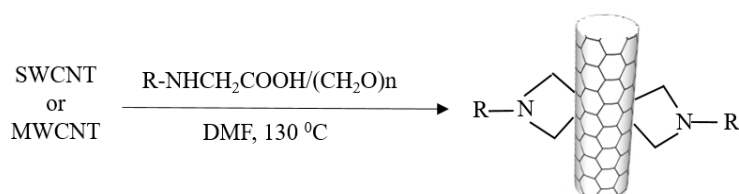
Figure 2.13: 1,3-Dipolar cycloaddition of azomethine ylides

functional group as compared to others one due to multiple chemical reactions conducted with this group. It also supports the attachment of organic or inorganic materials, which is essential for solubilizing nanotubes [73]. The crosslinking between CNTs can done with covalent functionalization via thiolation and esterification reaction [74]. Mickelson *et al.* [75] reported the fluorination of SWCNT at the side walls by passing fluorine element at different temperatures. The solubility of organolithium and Grignard reagent in chloroform convert the fluorinated SWCNTs into alkylated SWCNTs (**figure 2.11**). It can also be solubilized by direct functionalization of their side walls by cycloaddition reactions like carbenes addition, nitrenes addition (**figure 2.12**), nucleophilic cyclopropanol, Azomethineylides [76] (**figure 2.13**), Diel- Alder reaction and side wall osmylation. CNT can also functionalized with the addition of radicals, electrophilic addition, and nucleophilic carbene [77, 78].

2.3.2 Defect Functionalization

The oxidative treatment is used to eradicate amorphous carbon or metal particles from the raw materials. This methodology observes the defects at the open ends of CNTs. The oxidized carbon atoms in the form of carboxyl (-COOH) group were attached to the surface of CNT [79]. This treatment breaks the CNT in short segment of tubes with lengths 100–300 nm. Mawhinney *et al.* [80] reported the 5% of carbon atom at the localized defective site of SWCNTs by the evolution of carbon dioxide (CO_2), carbon monoxide (CO) at 1273 K temperature. Hu *et al.* [81] also described the 1-3 % of acidic sites using acid-base titration method. This method is not efficient for generating defective sites at the surface of CNT because of which CNT can not properly disperse in the polymer matrix. After the finishing, off weak van der Wall, forces functionalized CNT are more dispersible in an organic solvent than pristine CNT. This method is also proposed to get individual and soluble (in organic solvent) SWCNT macromolecules if reaction time increased for four days (at elevated temperature) in the presence of acid chloride group with amines [82].

2.3.3 Noncovalent Exohedral Functionalization

The non-covalent functionalization of the outer surface of CNTs widely interested in reserving the extended p-network of the nanotubes [83]. In this method, nanotubes can be moved to the liquid phase via non-covalent functionalization of the surface-active molecules, for example, sodium dodecyl sulfate (SDS) or benzalkonium(BKC).The hydrophobic surfaces of the CNTs can be changed to the hydrophilic surface using Triton X-100 as a surfactant [84]. As a result, CNT-Triton conjugate interacts with the reductase, both having hydrophilic surface creating a water-soluble complex of the immobilized enzyme. The interactions between the enzyme and CNT-Triton conjugates can confirmed by gel electrophoresis and Raman spectroscopy. As the micellar concentration reached to a critical point, SDS forms supramolecular structures made up of half cylinders on the nanotube's surface (**figure 2.14**).The observed rings, helices, or double helices depends on the symmetry and the diameter of the CNT [85]. Gul *et al*. [86] reported non-surfactant arbitrated immobilization of protein and DNA on the carbon nanotube. The water repelling sections of the proteins are essential for adsorption. Protein immobilization on nanotubes is a nucleophilic reaction which involves the substitution of N-hydroxysuccinimide by an amine (RNH_2) group on the protein. The mechanism of above reaction shows the interaction of movable π-bonds on the CNTs wall because of sp^2 hybridization with π-bonds of polymer

molecules [87]. The wrapping mechanism attributes the interactions between the polymer and the CNTs which results in improving the physical association of polymers with CNT, and further, it forms the supramolecular complexes [88]. The dispersion of CNTs in conjugated polymer,i.e., poly(m-phenylenevinylene-co-2,5-dioctyloxy-p-phenylenevinylene) (PmPV) which forms the wrapping of copolymer around the nanotubes [89, 90]. The prepared hybrid composites have better electrical properties than that of individual components. The dispersion of CNT in different solvents is also possible using non-wrapping methods [91].
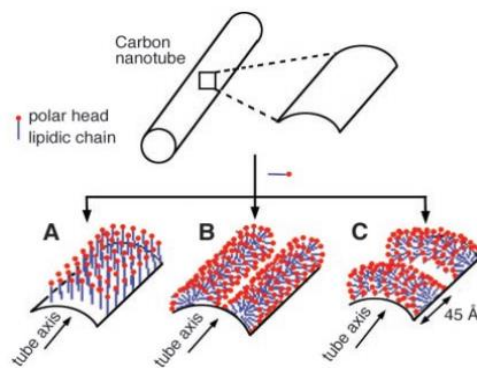
Figure 2.14: The possible organization of the sodium dodecyl sulfate molecules on the surface of a CNT. (a) The SDS molecules could be adsorbed perpendicular to the surface of the nanotube, forming a monolayer,(b) oriented parallel to the tube axis and (c). Half-cylinders oriented perpendicular to the tube axis. [85]

With this approach, dispersion of CNT can improve in a solvent with stabilized copolymers of various structures. The adsorption of block copolymers on nanotubes by non-wrapping mechanism leads to the formation of good dispersions of CNT. The non-covalent attachment has some shortcoming, i.e., the forces between the wrapping molecule and the filler might be weak results in a hybrid composite with the efficiency of the load transfer near to the ground.

2.4 Methods of Preparation of CNT/PANI Nanocomposites

The excellent properties of CNTs utilized in real-world applications with the development of hybrid CNT/polymer nanocomposites. At present, PMCs with CNTs as a filler used in various areas of applications like infrastructure sectors, energy, aerospace, defense, sporting goods, transportation and automotive. The potential of PMCs in these applications is due to their flexibility, light weight, design, high strength and high durability.

Among various polymer composites, hybrid CNT/PANI nanocomposites extensively used as electromagnetic interference (EMI) shielding and electrostatic discharge (ESD) material because of its high electrical conductivity. The higher level of conductivity was due to the creation of conducting path in the matrix material. The effective use of CNTs as a filler for producing nanocomposites depends on the homogeneous dispersion of nanotubes in the PANI matrix without finishing their integrity. Moreover, the mechanical properties of hybrid nanocomposites can also be improved with excellent interfacial bonding which helps in transferring the significant load across the CNT–matrix interface. This process is highly acceptable for getting good dispersion of nanotubes without affecting its property. The various method used for the synthesis of CNT/PANI nanocomposites are as follows:

2.4.1 Electrophoretic Method

In recent years, electrophoretic method received much attention toward itself, for developing dense and uniform films of conducting polymer. Some research papers published on the incorporation of CNT into a PANI matrix. Dhand *et al.* used electrophoretic route [92, 93] to prepare carboxylic-functionalized MWCNTs/PANI composite film [93] on indium tin oxide (ITO) coated the glass.
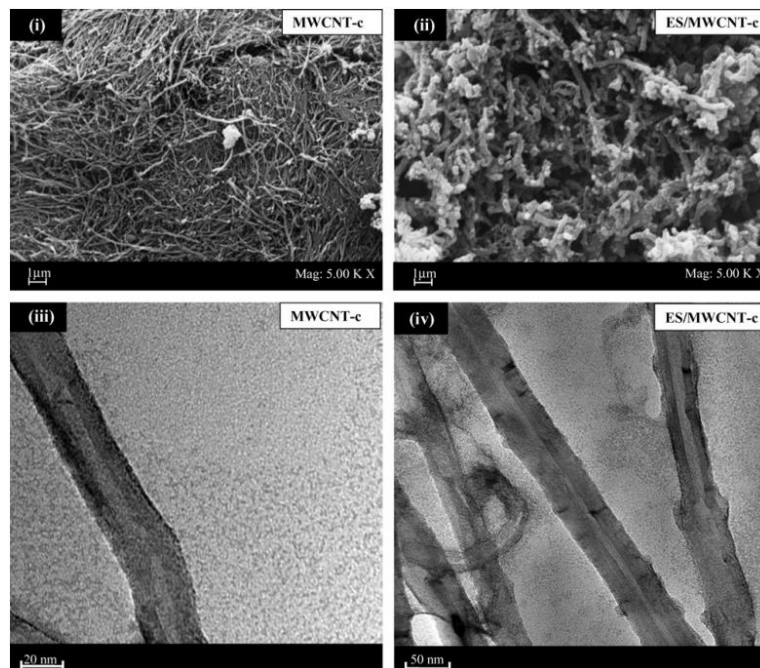
Figure 2.15: SEM (i and ii) and TEM (iii and iv) micrograph of c-MWCNTs and c-MWCNTs/ES composite. [92]

The thickness of the homogeneous composites film was about 200nm and having excellent electrochemical and charge transfer properties. SEM and TEM studies investigate the wrapping of carboxylic-functionalized MWCNTs (c-MWCNTs) with ES form of PANI. The surface morphology of carboxylic-functionalized MWCNTs and its composite with ES form of PANI after the film fabrication on the ITO plates depicted in **figure** (**2.15i and ii**). Furthermore, TEM images show the sharp and well-defined edges in MWCNTs (**figure 2.15iii**), however, the unclear ends of MWCNTs are noticeable in MWCNTs doped PANI nanocomposite (**figure 2.15iv**) along with ES wrapping onto MWCNTs. The limitation of the electrophoretic method compared to the other colloidal processes is that aquatic media cannot use during processing. The reason is that as the voltage applied to the liquid medium, the gasses like hydrogen and oxygen evolved at the electrodes. The evolution of these gasses has the negative effect on the deposits formed.

2.4.2 In-Situ Polymerization

In this polymerization method, a solution of dispersed CNT added in the aniline monomer. The desired solution of an oxidizing agent like APS, $K_2Cr_2O_7$, $KMnO_4$, KIO_3, $FeCl_3$, etc. is added dropwise to the mixture solution followed by polymerization. A higher percentage of CNTs can easily disperse via this route, form a strong interaction with the polymer matrixes. This method is useful for the preparation of composites with polymers that cannot be processed by solution or melt mixing, e.g., insoluble and thermally unstable polymers. Bachhav *et al.* [94] reported the synthesis of carboxylated multi-walled carbon nanotubes (MWCNTs) doped PANI nanocomposites by in situ chemical oxidative polymerization method using ammonium peroxodisulphate (APS) as an oxidant and HCl as a dopant. The ultrasonication treatment is given for uniform dispersion of MWCNTs in PANI matrix. **Figure 2.16a** depicts the combined ropes with the smooth surface of functionalized MWCNTs with lengths up to few micrometer and diameter is about 10 nm. Granular morphology of PANI with an average diameter of 100nm shown in **figure 2.16b**. This method intentionally used for grafting of PANI on the surface of MWCNTs. **Figure 2.16c** shows that with the addition of 4.0 wt.% MWCNTs in PANI matrix increased the diameter up to the range of 100-150 nm. The thin layer of PANI was deposited on the surface of MWCNTs with an average diameter of 15-20 nm at 8.0 wt% of MWCNTs **figure 2.16d.** The electrical conductivity increased gradually up to 1 wt% MWCNTs content but sharply

increase beyond it. The electrical conductivity of pure PANI was 0.17 S/cm and increase from 0.22 S/cm to 3.32 S/cm for 0.25 wt% and 8 wt%, respectively. Konyushenko *et al.* also followed same method [95] for the development of MWCNTs doped PANI nanocomposites with loading the filler up to 80 wt% (**figure 2.17**). They observed the uniform coating of PANI on the surface of MWCNTs and found that the diameter of MWCNTs increased with increasing the deposition of PANI. TEM images (**figure 2.18**) shows the clear view of
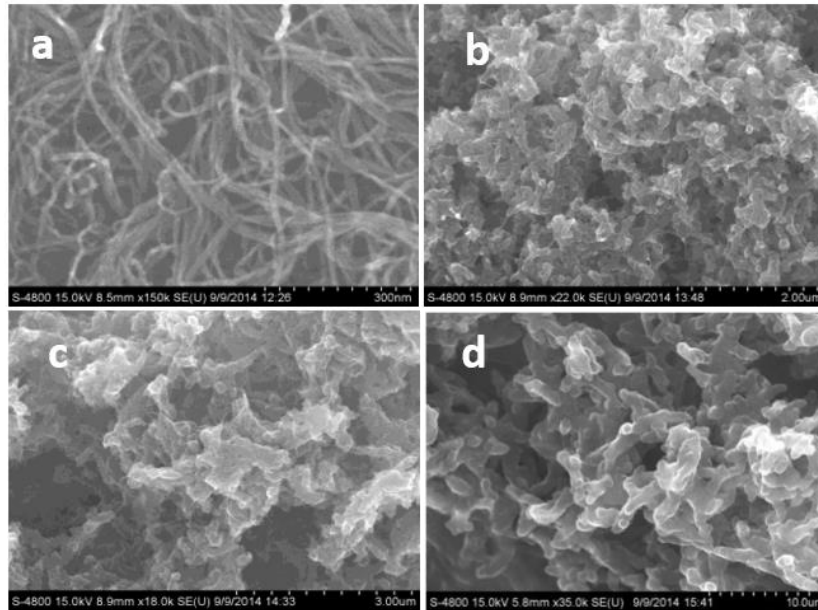
Figure 2.16: FE-SEM images of f-MWCNTs (a), PANI (b) and MWCNTs/PANI nanocomposites at MWCNTs contents of 4 wt.% (c) and 8 wt.% (d) [94].

MWCNTs (left), and bilayer structure of MWCNTs coated PANI nanocomposites (right). The visualization of internal cavity makes it sure that the coating of PANI takes place only at the outer surface of the CNT. In situ polymerization of aniline monomer inside the CNT hindered by the limited access of reactants to the interior of the CNT. It was found that resulting composites have the electrical conductivity of 7.7 S cm^{-1} for 70 wt. % CNT which was higher than that of pure PANI,i.e., 0.9 S cm^{-1}. Choudhury *et al.* [96] stated the average electrical conductivity of about 1.4 x 10^{-1} S/cm for f-MWCNTs/PANI nanocomposites loaded with filler concentration greater than1wt %. Philip *et al.* [97] also reported the MWCNTs coated PANI nanocomposites via in-situ polymerization method. For good dispersion of MWCNTs in PANI matrix, they functionalized the MWCNTs with *p*-phenylenediamine, which gave phenylamine functional groups on the surface. The composites of PANI prepared with a-MWCNTs (**C1**), and oxidized MWCNTs (**C2**) disclosed the tubular morphology with

core-shell structure in which **C1** composite also display the granular morphology. The electrical conductivity of PANI, **C1** and **C2** were 8.2 x 10^{-3} S/cm, 6.5 x 10^{-2} S/cm and 2 x 10^{-2} S/cm, respectively. PANI -coated and doped sulfonated multiwalled carbon nanotube (i.e., PANI-c-MWNT-$(OSO_3H)n$) and (PANI-d-MWNT-$(OSO_3H)n$) nanocomposites, respectively were prepared by in situ polymerization method [98]**.**
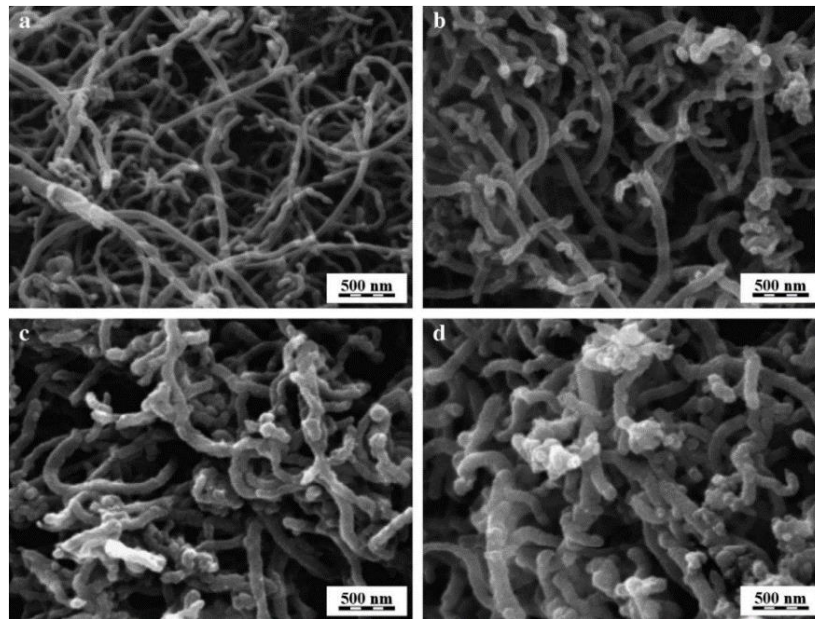
Figure 2.17: Original MWCNTs (a) and those coated with 50 wt% (b), 70 wt% (c) and 80 wt% PANI (d). [95]
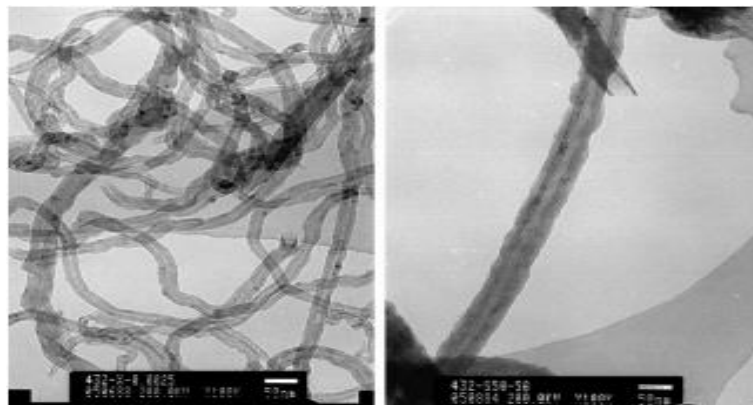
Figure 2.18: Original MWCNTs (left) and MWCNTs (50 wt%) after coating (right) with polyaniline at the same magnification. [95]

Figure 2.19a shows the diameter of the pure nanotube in the range of 10-100nm. The hollow core of nanotube and its crystalline nature can see in **figure 2.19b** and **figure 2.19c,** respectively. As aniline to MWCNTs-$(OSO_3H)n$ ratio was ≤ 1 (for example 1:2 or 1:1), the

prepared composites show the coating of PANI on the surface of MWCNTs-(OSO$_3$H)n (i.e., PANI-c-MWCNTs-(OSO$_3$H)n) (see **figure 2.19d and 2.19e**). The diffraction rings and spot in **figure 2.19f** reveals the characteristic of PANI "shell" and MWCNTs- (OSO$_3$H)n "core," respectively. The ratio of aniline to MWCNTs-(OSO$_3$H)n $\geq$ 2 (for example 2:1, 4:1 and 8:1) leads to the preparation of the composites via self-assembly process along with in-situ polymerization (**figure 2.19g and 2.19h**). It explained that the surface of PANI-d-MWNT-(OSO$_3$H)n was very rough compared to the PANI-c-MWNT-(OSO$_3$H)n nanocomposites.
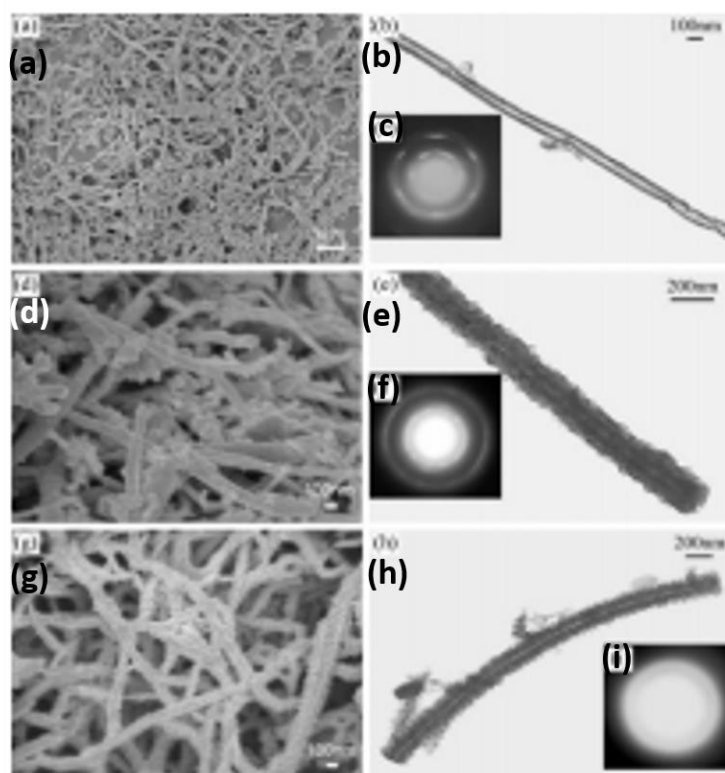
Figure 2.19: SEM images (a,d,g), TEM images (b,e,h) and electron diffraction patterns (c,f,i) of: a-c) MWNT-(OSO$_3$H)n; d-f) PANI-c-MWNT-(OSO$_3$H)n; g-i) PANI-d- MWNT-(OSO$_3$H)n nanotubes. [98]

The electron diffraction pattern of PANI-d-MWNT-(OSO$_3$H)n composites **(figure 2.19i)** displays the amorphous nature of composites. The electrical conductivity of PANI-c-MWNT-(OSO$_3$H)n and PANI-d-MWNT-(OSO$_3$H)n nanocomposites reported as 2.2 x 10^{-2} S/cm and 1.4 x 10^{-2} S/cm, respectively.

2.4.3 Interfacial Polymerization

Interfacial polymerization usually implemented in an organic/aqueous biphasic system with aniline monomer dissolved in an organic solvent followed by the addition of

oxidizing agent [99]. Usually, APS oxidant, dissolved in an aqueous acid solution [100, 101]. Interfacial polymerization is of two types,i.e., static (without stirring) and dynamic (with stirring). The preparation of PANI nanofibers highly desired through interfacial polymerization method. The reason behind that is reduced local dielectric constant of water at the organic/water interface would support the formation of phenazine nucleates at the interface. Huang *et al.* [102] also explained the reason for the development of fibers through interfacial polymerization. They observed organic phase eliminates an amount of aniline monomer from aqueous phase which promotes the stacking of nucleates over their random agglomeration. Jeon *et al.* [103] prepared the dispersion of carbon nanotube in the organic
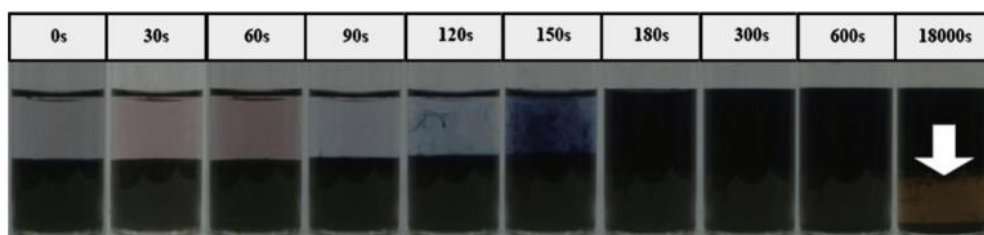
Figure 2.20: Photographs of reaction vials as a function of reaction time, the product in aqueous phase consists of PANI/PANI-g-MWCNTs mixture. The black residue at the bottom of organic phase identified as the unreacted NH$_2$-MWCNTs (white arrow). [103]
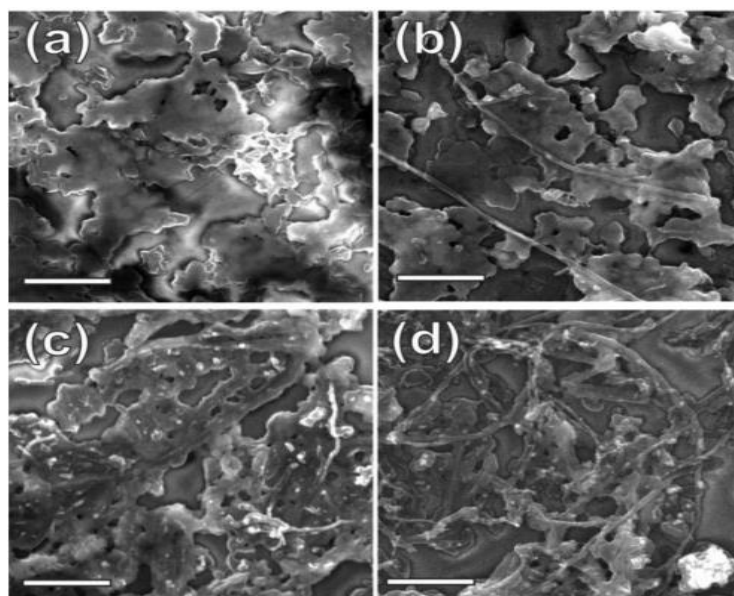
Figure 2.21: FEG-SEM images of the samples PANI (a), PANI + 0.25% CNT (b), PANI + 1% CNT (c), and PANI + 4% CNT (d). Scale bar is 1 μm. [104]

phase through static interfacial polymerization. By way of static polymerization taking place at the interface, PANI, and PANI-g-MWCNTs diffuse into the upper aqueous phase. **Figure**

2.20 shows static interfacial polymerization of aniline with respect to time. Salvatierra *et al.* [105] deposited a film of CNT-doped PANI nanocomposite over the glass substrate by interfacial polymerization method and studied the effect of CNT on the structure and conformation of polyaniline. They explained that carbon nanotubes bring vital modifications in the electronic structure of the polymer, resulting in a more polaronic organization. Mariano *et al.* also reported self- assembled films of CNT/PANI nanocomposites via using interfacial polymerization method [104]. They observed the granular morphology of PANI displays in **figure 2.21a.** The morphology of the films shows that at lower CNT (0.25 wt.%) content only rare tubes are detected (**figure 2.21b**). These tubes attractively distributed in the granular polymeric structure. PANI with 1 wt% CNT shows more discrete structures, where few tubes capped with a PANI layer (**figure 2.21c**). The CNT/PANI (4 wt. %) nanocomposite present large and plane structure with several CNTs (**figure 2.21d).** Consequently, the electrical properties of CNT-doped PANI films must depend on the size of PANI layer separating each CNT and the contact of filler with PANI matrix by the quantity of CNT. The electrical conductivity of these composites at low CNT concentration was the order of 10^{-7} S/cm. The slight change in electrical conductivity observed from 0.0 wt% to 0.25 wt% of CNT. The electrical conductivity of 4 wt% CNT with PANI matrix was approximately 0.06 S/cm.

2.4.4 Solution Mixing

This approach is very simple and efficient for the preparation of hybrid CNT/PANI nanocomposites. It involves the dispersion or dissolution of the nanotube with PANIeither in a same or different solvent [106]. The product obtained after the mixing of fillers and polymeric solution followed by drying treatment. Stirring is not sufficient condition for mixing of CNT in PANI matrix; a high power ultrasonic waves can also be used to emulsifying, crushing, and activating the particles. With this process, the aggregates and entanglement of CNTs effectively can broken which results in the easy dispersion. It has been reported the good dispersion of CNTs in polycarbonate matrix with ultrasonication at a frequency of 20 kHz for 10 minutes [107]. Ultrasonic waves and mechanical stirring play very vital role in the development of composites with an identical particle size. Li *et al.* [108] prepared the PANI nanofibers using irradiated ultrasonic polymerization with varying reaction temperature, ultrasonic power, and frequency of waves. The PANI prepared at higher frequencies showed higher purity as well as smooth surfaces than those at lower frequencies. The diameter and length of obtained PANI nanofibers were about 80 nm and 700

nm, respectively with ultrasonic power 250 W and frequency 50 kHz. Husin*et al.* [109] also reveals the formation of PANI nanofibers with ultrasonic polymerizations at a different frequency. They prepared the nanofibers at the frequency of 5-20 kHz and found the diameter of ~25 nm. Gajendran *et al.* [110] adopted solution mixing method for the preparation of CNT-doped polyaniline nanocomposites. The results obtained by mixing method reveals the favorable interaction between PANI and CNTs. The amount of filler used in PANI matrix controls their mechanical, conductive, and thermal properties. CNT/PANI composite synthesized via direct mixing (DM) mixing method and in situ polymerization also reported in the literature [111]. After that, three types of nanofibers for PANI, CNT/PANI, and DM-CNT/PANI fabricated via an electrospinning process. Authors compared the morphological feature of PANI, CNT/PANI, and DM-CNT/PANI composite. The fibers of DM-CNT (40 wt. %)/ PANI nanocomposites have a diameter about 50 nm which is less than that of PANI and CNT(40 wt%)/PANI nanocomposites fibers,i.e., 50-200 nm **(figure 2.22)**.The clear view of three types of nanofibers also shown with the TEM images (inset of **figure 2.22**).PANI
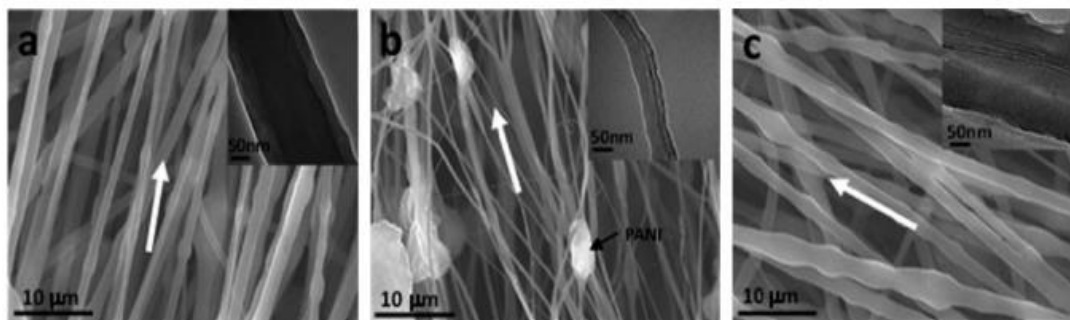
Figure 2.22: SEM images of the fiber mats of PANI (a), DM-CNT (40 wt.%) /PANI (b), and CNT(40 wt%)/PANI (c). The inserts are the TEM images of a single fiber. Arrows denote the alignment direction of fibers. [111]

particles segregated in DM-CNT/PANI composites, however in the case of CNT/PANI composites nanotubes were homogeneously covered by PANI and aligned in the direction parallel to the nanofibers axis. The electrical conductivity of CNT (40 wt %)/PANI nanocomposites fibers was about 17.1 S/cm which was ten times greater than the electrical conductivity of pure PANI. The direct value of electrical conductivity not reported for DM-CNT/PANI nanocomposite [111]

2.5 Properties of CNT/PANI Nanocomposites

2.5.1 Electrical Property of CNT/PANI Nanocomposites

The electrical conductivity and aspect ratio of CNT is high because of which it considered as exceptional candidates for the preparation of conducting composites. The incorporation of the conductive fillers in insulating polymer matrix gradually enhance the dielectric constant up to a critical volume fraction of the conductive filler. Beyond this critical volume fraction, the composite makes a transition from insulating to conducting nature. This transition is known as percolation threshold. According to classical percolation theory, the variation of electrical conductivity of nanocomposite beyond the percolation threshold can express by scaling law [94, 112].

$$\sigma_c = A.\,(\rho - \rho_c)^t \qquad\qquad (2.1)$$

where σ_c is the electrical conductivity of nanocomposite, A is a constant, ρ_c is the volume fraction of PANI at the percolation threshold. The symbol ρ is the volume fraction of filler near the percolation threshold, and t is the critical exponent which governs the scaling behavior in the region of ρ_c. **Equation (2.1)** is valid for both insulating as well as conducting matrix [94]. They reported electrical conductivity for pure PANI is about 0.17 S/cm. The level of electrical conductivity was increased to 0.22 S/cm to 3.32 S/cm for MWCNTs/PANI with 0.25 wt% to 8 wt% filler. The percolation threshold for MWCNTs/PANI nanocomposites is at 1 wt% MWCNTs. The filler content and its aspect ratio both are the important parameter to determine the electrical conductivity of the composite. CNT is an appropriate conducting filler to produce a low percolation threshold. Sandler *et al.*[113] reported the percolation threshold ranging from 0.0025 wt. % to several wt. % of filler. The percolation threshold for the electrical conductivity in CNT/polymer nanocomposites depends on polymer types [114], the degree of surface modification [72] of CNTs, aspect ratio [115], on dispersion [113], alignment [116], and composite processing methods [115]. It is well known that surface treated CNT generally, increase the dispersion of CNT in a polymer matrix which leads to enhancing the electrical conductivity of composites materials. There are some reports available on the functionalization of CNTs with an improved electrical conductivity of the composites [117]. Tamburri *et al.* [118] reported that the electrical conductivity of carboxylic (–COOH) functionalized SWNTs has higher than that of

untreated SWNTs. Aspect ratio plays a very important role in the percolation threshold of the polymer nanocomposites. Aspect ratio is defined as the ratio of the longest dimension to shortest dimension. Aspect ratio for planer fillers like graphene and graphite flakes is the ratio of lateral dimension to sheet thickness, whereas for rod-like nanostructures (such as carbon nanotubes and nanowires) is the ratio of thelength to its diameter. Fillers with higher aspect ratio percolate atlower concentration because of the formation of more efficient network with fewer contacts required to form a spanning cluster. Literature shows the electrical percolation threshold at 1wt.%, 0.1 wt.% and lower than 0.1 wt.% typical for CNT/polymer composites [119]. The conventional fillers such as carbon black used in matrix material found the percolation threshold between 3 and 15 wt. %. The range of percolation threshold can increased to 60 wt. % for metallic powders filler [115]. The size of filler affects the percolation threshold in the composites. In polypropylene-Cu composite small sizeCu particles shows the percolation threshold at lower volume percent than that of larger size filler [120]. Some researchers report the percolation threshold of MWCNTs filled polystyrene nanocomposites from 2 wt. % high-aspect ratio CNT grown in vertically aligned films was 0.1 to 0.5 wt.%. It was five times lesser than that for low aspect ratio industrially developed CNT-polymer nanocomposites; the achieved electrical conductivity with 2wt.% CNTs was 10^3 S/m [121]. The non-covalently functionalized SWCNT in PS matrix shows the percolation threshold at 0.045 wt. % with a maximum electrical conductivity of 6.89 S/m at 7wt. % of CNT. The similar route was also used for the preparation of PC/SWCNT nanocomposites and found that measured electrical conductivity increased to 4.81×10^2 S/m at 7 wt. % of nanotubes. The percolation threshold for this nanocomposites reached to 0.11 wt. % of SWCNT fillers. Sarvi*et al*. [122] reported PANI coated MWCNTs and uncoated MWCNTs dispersed in the matrix of polystyrene. They observed the electrical percolation threshold for PANI-coated MWCNTs and uncoated MWCNTs at 0.4 wt. % and 0.7 wt. %, respectively. The lower percolation threshold value in PANI-coated MWCNTs was due to the well dispersion of PANI-coated MWCNTs in a PS matrix. Many research group also studied the effect of morphology on the percolation threshold. They found that fibrous shape is the most favorable for achieving low percolation threshold [123, 124]. The shortcoming of fibrous shape filler is only the narrow smearing region. It is the region in between the onset and offset of percolation where electrical conductivity increases abruptly. George *et al*. [125] reported higher dielectric constant of the composite in the broad smearing region. To achieve the percolation value at lower filler concentration, the distribution of filler in the matrix should be uniform throughout the composite. The non-uniform distribution or formation of

aggregates disturbs the formation of a 3D path for charge carrier which leads the concentration of fillers toward higher sides [126].

2.5.2 Thermal Property of CNT/PANI Nanocomposites

Thermally stable polymer nanocomposites extensively used in automotive, aerospace industries, electrical and electronics applications. The aerospace industries are a major driving force for the advancement of new materials. Thermogravimetric analysis (TGA) is a very prominent technique used to know the thermal stability of nanocomposites. Among various composites, CNT-doped PANI nanocomposites because of thermal stability are widely used applications mentioned above. In general, the thermal stability of MWCNTs in the air is up to 650 °C and completely decompose beyond 750 °C. The first weight loss of emeraldine salt form of PANI (without considering the moisture) is due to the removal of dopant which converts emeraldine salt form of PANI to emeraldine base form. This step occurs at the same temperature range in air and nitrogen which means it is independent in the atmosphere [127]. Beyond this step, the major decomposition of PANI is taking place [128]. In an air atmosphere, PANI is completely decomposed at 700 °C however, in a nitrogen atmosphere, it converted into nitrogen-containing carbon [127]. With increasing the concentration of CNT fillers in the PANI matrix, the thermal stability of nanocomposites increased. The increase in thermal stability is due to the following reason.

a) The long conjugate π–π bond formed between PANI and MWCNTs
b) The existence of polymeric-filler interaction along with filler-filler interaction.

The degradation of emeraldine salt form of PANI with CNT nanocomposite in air atmosphere is complex because the loosed dopant in this atmosphere moderately overlaps with the degradation of the PANI backbone. To avoid the overlapping of dopant and getting a simplified interpretation of TGA data emeraldine salt is de-doped to emeraldine base before TGA measurement [129]. The volume contraction during the conversion of emeraldine salt into emeraldine base breaks the contact between MWCNTs fillers and PANI matrix. This contraction leads to lower the thermal stability of nanocomposites at a higher temperature. It also reported that volume contraction could be avoided by thermal deprotonation of thermally aged MWCNTs/EB nanocomposites at high temperature [130].

2.6 Applications

The conducting nature of PANI makes it suitable for many applications in multidisciplinary areas like conductive paint, conductive ink, conductive adhesive and electrostatic discharge (ESD) materials [131, 132]. To make the conductive paint on an industrial scale, DBSA-doped PANI commonly dispersed in the insulating poly(methyl methacrylate) (PMMA) matrix in an organic solvent [133]. The desired pattern can be obtained with inkjet cartridge loaded with the suspension or solution of conducting polymer. The conductive adhesive prepared with the dispersion of PANI as a filler in epoxy resin with different concentration as reported by Hino *et al.* [132]. The addition of doped PANI (10wt %) in the matrix of epoxy resin generates the electrical conductivity of the level of 10^{-1} S/cm. Wet spinning method is used to prepare the conducting textile fibers of high molecular weight PANI. The conducting fillers in insulating matrix avoid static charge generation for electrostatic discharge protection application [134]. Carbon nanotube doped PANI nanocomposites have great attention in numerous applications because of facile synthesis, easy processability. Another reason is the combination of various properties of CNT filler and matrix PANI which explains the synergistic effects in prepared nanocomposites. The properties of filler and PANI includes large surface area, high mechanical strength, high conductivity and exceptional case of doping by oxidation/ protonation, electrical conductivity respectively. The various application where CNT/PANI nanocomposites extensively used are as follows:

2.6.1 Actuators

Most advanced application of conducting polymers in the scientific community include actuators [135]. Actuators convert electrical energy into mechanical energy. The conducting polymer actuators are fully developed and demonstrate a solid-state actuating device to accelerate the commercial application. The bending operation of an actuator is comprising of the membrane and gold. Carbon nanotubes extensively used in actuators [136]. The excellent properties of CNTs like electronic, electrochemical and mechanical in PANI nanofibers leads to improve the electromechanical actuation [137]. The PANI and CNT have high actuation strain and high modulus, respectively, because of which nanocomposites display higher actuation strain in the range of 0.2–0.5% [138]. With the same objective, Yun *et al.* [139] reported the MWCNTs doped PANI nanocomposites coating for electroactive

paper actuators. The paper actuators were prepared using cellulose sheet coated with a thin electrode on its both sides. The electric field was applied to these electrodes, generating a bending displacement in a paper. The PANI and co-spun fibers of a chitosan hydrogel reveal electrochemical actuation responses. There are various advantages of electro-active actuator materials, for example, biodegradability, low price, dryness, low power consumption, actuation voltage and lightweight.

2.6.2 Sensors

A sensor is a device that detects and responds to some input (light, heat, motion, moisture, pressure, etc.) from the physical environment and converts it into a signal which can be read by an observer or by an instrument. Conducting polymers broadly used in the field of sensors, especially in the biological and chemical field [106]. The reason of wide interest is the interactions of these polymers with various analytes which may affect the redox and doping states of conducting polymers. The influenced state of these polymers leads to a change electrochemical potential, resistance, or current [140]. It is believed that conducting polymers are a good candidate for biological and chemical sensing, but their poor selectivity and low sensitivity are its short-coming and must be improved. The capability of PANI to change the color and electrical conductivity dopant make it useful in the field of the detector, sensor, and indicator [141, 142]. The limitations mentioned above can be overcome using various fillers in PANI matrices like metal and metal oxide particles, biological materials, metal salts, and carbon nanotubes. The reason for using these fillers is to alter the affinity of composite/nanocomposites, raise the chain mobility of PANI. The gas sensor improves its sensing characteristics in the presence of carbon nanotube with PANI. The addition of CNT in PANI increases its sensitivity. However, recovery times reduced. The network of the carbon nanotube is used as conductive and flexible electrodes to deposit the polyaniline via electrochemical method [143]. Sensors fabricated on Si surfaces with PANI/DNA composite nanowires established for the detection of HCl and NH_3. The outcomes revealed that the response time of prepared PANI/DNA composite nanowires to HCl and NH_3 was about 1s which was 100 times faster as compared to pure PANI nanofibers. The incorporation of metal oxide nanoparticle into PANI nanostructure spread their use in other gasses. Chemical polymerization route was also used to prepare the In_2O_3/PANI composite nanofibers for the detection of NO_2, CO, and H_2 gasses. The sensors based on In_2O_3 nanomaterial have a huge response to gasses mentioned above [144]. However, the operation temperature was

relatively high (100–350 ℃). Similarly, WO$_3$ doped PANI nanofibers composite based sensor also fabricated for the detection of H$_2$ gas, but its sensitivity was not superior as compared to In$_2$O$_3$ doped PANI nanofibers composite based sensors [145]. Dhand *et al.* fabricated SWCNT/PANI nanocomposites film on indium-tin-oxide (ITO) coated the glass. Co-immobilization of lipase and glycerol dehydrogenase were carried out through N-hydroxy succinimide and N-ethyl-N'-(3-dimethylaminopropyl) carbodiimide for triglyceride (tributyrin) sensing application. Biological molecule dopamine could identified with the modified electrode surface. The modification of electrode done with a thin layer of the highly perm-selective Nafion film and in situ polymerized CNT/poly(aniline boronic acid) composite [146]. Moreover, CNT based composite wrapping with DNA improves the electrochemical activity of the composite along with effective electrode surface area. Hence, dopamine binding taking place with highly dense boric acid which supports the sensitivity enhancement for dopamine detection. The improved selectivity and sensitivity of the sensors make it capable for the remedies of Parkinson's disease. Conducting polymers like PANI and PPy deposited on the thin film of CNT used as a conductive, transparent and flexible electrode for electrochemical sensor [143]. In the case of CNT/PANI nanocomposites, the variation of color of PANI with pH make it suitable for the optical sensor. The CNT/PPy and CNT/PANI devices might be applicable for solid state gas sensor or biosensor deposited on any shape of the surface that can be transparent and flexible.

2.6.3 EMI Shielding

Research extensively attracts EMI shielding materials because of their rapid proliferation of electronics and instrumentation in defense and commercial defense sectors [147].This phenomenon can be easily predictable by even a common man as flashes on the television screen and click heard on audio systems when a light is switched on. EMI also sources of some disease as insomnia; nervousness, symptoms of languidness and headache on exposure to electromagnetic waves.

Theory on shielding of electromagnetic interference

Once an electromagnetic wave permits through a shield, two phenomena are taking place,i.e., absorption and reflection. The energy which is not reflected and absorbed by the shield, but emerged out from the shield called residual energy. The electromagnetic waves

comprise of two essential part one is a magnetic field (H), and other is an electric field (E) (**figure 2.23**). The magnetic and electric fields are mutually perpendicular to each other, and the direction of wave propagation is at right angles to the plane comprising the two components. Wave impedance is the ratio of electric field to magnetic field, the intrinsic impedance of free space is 377 ohm. The near field shielding and far field shielding are the two regions involved in EMI shielding. The far field shielding is that region where the distance between the radiation source and the shield is larger than $\lambda/2\pi$ (where λ is the wavelength of the source). Electromagnetic plane wave theory applied for EMI shielding is in far field shielding region [148]. However, the region when the distance is less than $\lambda/2\pi$ called near field shielding and the concept centered on the involvement of electric and magnetic dipoles used for EMI shielding [149]. Shielding effectiveness (SE) is the ratio of the field before and after attenuation of the electric and magnetic field and can be stated as (**equation 2.2 and 2.3**).

$$SE = 20 \, log \, (E_I/E_T) \hspace{3cm} (2.2)$$

$$SE = 20 \, log \, (H_I/H_T) \hspace{3cm} (2.3)$$

Where E and H refer as electric and magnetic fields, respectively. The subscripts I and T denote to incident and transmitted waves, respectively. E measured in volts/m and H in amps/m. There are three primary mechanisms contributing to SE. Part of electromagnetic radiation absorbed within the shield material (A), part of the incident radiation reflected from the front surface of the shield (R), and part is reflected from the rear surface to the front (B), as exposed in **figure 2.24.** Hence, shielding effectiveness is the sum of all the three parts (**equation 2.4**). In last four decades, conducting polymers, PANI and PPy received great

$$SE = A + R + B \hspace{3cm} (2.4)$$

intention toward EMI shielding because of their corrosion resistance and light weight. The usual difficulties with intrinsically conductive polymers (ICP) are the lack of ability to process into useful articles. It is mainly true for PANI, which is known for its redox behavior, environmental stability and has adequate electronic conductivity. The good electrical conductivity of the material is required to achieve the excellent EMI shielding efficiency. Mostly, Metals used for EMI shielding applications, but due to their

heavyweight, natural corrosion, and uneconomic processing, it gets replaced by polymeric materials. The electrical conductivity required for electrostatic dissipating are approximately 10^{-5}-10^{-9} S/cm and should be greater than 10^{-4} S/cm for electromagnetic shielding applications [150]. The SE depends upon the thickness of conducting coating, type, level of doping and time interval given for each measurement in the point-by-point method. Lee *et al.* [151] stated the EMI shielding efficiency of the mixtures of PANI and conducting fillers such as graphite, carbon black and silver in the frequency range from 10 MHz to 1 GHz. They reported the shielding efficiency for graphite/PANI and Silver/PANI are 27 and 46 dB respectively, however, PANI without mixing of filler was merely 17dB. SE increases with increasing direct current electrical conductivity. They also saying that SE in contrast to
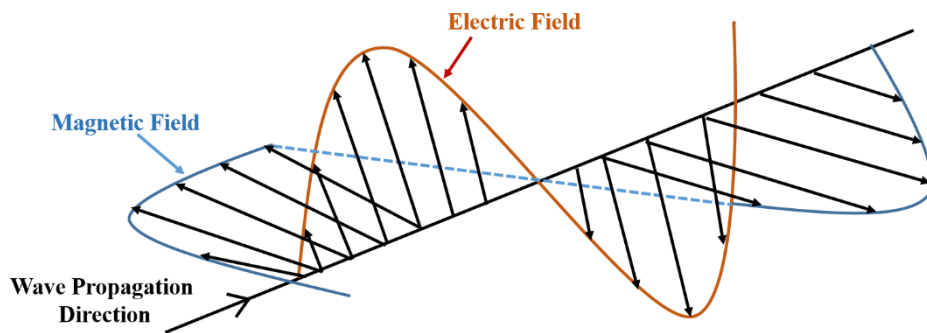
Figure 2.23: Electromagnetic radiation vector
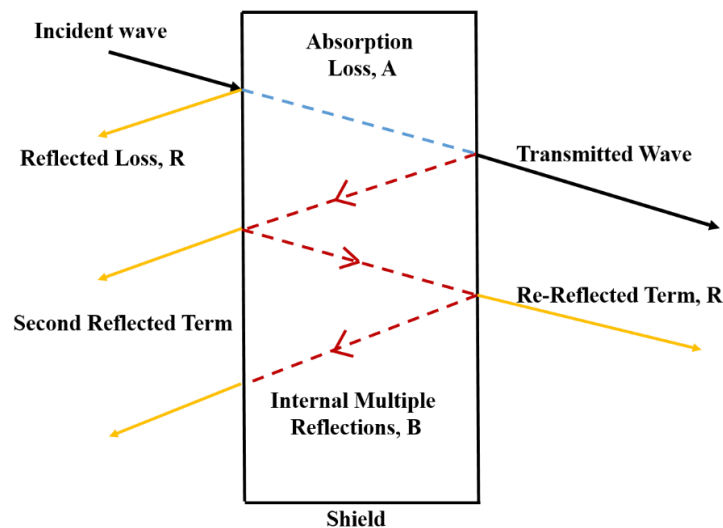
Figure 2.24: Attenuation of an electromagnetic wave by a shielding material

electromagnetic radiation increases through chemical doping and mixing with the addition of conducting filler. Koul *et al.*[152] used organic dopant like dodecyl benzene sulfonate and p-toluene sulfonate to prepare the PANI blend with acrylonitrile-butadiene-styrene (ABS) and measured their EMI/ESD response at 101 GHz. It was found that loading of PANI in (PAn/ABS: 10:90) composite illustrate SE of 11dB. 5% loading of PANI in ABS provides an SE of the order of 6dB, this order of SE is not sufficient to control the interference in the material having a thickness in the mm range but can use for the dissipation of static charge. Saini *et al*. studied the microwave absorption properties of PANI/CNT nanocomposite prepared via in situ polymerization [153]. The synergistic effect of CNT in PANI matrix shows that the conductivity of CNT/PANI nanocomposites was higher compared to neat PANI. These nanocomposites can apply for EMI shielding in the Ku-band,i.e., 12.4–18.0 GHz with the shielding effectiveness of −27.5–39.2 dB. Makeiff *et al.* [154] reported the composite of PANI-pTsA (*para*-toluene sulfonic acid)-coated MWCNTs and PANI-pTsA or MWNTs with an insulating polymer. They measured the microwave absorption (at X-band frequencies (8–12 GHz) of these composites and described that composites prepared with the mechanical mixing of separate synthetic PANI-pTsA and non-coated MWNT are good absorbers, having stronger absorption as compared to the composite of PANI-pTsA or MWNTs. Han *et al.* [155] reported the estimated EMI SE for CNT-doped polycarbonate (PC) in the range of 1.54 – 14.26 dB. They calculated the EMI SE both experimentally and theoretically and compared the data. Based on the EMI shielding theory (far-field shielding), it is observed that EMI SE increases with increasing the electrical conductivity (σ) of shielding material (**see equation2.5**). The electrical conductivity obtained for these composites were in the order of 2.06 x 10^{-4} S/cm.

$$EMI\ SE = 20\ log\ [1\ + (1/2)\sigma.L.Z_o] \qquad (2.5)$$

where σ is the conductivity of nanocomposite pellets, L is the thickness of the pellets and Z_o is the free space impedance (constant: 377 S^{-1}). Ghasemi *et al.*[156] also reported the polystyrene/polyaniline (PS/PANI) composites with EMI SE up to 8dB. Aggregates of PANI used for the preparation of composite showed the value of electrical conductivity about 3.4×10^{-2} S/cm.

2.6.4 Electronic Nanodevices

The versatile properties of conducting polymers like electrical conductivity, mechanical flexibility, and low-cost availability widely attracted for the fabrication of electronics devices. Among one dimensional, two dimensional and three-dimensional structures of conducting polymers one-dimensional nanostructured (like nanofibers, nanorods, nanotubes, and nanowires) are the excellent candidates for nanoelectronic devices. The use of various fillers like metals, carbon nanomaterials, semiconductors and even insulating polymers in conducting polymers matrix facilitate the formation of the one-dimensional nanocomposite. It believed that one-dimensional nanocomposite has good electrical conductivity than their 2D/3D counterparts or induce efficient electron transfer. The availability of free charge carriers makes them suitable for various electronic devices like transistors, memory, light emitting diodes, and photovoltaic devices [157-159]. Gold-doped-PANI composites extremely used by some researchers for the fabrication of memory devices [160].

2.6.5 Fuel Cell

In the recent decade, the energy conversion and storage attract the intention scientific society toward itself. Fuel cells are the most promising applications for electric vehicles; it converts the chemical energy of a fuel directly into electricity by electrochemical reactions. The advantages of fuel cell-like environment friendliness, fuel portability, high energy conversion efficiency and direct methanol fuel cells (DMFCs) has a great impact in the area of energy applications [161]. In the current scenario, carbon nanofibers and carbon nanotubes are the decent candidate for Pt nanoparticle filling for the reason of their large surface area and superior electrical conductivity. The 1D nanostructure of conducting polymer make it a more supportive for electrocatalyst [66, 162, 163]. The catalytic activity CNT/PANI nanocomposite is higher than that of pure PANI for formaldehyde [164], methanol [165], and formic acid [166]. Manish *et al*.[167] reported MWCNTs-coated-PANI nanocomposite which altered glassy carbon electrode for oxygen reduction and improvement in the amperometric current. Researchers put their efforts on the cathode modification and the optimization of bacterial inoculums to increase the power output of microbial fuel cells [168]. CNT filled PANI nanocomposites broadly used as an anode material meant for high power microbial fuel cells [169, 170]. The reason for using CNT is that it has high surface area and electrical

conductivity which increase the electrochemical activity of the anode reaction because of which high power output is there. The host PANI provides the electron transfer through its matrix, as PANI is a good electron donor.

2.6.6 Supercapacitors

A lot of efforts have been dedicated to the fabrication of nanostructured conducting polymer nanocomposites as electrode materials in energy storage devices such as supercapacitors [171]. It was predicted that the synergistic action of an individual constituent in the nanocomposites could expressively increase the performance of the energy devices. The supercapacitors, also named as ultracapacitors or electrochemical capacitors have the capacitance of 10^5 times higher as compared to the normal capacitors. Supercapacitors can work significantly at higher specific power than batteries due to the cyclic redox capability. The charge storage in supercapacitors depends upon the ion absorption of the electrically binary layer on the electrode and electrolyte interface for electrochemical double layer capacitors. [7, 172] In recent time, various fillers like TiO_2, WO_3, graphene, titania nanotubes, SWCNT, MWCNTs,etc.are widely used in the matrix of PANI for supercapacitors application. Singu et al. [173] used TiO_2 and MWCNTs as fillers in PANI to improve the pseudo-capacitance and cycle stability of pure PANI. They prepared ternary PANI–MWNTs–TiO_2 composite via in-situ chemical polymerization and exposed that specific capacitance of MWCNTs (30 Fg^{-1}) and PANI (210 Fg^{-1}) electrodes increased to 270 Fg^{-1} in PANI–MWNTs–TiO_2 composites. It shows that PANI–MWNTs–TiO_2 composites has excellent cycling stability and good rate capability. Yuksel et al. [174] also fabricated thin film supercapacitor electrodes invented of binder-free single-walled carbon nanotube (SWCNT) thin films deposited onto glass substrates. They used pseudo-capacitive PANI and WO_3 to deposits through electro-deposition on the SWNT thin films. The synergistic and complementary effect of SWNTs and WO_3 & PANI increase the electrochemical energy storage capacity. A specific capacitance of ternary nanocomposites was 28.5 mF/cm^2 acquired at a current density of 0.13 mA/cm^2. Yu et al. [175] developed the micro-spherical PANI/graphene composites prepared using sheet-like graphene oxide/PANI (GO/PANI) composites as raw materials. The results revealed that because of the special structure the electrochemical capacitance of micro-spherical graphene/PANI composite obtained as 596.2 and 447.5 Fg^{-1} at a current density of 0.5 and 20 Ag^{-1}, respectively, representing superior rate capability. Some researchers align the MWCNTs in the matrix of PANI via electro-

deposition process [176]. The specific capacitance of these electrically conductive composite films obtained about 233 F/g at a current density of 1 A/g. It also reported that the cyclic stability of these unique supercapacitors were much high.

CHAPTER THREE

Methodology

In this chapter, the information about the materials and purchased along with methods that adopted for the synthesis of PANIs (with and without solvent), functionalization of MWCNTs and preparation of hybrid MWCNTs/PANI nanocomposites given in details. The methodology adopted for the synthesis of self-standing film of PANI also explained in detail. Details about the characterization techniques like density kit, XRD, FT-IR, Raman spectroscopy, I-V measurement, SEM, TEM, TGA and UV-Vis spectroscopy used for reported materials also given in this chapter.

==

Chemical oxidative polymerization and solid state oxidative polymerization methods were used to prepare the PANIs with solvent (PANI 1) and without solvent (PANI 2), respectively. The PANIsalso prepared under vacuum drying conditions namely, PANI 1VD and PANI 2VD.Among all prepared PANIs, PANI 1VD selected as a matrix for further preparing hybrid nanocomposites using functionalized MWCNTs as a filler material. PANI 1VD also used for the synthesis of self-standing film of non-protonated and protonated (with hydrochloric acid) PANI system namely PANI A and PANI B, respectively.

3.1 Materials

We select PANI as a matrix materials. The conducting MWCNTs were used as a filler in dual morphology (fibrillar and granular) PANI matrix. Before using, functionalization of as- received MWCNTs were carried out to for good dispersion in PANI matrix. The conducting filler was used to enhance the level of electrical conductivity of dual morphology PANI composites.

The following chemical used to prepare all samples; Aniline ($C_6H_5NH_2$; 99%purity, Merck) as a monomer double distilled before use. Ammonium peroxodisulfate [$(NH_4)_2S_2O_8$or APS; 98% purity, Merck)] were used as an oxidant.To prepare PANI, deionized water was used as a solvent.Sulfuric acid (H_2SO_4; purity 98%, Merck make), Nitric acid (HNO_3, Fisher Scientific;Qualigens make) and hydrochloric acid (HCl; 37% purity, Merck) as a dopant. The 1-methyl-2-pyrrolidinone (NMP) (99%purity, Alfa Aesar), heptamethyleneimine (HPMI) (99% purity, Alfa Aesar), 1,3-Dimethyl-3,4,5,6-tetrahydro-2(1H)-pyrimidinone (DMPU) (99% purity, Alfa Aesar),dimethyl sulphoxide (DMSO) (C_2H_6OS, purity >99%, Merck make) were used as solvent. The MWCNTs (density 2.1 g/cc) purchased from Sigma-Aldrich. For good dispersion, the surface treatment of pristine MWCNTs was done by oxidative treatment as reported by Z. Zhao *et al*. According to the manufacturer, the diameter and length of MWCNTs were (16-20 nm) and (3-8 µm) respectively.

3.2 Synthesis of Polyaniline

PANI was synthesized with and without solvent under different drying conditions. APS used as an oxidizing agent. The oxidation potential of APS oxidant was (2.01 V); [63]. Due to its higher oxidation potential, this, in turn, accelerated the polymerization mechanism. A previous study [177] revealed that PANI prepared with APS oxidant (with solvent) exhibited a granular morphology.

3.2.1 With Solvent

PANI synthesized in the presence of solvent by the chemical polymerization of the aniline monomer. A solution of APS (4.564 g) prepared in 200 ml of 2.5M HCl (**figure 3.1**). Distilled aniline (4 ml) was added to the previous solution for complete solubility of the monomer and stirred vigorously in a chemical bath kept below 5 ^{0}C. A volume of 2 ml of aniline was added dropwise (one drop every 10 s), whereas the remaining 2 ml added at once. The pH of the solution maintained in acidic medium (pH < 3). The solution stirred in an airtight flask for another 3 h, and after that, it left for 10–12 h at room temperature to completely polymerize aniline [178]. During polymerization, the color of the solution gradually turned green. The solution was filtered and washed with deionized water to remove the unreacted soluble component, with a 0.1 M HCl solution to eliminate the unreacted aniline monomer and finally with acetone to remove water. The precipitate was dried separately in the air (PANI 1) and a vacuum oven at 90 ^{0}C (PANI 1VD) for 18 h.

3.2.2 Without Solvent

Solid state oxidative polymerization can be used for the synthesis of PANI without solvent. First, distilled aniline (4 ml) poured into a porcelain mortar and HCl (2.4 ml) was added dropwise followed by simultaneous grinding (a white paste formed during this process) for 10 min at room temperature **(figure 3.2).** Subsequently, fine APS powder (11.409 g) was added slowly (to prevent overheating due to the highly exothermic reaction) [179]. After the addition of APS, the color of the paste changed from white to green; this confirmed the doping of HCl. This paste transferred into a 2-L beaker containing a solution of acetone, ethanol, and deionized water in a 1:1:8 ratio and left for 1h. The previous solution was washed with deionized water, acetone, and ethanol, respectively, until the brown filtrate became colorless, as also reported by Tantawy *et al*. [180]. The obtained product was dried separately in air (PANI 2) and, after that, in a vacuum oven at 90 ^{0}C (PANI 2VD) for 18 h.
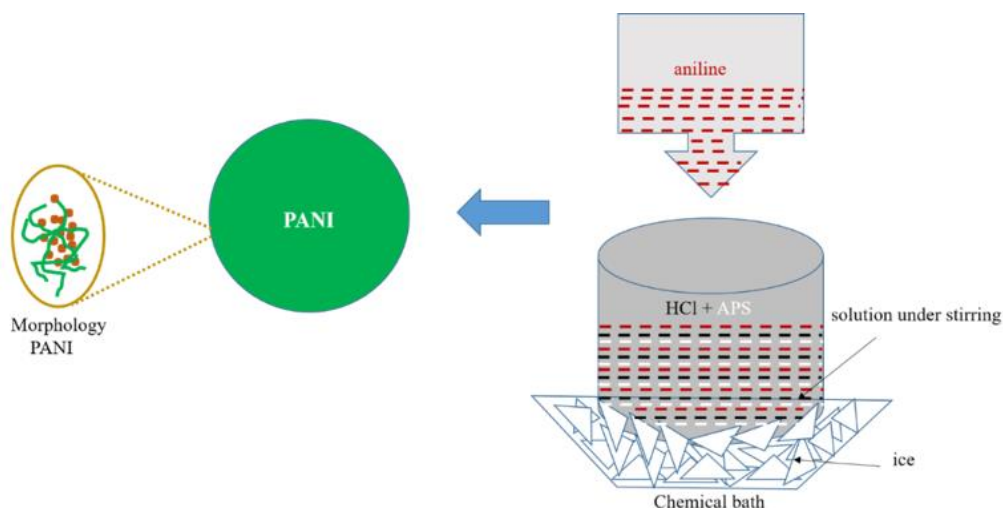
Figure 3.1: Schematic of preparation of PANI with solvent
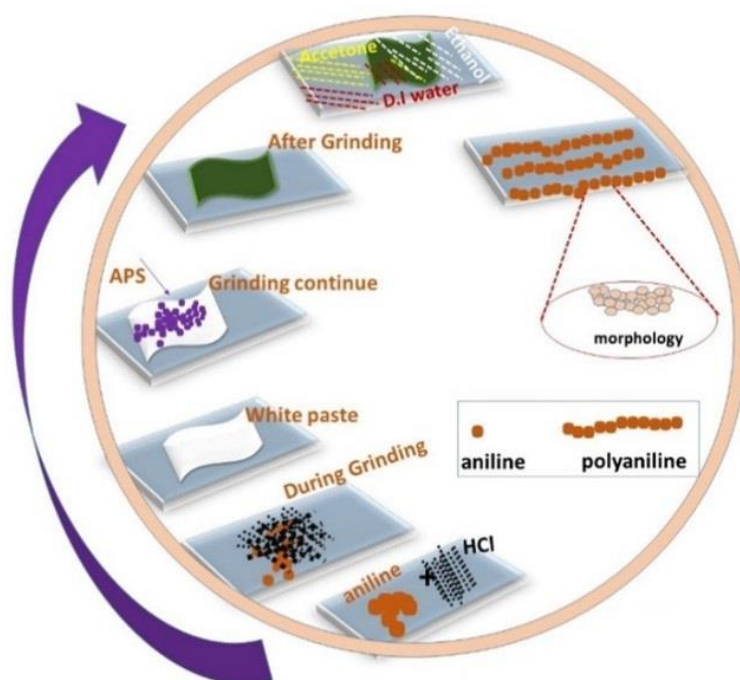
Figure 3.2: Schematic of preparation of PANI without solvent

Among all prepared PANIs, PANI 1VD selected as a matrix for further preparing hybrid nanocomposites using functionalized MWCNTs as a filler material. PANI 1VD also used for the synthesis of self-standing film of non-protonated and protonated (with hydrochloric acid) PANI system namely PANI A and PANI B respectively.

3.3 Functionalization of Pristine MWCNTs

The chemical functionalization of pristine MWCNTs has been carried out using oxidative treatment. CNT has the weak van der Wall forces because of which it strongly agglomerated. The creation of an additional functional group on its surface diminishes the van der Wall forces due to the existence of repulsive forces. The reduction in van der Wall forces, increase its dispersion in the nanocomposite materials. To create identical functionality by oxidative treatment, around 1g pristine MWCNTs was ultrasonicated in a mixture of concentrated H_2SO_4 and HNO_3 (3:1, 60ml and 20ml, respectively) for 2h as reported in the literature [181] (**figure 3.3**). After that, the dispersion refluxed in a triple-neck flask (volume 1.0 L), equipped with an external heater, control thermocouple, magnetic stirrer and condenser under vigorous stirring at 80 °C for 60 minutes. The suspension was kept for some time until it gets cooled. After acid treatment, above acidic suspension of MWCNTs slowly added into the deionized water (to avoid the excess exothermic reaction). The above solution was filtered through centrifuge process, washed the suspension thoroughly with deionized water (this process was repeated several times until neutral pH). The collected suspension dried in air, and after that, the dried powder was kept in vacuum oven (-70Kpa) overnight at 60°C. The functionalized MWCNTs, with acid treatment, were assigned as COOH-MWCNTs (f-MWCNTs).

3.4 Nanocomposites Preparation

Initially, different weight percent of functionalized MWCNTs (f-MWCNTs) was ultrasonicated in 10ml DMSO solvent for 1h. After that, 0.5g of PANI added during ultrasonication followed by constant stirring for 2h at room temperature to ensure complete mixing. During solution processing, hydrophobic chains of polymer attached to the surface of individual f-MWCNTs due to hydrophobic-hydrophobic interactions. The surface treated nanotubes with –COOH group by the chemical treatment enhance the dispersion of nanotubes in PANI matrix. A carbonyl is a hydrophilic group but polyaniline and nanotubes both have hydrophobic benzene rings. The presence of benzene ring in PANI and nanotubes leads to enhance the hydrophobic interactions [182].The obtained composite was filtered and washed

Table 3.1. Weight and volume percentages of the f-MWCNTs filler in PANI matrix

Sr. No.	Weight%	Volume%
1	0	0.0
2	0.25	0.1
3	0.5	0.3
4	1.0	0.6
5	1.5	0.9
6	2.0	1.3
7	3.0	1.9
8	5.0	3.3
9	10.0	6.7
10	20.0	13.9
11	30.0	21.0

with DI water and acetone to remove unreacted soluble components and water molecules. The product was subsequently vacuum-dried (-70 Kpa) in the oven at 90℃ for 18h. Composites containing 0.1, 0.3, 0.6, 0.9, 1.3, 1.9, 3.3, 6.7, 13.9 and 21 vol. % of f-MWCNTs were prepared. The volume percent of f-MWCNTs (**table 3.1**) for selected weight percent in PANI matrix was determined from the relation given as [183] (**equation 3.1**).

$$V_f = {W_f}\Big/{[W_f + (1 - W_f) \times (\rho_f/\rho_m)]} \tag{3.1}$$

where V_f the volume fraction of filler, W_f is the weight fraction of filler; ρ_f is the density of the filler, and ρ_m is the density of the PANI matrix.

3.5 Preparation of PANI Films

The self-standing PANI films were prepared via solution casting method. Initially, 0.1 gm of PANI 1VD powder was mixed with 0.1 ml of HPMI in a teflon vial for 10 minutes. With the addition of HPMI, the color of the PANI changed to blue which indicates that the emeraldine salt form of PANI converted to the emeraldine base form. After that, 1.35 ml of
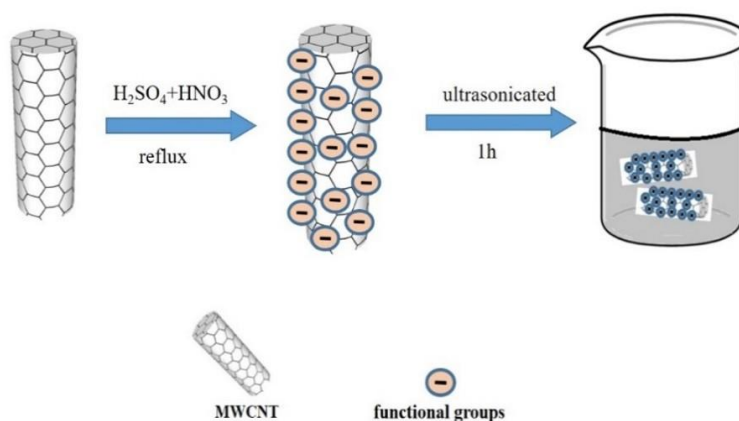
Figure 3.3: Schematic of functionalization of pristine MWCNTs
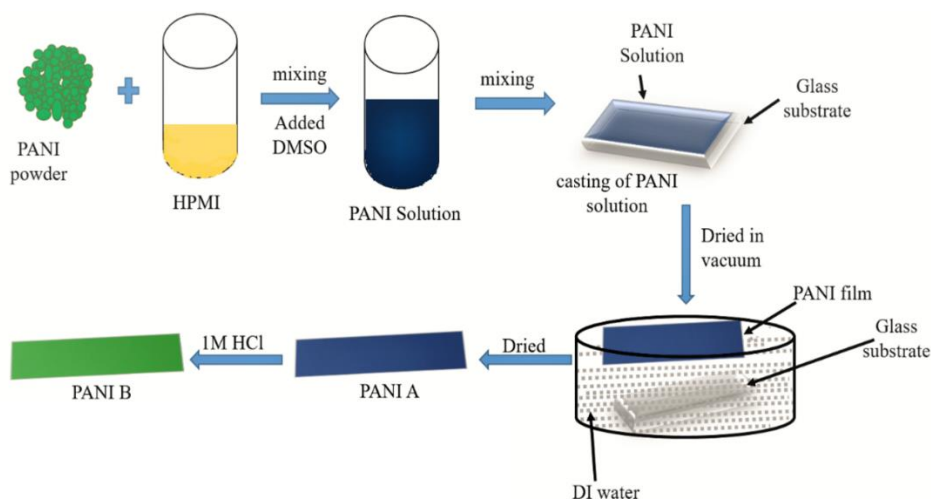
Figure 3.4: Preparation of self-standing film of PANI A and PANI B

DMPU solvent was added to above mixture and stirred mildly for 30 minutes to disperse the visible solid particle of PANI. After that, PANI solution was filtered through the cotton plug followed by casting on a glass substrate and put in the oven at 60 ℃ for two days. It was found that the color of the film turned to green. To detach the dried film from the glass substrate, it immersed into the water container for overnight. The exchange of water with the solvent was taking place. Previous water was changed with a fresh one and keep the film again for the next 4 hour to ensure the complete removal of residual of NMP and HPMI. The obtained film was in blue color which indicates the formation of emeraldine base form of PANI (**figure 3.4**) and dry it in air for one hour. To reduce the chance of bending sandwich self-standing PANI film in between two Kim Wipes under the load of 5 kg for one day. The

obtained film in blue color leveled as PANI A. Afterward, the self-standing film was protonated with 1M HCl. The color of the film turned to green which shows the emeraldine salt form of PANI. Dried it in the air for one h and sandwich between two Kim Wipes under the load of 5 kg for one day; the obtained film labeled as PANI B.

3.6 Characterizations of PANI (powder and film) and PANI based nanocomposites

Many characterization techniques were used to analyze filler component, matrix, and hybrid composites/nanocomposites. The used techniques discussed as follows in subsequent paragraphs.

3.6.1 Density Determination

The experimental density (ρ_{exp}) of hybrid nanocomposites were measured using density kit (Mettler Toledo, ME-DNY-4) according to **equation 3.2** based on Archimedes principle. The theoretical density(ρ_{th}) of hybrid nanocomposites was calculated using the rule of mixture (ROM) **equation 3.3**: [184]

$$\rho_{exp} = [A/A - B\,(\rho_o - \rho_L) + \rho_L] \tag{3.2}$$

$$\boldsymbol{\rho_{th} = \rho_m \times \left(1 - V_f\right) + \rho_f \times V_f} \tag{3.3}$$

where A and B is the weight of nanocomposites pellet in the air and distilled water medium, respectively.ρ_o and ρ_L are the density of the distilled water (i.e. 0.9967 gcm^{-3}) and density of air (i.e., 0.0012 g cm^{-3}) respectively. ρ_m and ρ_f are the densities of PANI matrix and filler, respectively. V_f is the volume fraction of the filler. After preparation of hybrid nanocomposites, further characterizations has done.

3.6.2 X-ray Diffractometry (XRD)

Information related to the crystallinity in the samples (PANI 1, PANI 1VD, PANI 2, PANI 2VD, hybrid MWCNTs/PANI nanocomposites, PANI A and PANI B) collected with the help of X-ray Diffractometry (XRD; PaNalytical X'Pert Pro, Cu Kα radiation, wavelength = 1.54 Å). The XRD data collected in the 2θ range from 10 to 60°; step size 0.02°

with a scan rate of 0.7s. From XRD pattern, the total area could divide into crystalline and amorphous components. The degree of crystallinity (X_c) was determined as the ratio of the crystalline area to the total area, as indicated in **equation (3.4)**:

$$X_c(\%) = [A_c/(A_c + A_a)] \times 100 \qquad (3.4)$$

where A_c is the area of the crystalline phase, and A_a is the area of the amorphous phase.

3.6.3 Fourier Transform Infrared (FTIR) Spectroscopy

The bonding characteristics of all samples which include (PANI 1, PANI 1VD, PANI 2, PANI 2VD, hybrid MWCNTs/PANI nanocomposites, PANI A and PANI B) were studied with Fourier transform infrared (FTIR) spectroscopy (Perkin Elmer). Random sample of PANI has been selected for the measurements. PANI in the form of powder was mixed with vacuum dried KBr powder. The mixed powder was compressed using hydraulic press for FTIR measurement.

3.6.4 Raman Spectroscopy

Raman spectroscopy was carried out to characterize pristine MWCNTs and f-MWCNTs to know the disorders in functionalization of MWCNTs. Raman spectrometer STR 500 Airix equipped with a single grating and an electrically cooled CCD detector used for this purpose. Excitation was at 532 nm from a solid state laser.

3.6.5 Scanning Electron Microscopy (SEM)

Scanning electron microscopy (SEM) measurements were carried out under FESEM (Nano 450, FEI). The cross-sectional images of the PANI and f-MWCNTs filled PANI nanocomposites were taken at 5000-X, 25000-X and 50000-X. For good quality SEM images, the sample should be electrically conductive. As prepared PANI was conducting in nature. It was directly used in the holder in the form of pellets (fractured surfaces).

3.6.6 Transmission Electron Microscopy (TEM)

To know the internal structural information of matrix material, functionality of filler material and nanocomposite it is very important technique. The morphology of PANI, CNT and

hybrid PANI nanocomposites were investigated by transmission electron microscopy (TEM) and high-resolution TEM (HRTEM) [FEI: TECNAI G^2 operated at 200kV]. Samples for TEM study were prepared by dispensing a small amount material in DMSO; a single drop of the suspension dropped on a 300 mesh carbon coated copper grid with the help of micropipette. To dry the copper grid keep it for overnight and then next day used under TEM. The high-resolution mode of TEM (HRTEM) was used to investigate the characteristic features of pristine and functionalized carbon nanotubes.

3.6.7 Thermogravimetric Analysis (TGA)

The thermal stability of the samples were examined using a thermogravimetric analyzer (TGA) STA 6000, Perkin Elmer). The operation was taken under nitrogen gas with a flow rate of 10 ml/min and a heating rate of 10°C/min.

3.6.8 Ultra Violet-Visible (UV-Vis) Spectroscopy

The absorption spectra of matrix material were recorded using ultraviolet–visible spectroscopy (C60, Agilent Technologies, 300–900 nm). The samples were prepared in a 1-methyl-2-pyrrolidinone (NMP) solvent for the absorption study. The purpose was to know the presence of benzenoid and quinoid rings in PANI.

3.6.9 Current-Voltage Measurements

For the electrical measurements, pure PANI pellets were prepared with 2mm thickness whereas PANI/CNTs nano-composites pellets were prepared with 1mm thickness. In both the conditions, the diameter was 13mm. In case of self-standing film of PANI, the thickness of prepared film was 36 micron. The DC electrical resistance of PANI pellet, PANI/CNTs nano-composites pellets and PANI films were measured using electrometer (2601B, Keithley). The silver paste applied on the cross-sectional faces of the pellets prior the electrical measurements. Standard two-probe and four-probe method used for this measurement. In case of two probe methods, pellets were sandwich between two electrodes and for four probes the distance between the probes was 0.2 cm. The **equations 3.5 and 3.6** were used to calculate the DC electrical conductivity of PANI and f-MWCNTs filled PANI

composites pellets. The electrical conductivity of self-standing PANI films were calculated using **equation 3.6 and 3.7.**

$$\rho = RA/L \qquad (3.5)$$

$$\sigma = 1/\rho \qquad (3.6)$$

$$\rho = 4.5324 \times w \times \frac{V}{I} \qquad (3.7)$$

where ρ is the resistivity of the PANI pellet and PANI film, R is the resistance of the PANI pellet; A is the area of the pellet, L is the thickness of the PANI pellet and σ is the conductivity. w , V and I is the thickness of PANI films, voltage and current, respectively.

3.6.10 Estimated Far-Field EMI Shielding

The estimated far-field EMI shielding efficiency of f-MWCNTs filled PANI nanocomposites was calculated using equation **(3.8)**

$$EMI\ SE = 20\ log\ [1\ +\ (1/2)\sigma.L.Z_o] \qquad (3.8)$$

where σ is the conductivity of nanocomposite pellets, L is the thickness of the pellets and Z_o is the free space impedance (constant: 377 S^{-1}).
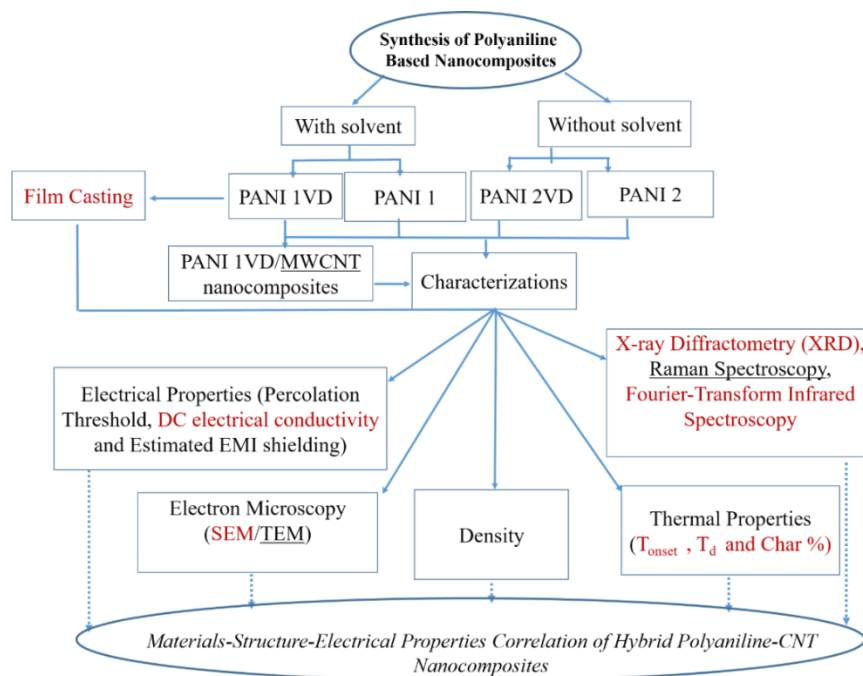
Figure 3.5: Flow diagram showing methodology for preparation and characterizations of PANI and PANI-based nanocomposites

The methodology adopted in research work summarized with flow diagram (**figure 3.5).**

CHAPTER FOUR

PANI Characterizations

The present chapter has given detail about the structural, electrical, morphological, thermal and optical study of PANI 1, PANI 1VD, PANI 2and PANI 2VD. XRD results showed that PANI prepared with solvent has more crystallinity than that of without solvent. FTIR results confirmed the presence of dopant in the air and vacuumdrying conditions. The direct current electrical conductivity of PANIs prepared with solvent is higher as compared to the without solvent due to mixed (granular and fibrillar) morphology. The growth mechanism of PANI nanofibers and granular structure along with morphology of PANI changed from one-dimensional to granular shape also explained in this chapter.

===

4.1 PANI with and without Solvent

The prepared PANIs samples were characterized using XRD, FTIR, SEM, TEM, UV-Vis and TGA techniques. Electrical resistance of all samples were measured with an electrometer. The effect of drying conditions on the DC electrical conductivity of PANI also investigated in detail.

4.2 Density Determination

The experimental densities of PANI 1, PANI 2, PANI 1VD, and PANI 2VD were found to be 1.327, 1.331, 1.361, and 1.335 g/cm³, respectively. These densities were very close to the density of the commercially available PANI (i.e., 1.36 g/cm³). The density of the vacuum-dried PANI 2VD was slightly higher than that of the air dried PANI 2. However, the higher density of PANI 1VD compared to PANI 1 may have been due to the removal of defects and free volume and similarly for PANI 1VD and PANI 1. Another reason may have been the good ordering of the polymeric chain and the change in the molecular weight of the polymers processed under different conditions. The molecular weight of PANI 1 prepared in solvent could be on the higher side because of the presence of air, moisture, and solvent. On vacuum treatment, the PANI prepared below 5 °C (having high molecular weight) has released air and moisture which could lead to an enhancement in the density. It reported that high-molecular-weight PANI could achieve when it prepared below room temperature [185].

4.3 Structural Study and Crystallinity Determination

The analysis of XRD patterns (**figure 4.1**) confirmed the formation of PANI and the percent crystallinity. The three main peaks observed at 2θ values of 14.2, 20.2, and 25.2° correspond to (010), (100), and (110) crystal planes (JCPDS 00-060-1167) of PANI salt [180]. Peaks of relatively lower intensity at 27.3 and 30° also observed in PANI 1 and PANI 1VD. It was evident from the XRD data that PANI prepared with a solvent had a greater
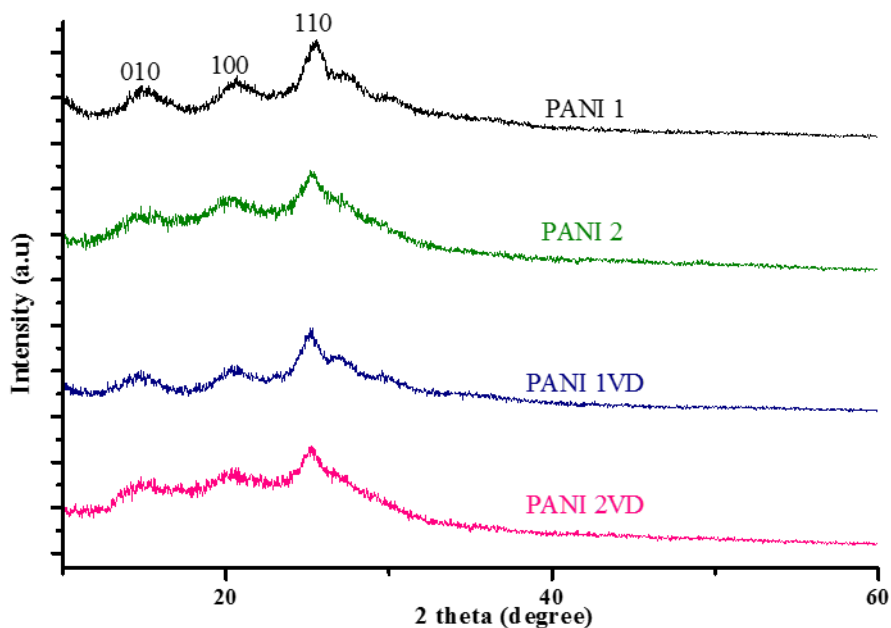
Figure 4.1: XRD patterns of PANI 1, PANI 1VD, PANI 2, and PANI 2VD.

extent of crystallinity. This may have been due to the orientation of polymeric chains during solution evaporation [186] this, in turn, produced larger crystalline domains embedded in the amorphous region. We found that the crystallinity of PANI decreased slightly during the vacuum drying treatment. The percentage crystallinity values for PANI 1, PANI 1VD, PANI 2, and PANI 2VD calculated as approximately 45, 38, 20, and 15, respectively. It was the
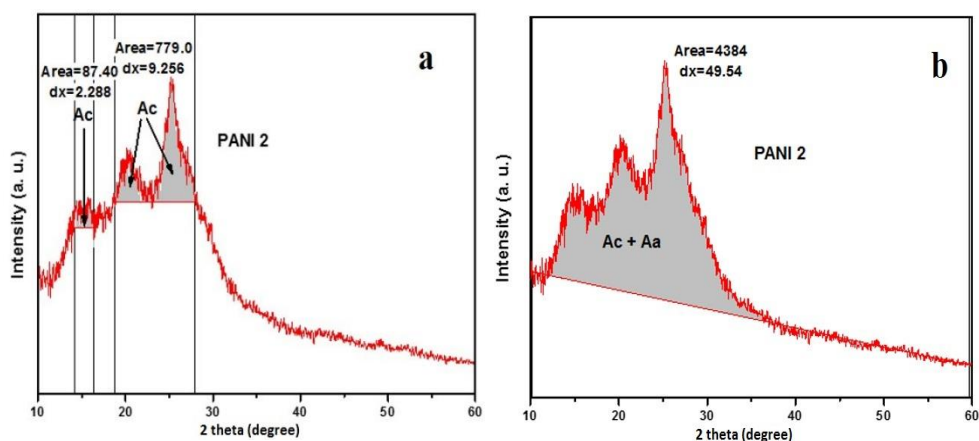
Figure 4.2: Percent of crystallinity of PANI 2; (a) area of crystalline phase (A_c) and (b) area of crystalline and amorphous phase ($A_c + A_a$).

approximate measurements of the crystallinity. These changes in crystallinity were due to the loss of dopant, which confirmed from FTIR spectroscopy. **Figure 4.2** shows the plots for

percent of crystallinity calculated from XRD data, for PANI 2. Similarly, the percent of crystallinity was calculated for PANI 1, PANI 1VD and PANI 2VD.

4.4 Structural Study

The FTIR spectra (**figure 4.3**) of the PANI 1, PANI 1VD, PANI 2 and PANI 2VD were analyzed to confirm the presence of a dopant in the air- and vacuum-drying conditions. For FTIR measurement, the samples were placed inside the holder. As expected, the crystallinity of the vacuum-dried PANI was lower compared to that of the air-dried PANI. This change in the crystallinity may affect the area of the absorption band. The band at 1292 and 1245 cm^{-1} assigned to the bending vibrations of C-N for aromatic amines and C-N$^{+\bullet}$ stretching vibrations in the polaron structure represented the existence of conducting protonated PANI [153]. The moisture content in the polymer was measured with the vibrations at 1620 cm^{-1} in their FTIR spectra [187].The characteristic peaks at 1564 and 1490 cm^{-1} represented C=C stretching of quinoid (N=Q=N) and benzenoid (N=B=N) rings, respectively [188]. The strong band at 1143 cm^{-1}attributed to the vibration
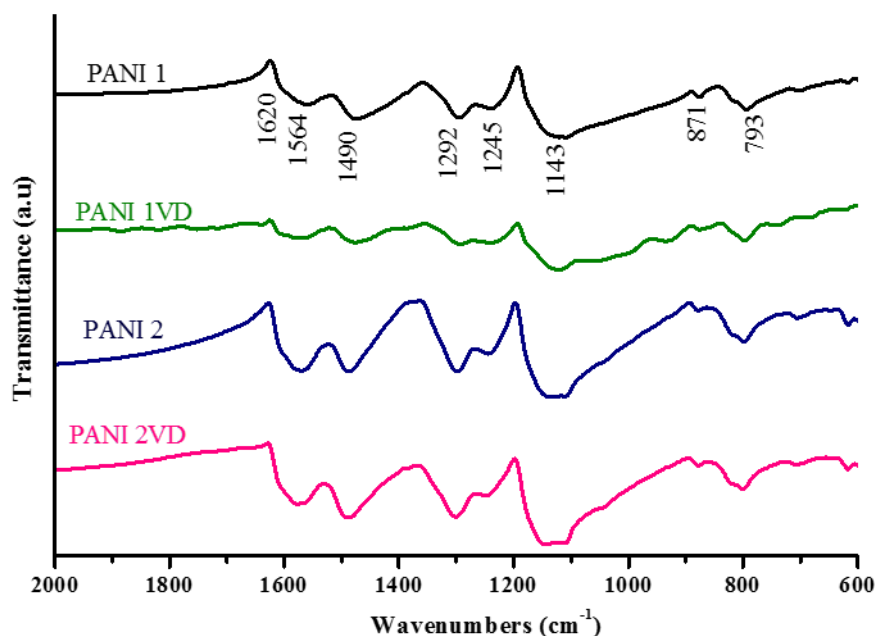
Figure 4.3: FTIR spectra of PANI 1, PANI 1VD, PANI 2, and PANI 2VD.

mode of the –NH^{+}= structure and/or C-H in-plane bending vibrations [189]. The bands observed at 871 and 793 cm^{-1} and corresponding to ring deformation were related to the C-H

out of plane bending vibrations of the benzene ring. There was no obvious change in the characteristic peaks of any of the PANIs; however, the intensity changed as follows: PANI 2 > PANI 2VD > PANI 1> PANI 1VD. The decrease in the intensity was due to the removal of a small amount of HCl dopant from PANI with the vacuum-drying treatment [190]. For instance, the intensity of the band at 1143 cm^{-1} was higher in the case of PANI (without solvent); this was ascribed to the higher degree of protonation in the backbone due to concentrated acidic medium. This resulted in a higher degree of electron delocalization. The higher degree of protonation may have increased the electrical conductivity of PANI.

4.5 Electrical Conductivity

The current–voltage characteristics of PANI 1, PANI 2, PANI1VD, and PANI 2VD are shown in **figure 4.4** and indicate their cubical parabolic nature at room temperature.
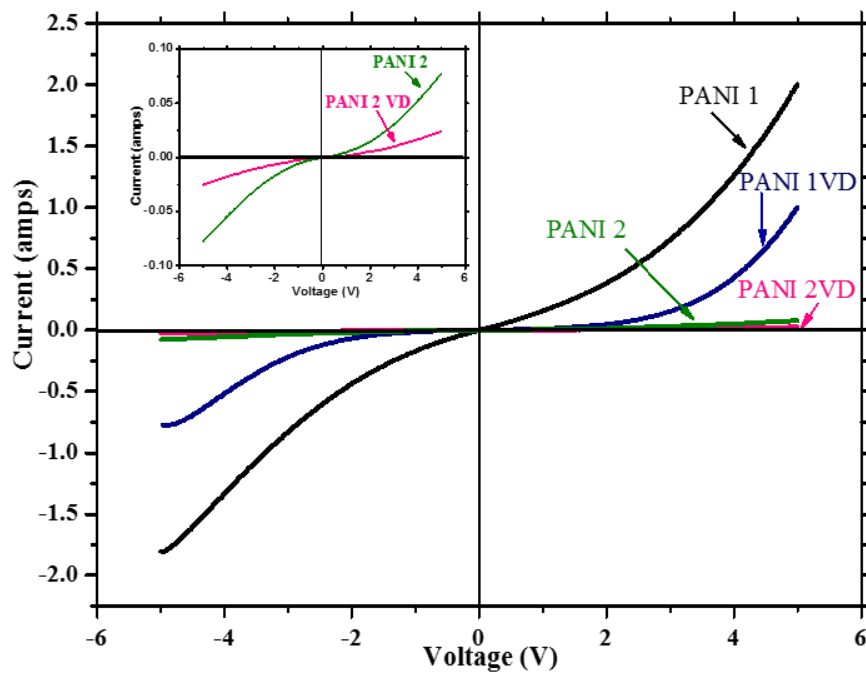
Figure 4.4: Current–voltage characteristics of PANI 1, PANI 2, PANI 1VD, and PANI 2VD.

The electrical conductivity values of PANI 1 and PANI 1VD were greater than those of PANI 2 and PANI 2VD. However, the degrees of electron delocalization in PANI 2 and PANI 2VDwere greater than those of PANI 1 and PANI 1VD. This contradiction could explain by the mixed (granular and fibrillar) morphology of PANI 1 and PANI 1VD.Due to fibrillar (almost one-dimensional system) morphology, the resistance experienced by the

charge carriers would be lesser than that experience in the granular morphology,i.e., in PANI prepared without solvent.An enlarged view of the current–voltage characteristics of PANI 2 and PANI 2VD shown in the inset. The values of the dc electrical conductivity of PANI 1, PANI 2,PANI 1VD, and PANI 2VD were calculated as 3.3 X 10^{-2}, 0.1 X 10^{-2}, 0.3 X 10^{-2}, and 0.3 X 10^{-3} S/cm, respectively (**table4.1**).The higher conductivity of PANI 1 may have been due to the presence of nanofibers, moisture content, and strong interior intrachain interactions [191]. In addition, the crystallinity of PANI 1was higher than the values of 7, 25, and 30% for PANI 1VD, PANI 2, and PANI 2VD, respectively. The higher the crystallinity, the fewer were the number of defects in the polymer, and this resulted in an enhancement in the conductivity. The crystalline phase may also be responsible for the percolation pathway of the systems. The reduced resistance of the nanofibers facilitated the drifting of the charge carriers. On vacuum treatment, the slight decrease in the electrical conductivity of PANI 1VD may have been due to the removal of moisture and the formation of branched nanofibers. The

Table 4.1 Morphology, DC electrical conductivity and band gap of prepared PANI 1, PANI 2, PANI 1VD and PANI 2VD

Materials	Oxidising Agents	Morphology	Conductivity	Band gap
PANI 1	APS	hair like nanofibers & granular	3.3 x 10^{-2} S/cm	3.25 and 1.67 eV
PANI 2	APS	Granular	0.1 x 10^{-2} S/cm	3.24 and 1.68 eV
PANI 1VD	APS	branched nanofibers & granular	0.3 x 10^{-2} S/cm	3.27 and 1.67 eV
PANI 2VD	APS	Granular	0.3 x 10^{-3} S/cm	3.20 and 1.63 eV

branching of nanofibers enhanced the separation, and this reduced interior intrachain interactions and coupling between the polymeric chains [192].The lower conductivity of PANI 2 and PANI 2VD may have been due to the irregularly shaped granular morphology and less contact between the monomer and oxidant molecule; this may have decreased the oxidation level in PANI prepared without solvent. The weak secondary bonding separated the particle phase, and this may have also favored the decline in the dc electrical conductivity of PANI. Riaz *et al.* [193] reported that irregular agglomerates decreased the desired properties of the polymer. The dc electrical conductivities of one-dimensional/two-dimensional structures are greater than those of their three-dimensional counterparts.

4.6 Morphological Analysis

Figure 4.5 and 4.6 show the morphological features of air dried PANI 1 and PANI 2 respectively. The air dried PANI 1 shows the dual (granular and hair like nanofibers) morphology of PANI. These grains and hair like nanofibers at different magnifications
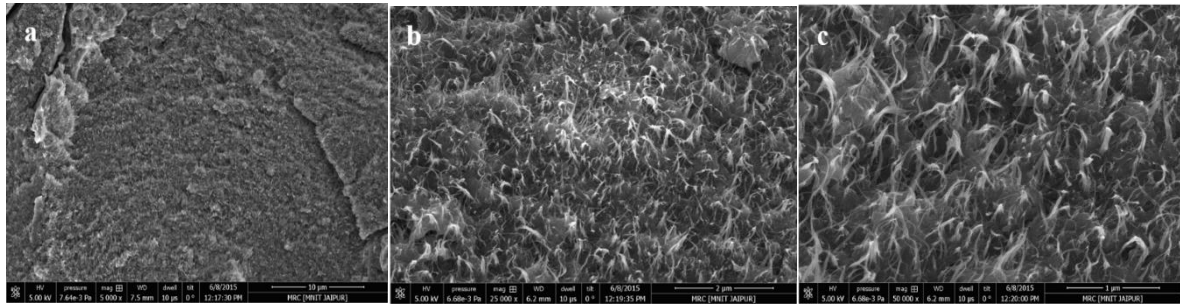
Figure 4.5:SEM images of PANI 1 at (a) 5000X, (b) 25000X and (c) 50000X magnifications
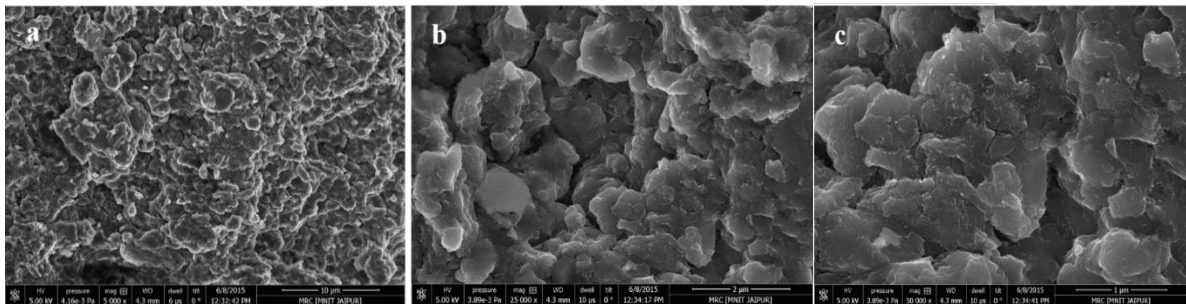
Figure 4.6: SEM images of PANI 2 at (a) 5000X, (b) 25000X and (c) 50000X magnifications
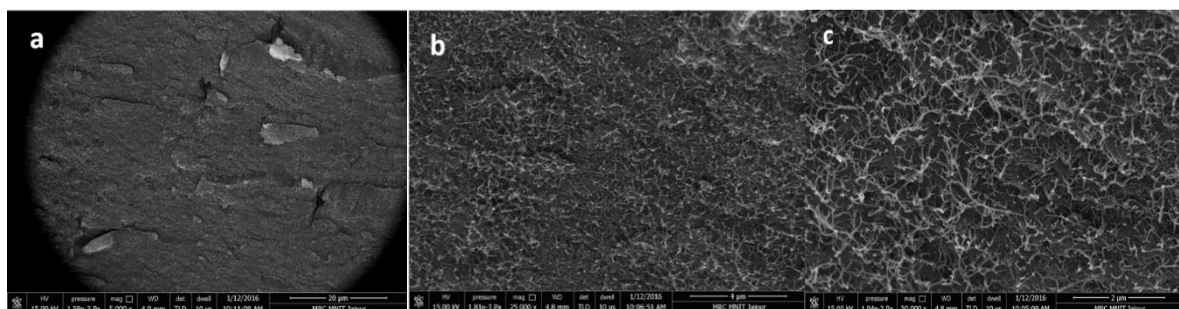
Figure 4.7: SEM images of PANI 1VD at (a)5000X, (b)25000X and (c)50000X magnifications
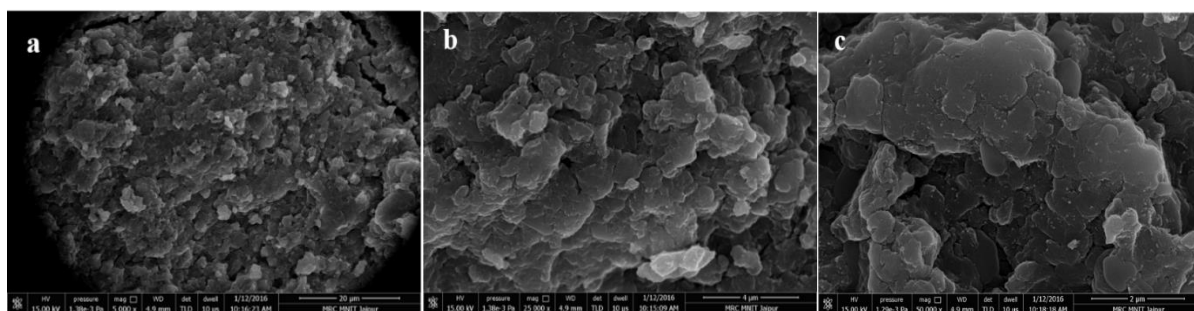
Figure 4.8: SEM images of PANI 2VD at (a) 5000X, (b) 25000X and (c) 50000X magnifications

depicted in **figure 4.5(a-c). Figure 4.6** shows the granular morphology of PANI 2 at different magnification. It was very interesting to note that after vacuum dried treatment the morphology of PANI 1 gets changed from hair like nanofibers to branched nanofibers (PANI 1VD). However, there was no change in the morphology of PANI 2. The obtained morphology of PANI 1VD and PANI 2VD at different magnification are depicted in **figure 4.7 and 4.8**, respectively. The TEM images (**figure 4.9**) shows the clear view of PANI (PANI 1) nanofibers along with granular morphology.
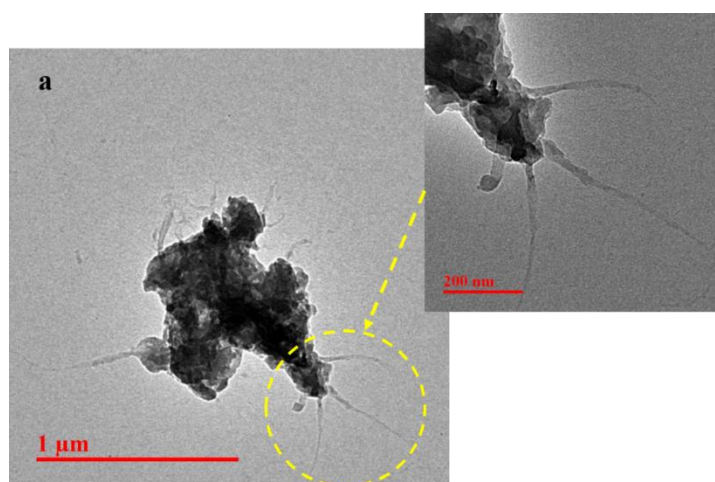
Figure 4.9: TEM images of dual (granular and fibrillar) morphology PANI 1

The formation of PANI nanofibers along with grains observed without the addition of any structural directing agent was very interesting and might be the natural morphology of PANI. Such a mixed morphology has rarely reported in the literature. The reason for the dual morphology in the case of PANI 1 might have been the rate of addition of aniline. Initially, 2 ml of reagent added dropwise; this formed nanofibers. The remaining 2 ml added at a once, and this produced the granular morphology [100]. **Figure 4.7(a-c)** reveals the branched

nanofibers network along with a granular structure for PANI 1VD. On removal of a small amount of HCl dopant, as confirmed by the FTIR spectra, intermolecular hydrogen bonding occurred in PANI, and this resulted in the branching of nanofibers networks [193]. TGA also did the confirmation of the removal of the HCl dopant. The hair like nanofibers may have increased the free volume and, hence, decreased the density of the materials. In the case of PANI prepared without a solvent, the irregularly shaped grains were interconnected well with each other, and this represented a sufficient binding energy to combine with nearby grains or molecules.

4.6.1 Growth Mechanism of the PANI Nanofibers and Granular Structure

The dropwise addition of the aniline monomer into the oxidant solution enhanced its solubility to a larger extent, and this led to the formation of nanofibers. The complete solubility of the monomer formed primary nanofibers, and the secondary chain growth of the nanofibers suppressed. Wang and Jing [194] reported that a depleted region of oligomeric intermediate and aniline cation created that surrounded the PANI nanofibers; this assisted the growth and elongation of the nanofibers in one direction because their ends extended to the less depleted region. In addition, the lower nucleation site on the surface of the PANI nanofibers also confirmed the continuity of the PANI nanofibers at the end of polymerization. In the case of PANI prepared without a solvent, the reactions mainly occurred at the surface of the solid-state reactant. The reported literature shows that the morphology of a product depends on the rates of nucleation and growth of the product. The inter-diffusion rate of the reactant was very slow; this may have been due to less contact between the monomer and oxidant molecules. This may have weakened the secondary bonding (van der Waals interactions) and favored the phase separation of the particles.

4.6.2 Morphology of PANI Changed from a One-Dimensional Shape to a Granular Shape

The dropwise addition of aniline into APS produced clean nanofibers at the early stage of the polymerization process. The initially formed nanofibers acted as nucleation centers for the further precipitation of PANI. With the extreme surplus of APS, the nanofibers became thicker and coarser, and this led to irregularly shaped agglomerates. The relative fraction of nanofibers and granular particles depended on the ability to separate the formation of nanofibers from the secondary growth of the polymer.

4.7 Thermal Analysis

The TGA and differential thermogravimetric (DTG) curves of the PANI samples depicted in **Figure 4.10 (a,b)**. A three-step weight loss process was evident in the TGA curve of the pure PANI. Three major minima observed in the DTG curve, which showed the majority weight loss of the respective steps [195, 196]. The initial weight loss about 100°C
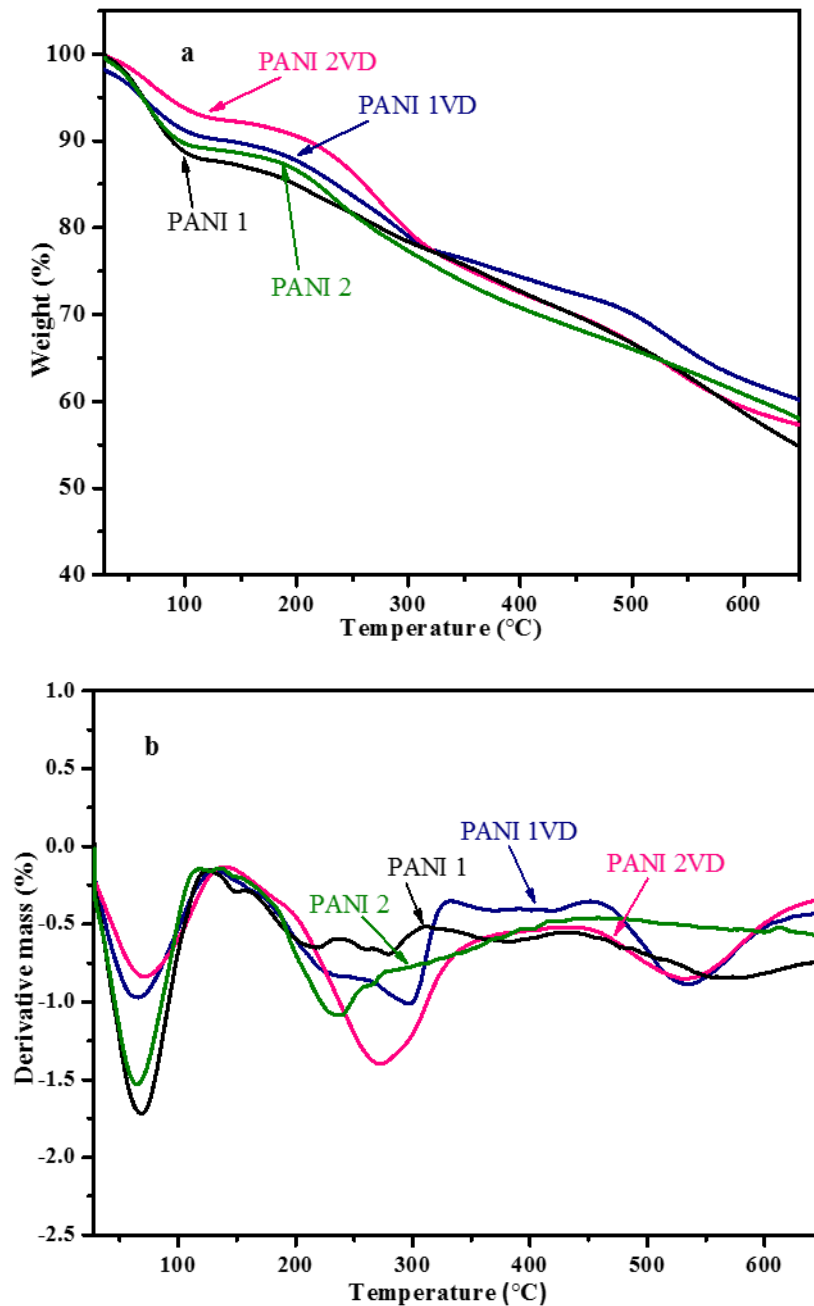
Figure 4.10: TGA (a) and DTG (b) curves of PANI 1, PANI 1VD, PANI 2, and PANI 2VD.

attributed to the loss of small amounts of absorbed water and unreacted monomers [162]. The second weight loss between 150 and 300 °C was believed to have been due to the decomposition of dopant and low-molecular-weight oligomer [197]. We observed that the third weight loss started close to 400 °C, and it ascribed to the degradation and decomposition of the backbone units of PANI [198].

The degradation of the PANI backbone units resulted in the formation of substituted aromatic fragments and the extended aromatic fragment, as confirmed by the bands at 871 and 793 cm^{-1} in the FTIR spectra. **Figure 4.10a** reveals that there was a lower content of moisture and dopant expelled from the polymeric chains in the vacuum-treated PANIs compared to those that were air dried. The onset temperature is the temperature up to which a material has thermal stability. For PANI 1, PANI 1VD, PANI 2, and PANI 2VD, the onset temperatures were 520, 510, 530, and 515 °C, respectively **(table 4.2)**. The main decomposition temperature and residual weight values for PANI 1, PANI 1VD, PANI 2, and PANI 2VD were 560 °C and54.72%, 565 °C and 60.18%, 550 °C and 58.03%, and 555 °C and 57.38%, respectively. The order of moisture percentage, as observed in **figure 4.10a**, was as follows PANI 1 > PANI 2 >PANI 1VD > PANI 2VD. The higher percentage of

Table 4.2: Calculation of T_{onset}, T_d and char% of prepared PANI 1, PANI 2, PANI 1VD & PANI 2VD

Materials	T_{onset}	T_d	char%
PANI 1	520 °C	560 °C	54.72%
PANI 2	530 °C	550 °C	58.03%
PANI 1VD	510 °C	565 °C	60.18%
PANI 2VD	515 °C	555 °C	57.38%

moisture content in PANI 1 and PANI 2 compared to PANI 1VD and PANI 2VD, respectively, showed the higher value of dc electrical conductivity. Bellucci *et al.* [199] reported that in the presence of moisture, the electrical conductivity of polyimide increased. A very slight change in the percentage of counter ion of the dopants moieties (Cl_2) may have also affected the mobility of the charge carrier. It has reported that the higher electron affinity and lower thermal conductivity in the dopant counter ion (Cl_2) increased the conductivity of PANI. The presence of moisture could have enhanced the electrical conductivity of PANI. Among all of the PANIs, PANI 1 showed a higher content of moisture, and this resulted in a higher conductivity compared to those observed in the others.

4.8 Absorption Study

To prove the presence of benzenoid and quinoid rings in the PANI samples, absorption spectra (**figure 4.11**) recorded. The spectra taken in NMP solvent; this turned the color of PANI from green to blue (i.e., indication of the conversion of emeraldine salt to emeraldine base). There were no changes in the absorption spectra of all of the samples; this may have been due to the same dopant used during the preparation of PANI.
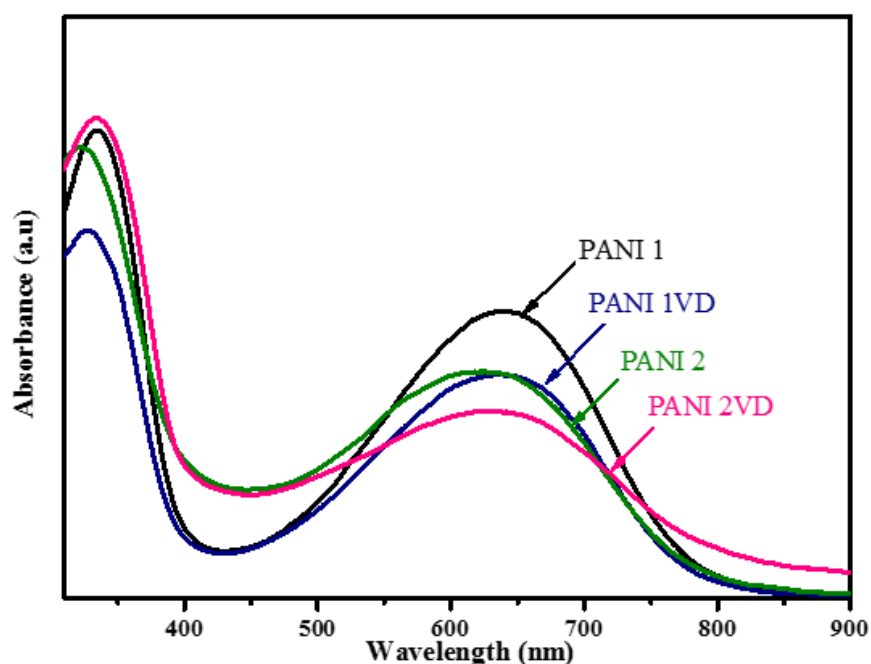
Figure 4.11: Absorption spectra of PANI 1, PANI 2, PANI 1VD and PANI 2VD.

Babu *et al*. [200] reported that PANI prepared with various oxidants had different absorptions. The absorption spectra showed intense and broad absorptions at 330 and 630 nm; this confirmed the formation of emeraldine base [201]. The absorption at 330 nm might have correlated with the pi–pi* transition within benzenoid rings, that is, the electronic transition from highest occupied molecular orbital to lowest unoccupied molecular orbital, and the absorption at 630 nm should have been pi–pi* transitions within the quinoid rings [202]. The intensity of the peak corresponding to the quinoid ring was relatively weak because the addition of HCl into the PANI backbone changed electron delocalization into the polymeric chains and led to charge equalization. The equalization of charge formed the
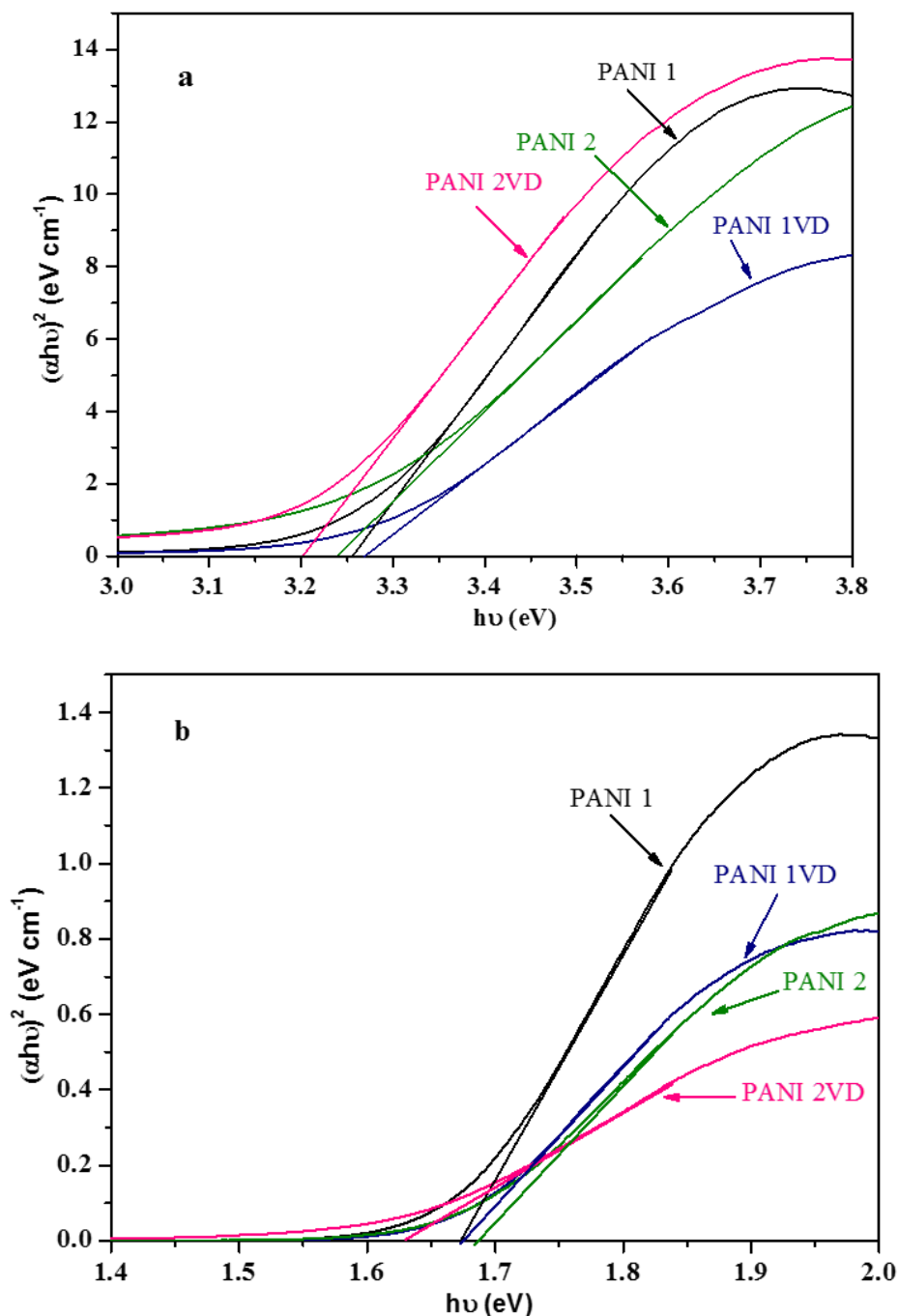
Figure 4.12: Optical band gaps of PANI 1, PANI 1VD, PANI 2, and PANI 2VD corresponding to (a) 330nm and (b) 630nm.

conjugated system and protonation occurred at the imine ion of the quinoid ring; this generated the excited polaron. The optical band gap (E_g) of the synthesized materials calculated by Tauc's relation [203] (**equation 4.1**):

$$(\alpha h\upsilon) = B\left(h\upsilon - E_g\right)^n \qquad (4.1)$$

where B is a constant, α is the absorption coefficient, h is Planck's constant (6.625 X 10^{-34} J s), and υ is the frequency of the incident photon. The exponent n has discrete values of 1/2,3/2, 2, and 3, and n = 1/2 is assigned to direct allowed transitions, n = 3/2 is assigned to direct forbidden transitions, n = 2 assigned to indirect allowed transitions, and n = 3 assigned to indirect forbidden transitions. For calculating the band gap, first the absorption spectra have been obtained with respect to wavelength using UV spectrometer. The graph was plotted between $(\alpha h\nu)^2$ and hν in origin software. The band gap was calculated by drawing a tangent in the graph with respect to both peaks at 330 nm and 630 nm which touches the hν value.

Tauc's plot for the calculation of the optical band gap (on both 330 nm and 630 nm peaks) shown in **figure 4.12 (a,b)**. Extrapolation of a tangent on both the peaks, obtained in the absorption spectra, indicated values of the optical band gap of 3.25 and 1.67 eV (PANI 1), 3.24 and1.68 eV (PANI 2), 3.27 and 1.67 eV (PANI 1VD), and 3.20 and1.63 eV (PANI 2VD). Our results suggest that the morphological and physical properties of PANI could be regulated through the selection of an appropriate route of preparation.

CHAPTER FIVE

MWCNTs/PANI Nanocomposites

In current chapter, discussion has given about the density, structural, electrical, morphological and thermal stability of hybrid f-MWCNTs/PANI nanocomposites. PANI 1VD selected as a matrix for further nanocomposites formation and their characterizations. The results about confirmation of functionalization of pristine MWCNTs with carbonyl group explained in this chapter. The electrical conductivity of nanocomposites is higher than that of pure PANI. The percolation threshold is found to occur at 0.1 vol. % of the filler. The electrical conductivity of nanocomposites is reaches up to the level which is required for EMI shielding applications.

==

5.1 MWCNTs/PANI Nanocomposites

Hybrid MWCNTs/PANI nanocomposites were prepared with different MWCNTs content as given in **table 5.1**. Before preparing nanocomposites pristine MWCNTs were

Table 5.1. Weight and volume percentages of the f-MWCNTs filler in PANI matrix

Sr. No.	Weight%	Volume%
1	0	0
2	0.25	0.1
3	0.5	0.3
4	1.0	0.6
5	1.5	0.9
6	2.0	1.3
7	3.0	1.9
8	5.0	3.3
9	10.0	6.7
10	20.0	13.9
11	30.0	21

functionalized by oxidative treatment designated as f-MWCNTs. Pristine and functionalized MWCNTs were characterized using FTIR spectroscopy, Raman spectroscopy and TEM. The prepared nanocomposites were characterized using XRD, FTIR, SEM, TEM, TGA techniques. The DC electrical conductivity was also measured using electrometer.

5.2 Density Determination

The theoretical and experimental density of hybrid f-MWCNTs/PANI nanocomposites shown in **figure 5.1**. It is clearly seen that the density of nanocomposites increased with increasing the content of f-MWCNTs which is due to the higher density of MWCNTs (2.1 g/cm^3) than the density of pure PANI (1.361 g/cm^3). The experimental density was in close agreement with the theoretical density at lower vol. %, however, at
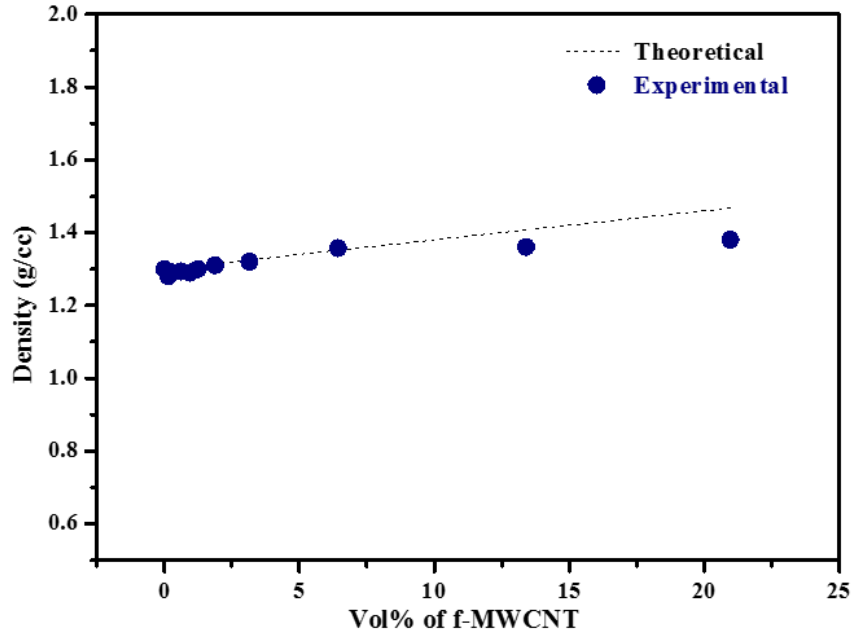
Figure 5.1: Theoretical and experimental densities of hybrid f-MWCNTs/PANI nanocomposites

higher vol. %(beyond 3.3 vol. %) it was slightly less than the theoretical density. The probable reason for lower density at higher vol.% is the agglomeration of CNT which hinders the infiltration of the polymer during processing [204].

5.3 Structural Study and Crystallinity Determination

The analysis of XRD patterns confirmed the formation of hybrid f-MWCNTs/PANI nanocomposites and percent of crystallinity (**figure 5.2**).The diffraction peaks (for f-MWCNTs) appeared at 2θ = 25.9°, and 43° correspond to graphite-like structure and catalytic particles encapsulated inside the wall of CNTs, respectively [205]. PANI shows broad peaks at 2θ = 14.2°, 20.2°, and 25.2° which is corresponding to (010), (100) and (110), crystal planes (JCPDS 00-060-1167) of polyaniline in the emeraldine salt form, respectively [180]. The peaks of relatively lower intensity also observed at 27.3° and 30°. In comparison to PANI, the XRD pattern of hybrid f-MWCNTs/PANI nanocomposite demonstrate noticeable differences in the sharpness of the peak which affects the crystallinity of nanocomposites**.**
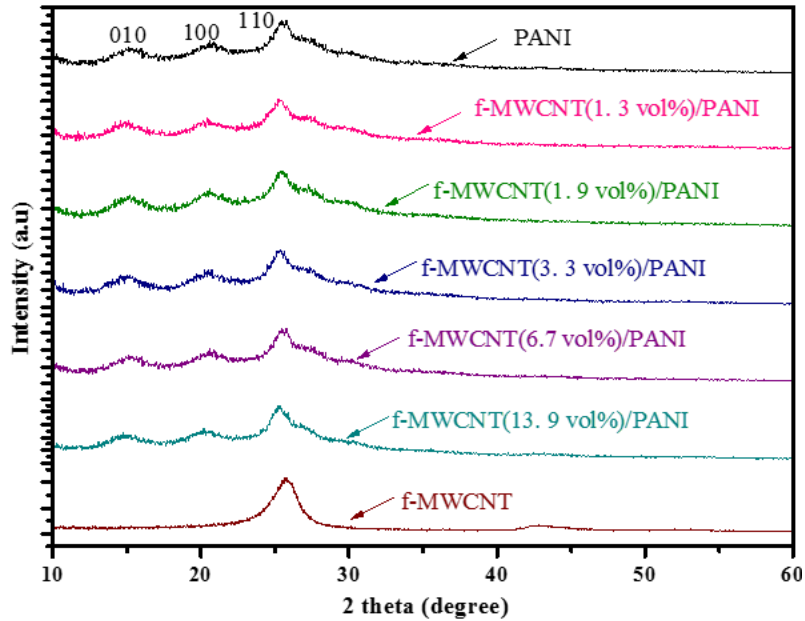
Figure 5.2: XRD patterns of PANI, f-MWCNTs, and hybrid f-MWCNTs/PANI nanocomposites

The value of percentage crystallinity for pure PANI and hybrid f-MWCNTs/PANI nanocomposite calculated as 38 (for PANI), 40 (1.3 vol % f-MWCNTs and 1.9 vol. % f-MWCNTs), 42 (3.3 vol. % f-MWCNTs), 43 (6.7 vol. % f-MWCNTs) and 46 (13.9 vol. % f-MWCNTs) (**table 5.2**). The increased crystallinity in nanocomposites compared to PANI was

Table 5.2. Percent of crystallinity for PANI and hybrid f-MWCNTs/PANI nanocomposites

Material	$A_c + A_a$	A_c	$X_c (\%) = [A_c/ (A_c+A_a)]$ X 100
PANI	3460	1305	38
f-MWCNTs(1.3 vol%)/PANI	3465	1383	40
f-MWCNTs(1.9 vol%)/PANI	3470	1379	40
f-MWCNTs(3.3 vol%)/PANI	3980	1664	42
f-MWCNTs(6.7 vol%)/PANI	3220	1380	43
f-MWCNTs(13.9 vol%)/PANI	3900	1790	46

due to ultrasonication treatment was given during solution processing. The ultrasonication has been applied to attain the better dispersion of f-MWCNTs and PANI in DMSO solvent. It causes the rapid motion of molecule resulted in efficient mixing leads to the ordering of PANI chains along the axis of CNT. Peng *et al.* [206] reported the higher crystallinity of poly(3,4-ethylenedioxythiphene) (PEDOT) with effective mixing by ultrasonication

treatment. The higher percent of crystallinity of PANI with 13.9 vol. % f-MWCNTs also shows high direct current electrical conductivity. FTIR spectroscopy also confirmed these changes in crystallinity of hybrid nanocomposites.

5.4 Structural Study

The FT-IR spectra (**figure 5.3**) of PANI and hybrid f-MWCNTs/PANI nanocomposites were analyzed to confirm the interaction of f-MWCNTs with PANI which affected the crystallinity of nanocomposites. In the case of PANI, the 1564 cm^{-1} and 1490 cm^{-1} bands attributed to the C=C stretching of quinoid and benzenoid rings, respectively [188] (**table 5.3**). The characteristic peaks at 1292 and 1245 cm^{-1} ascribed to the bending
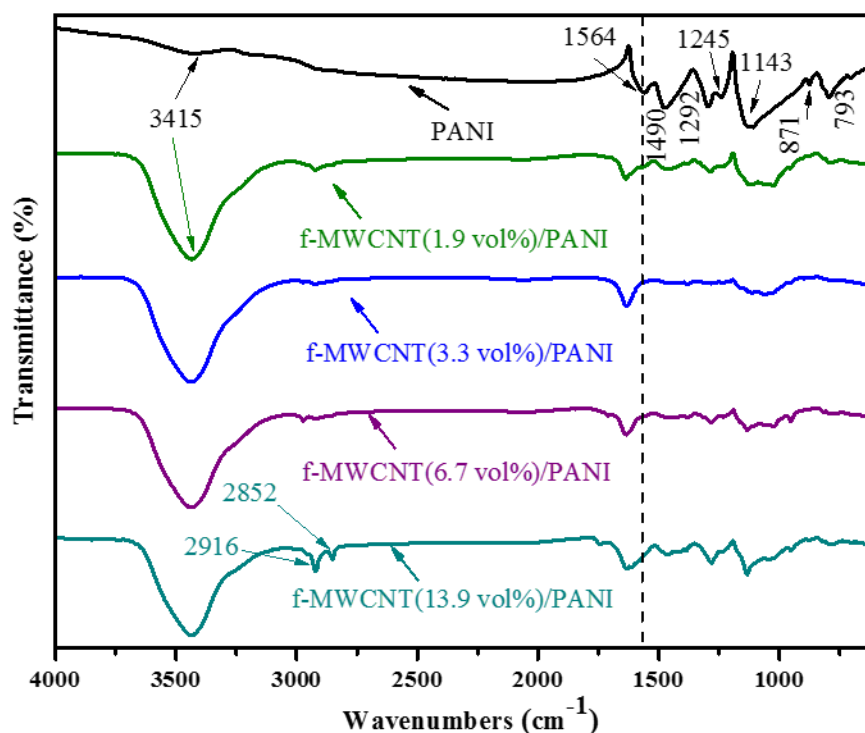
Figure 5.3: FTIR spectra of PANI and hybrid f-MWCNTs/PANI nanocomposites

vibration of C-N for aromatic amines and C-N$^{+\cdot}$ stretching vibrations in the polaron structure which signify the presence of conducting protonated PANI [153]. The strong bands at 1143 cm^{-1} assigned to vibration mode of –NH$^+$= structure and/or C-H in-plane bending vibration [189]. The observed band at 871 cm^{-1} and 793 cm^{-1} identified with the out-of-plane bending of C-H bond in the benzene ring. The signal observed at 3415 cm^{-1} (strong and broad for

nanocomposites and very weak for PANI) was assigned to the O-H stretching mode of carboxyl groups in functionalized CNT and absorbed water. The characteristics peaks at 2916

Table 5.3. Vibrational frequencies of PANI

interatomic bond	vibrational frequency (cm^{-1})
O-H stretching	3415
C=C (Qui)[a] stretching	1564
C=C (Ben)[b] stretching	1490
C-N bending (aromatic amine)	1292
C-N$^{+\cdot}$stretching (polaron structure)	1245
–NH^{+}=/ or C-H in plane bending	1143
C-H out of plane bending	871 & 793

[a]Qui=Quinoid, [b]Ben= Benzenoid

and 2852 cm^{-1} attributes to CH$_3$ (C-H stretching) and CH$_2$ (C-H stretching) group, respectively [207]. It found that with increasing the content of f-MWCNTs in PANI, the intensity of peaks at 2916 and 2852 cm^{-1} significantly increased which confirms the presence of f-MWCNTs in PANI. The quinoid band of PANI at 1564 cm^{-1}shifted to 1610 cm^{-1} with the addition of f-MWCNTs in PANI. The shifting of the band confirms the interactions of the carbonyl group of f-MWCNTs with the quinoid ring of PANI. The intensity of some of the peaks in nanocomposites decreased than that of pure PANI. The reason of decreased intensity was the adsorption of unreacted aniline monomer onto the surface of the functionalized CNT because of which polymer chains are forced to grow around the nanotubes [208]. The constrained motion of the polymeric chains and adsorption of monomer will limit the modes of vibration in PANI; the difference can see in FTIR spectra. By the strong interaction, it can assume that CNT is functioning as chemical dopants for PANI conductivity [209]. The interaction of conducting filler may have increased the electrical conductivity and EMI SE of hybrid f-MWCNTs/PANI nanocomposites.

5.5 Electrical Conductivity

The DC electrical conductivity of PANI and hybrid f-MWCNTs/PANI nanocomposites was plotted as a function of f-MWCNTs vol. % shown in **figure 5.4a**. the comparison of electrical conductivity of all the samples are depicted in **table 5.4.** For electrical resistance measurement, the silver paste was used on the both side of the PANI

pellet. It was used for making good connection of electrode (made up of copper material) on both side of the pellet. The diameter of the copper electrode on both side of the pellet was 14mm and area is 6.16 cm^2. It was found that with increasing the content of f-MWCNTs in PANI matrix, the DC electrical conductivity also increased. It was interesting to note that electrical conductivity increased very slowly up to 0.1 vol.% f-MWCNTs but increased rapidly beyond 0.1 vol.% f-MWCNTs content; this transition occurs known as percolation threshold. It resulted in the abrupt one order increment in the electrical conductivity level which is about twelve times higher than that of percolation threshold point. The reason for a sharp increase in electrical conductivity is the commencement of network between filler and PANI matrix, through which charge carrier get a physical path to move. It is believed that CNT is relatively good electron acceptor due to its similar structure as of fullerenes, while PANI is a decent electron donor.

There are several parameters upon which percolation threshold depends on, matrix type, synthesis method, and CNT type. MWCNTs having large surface area and aspect ratio because of which they may function as a "conducting bridges" connecting PANI conducting domains and improve the effective percolation in such heterogeneous systems. The electrical conductivity of dual morphology PANI was 0.3 x 10^{-2} S/cm and increased to 1.8 x 10^{-1} S/cm for f-MWCNTs/PANI nanocomposites (13.9 vol. % f-MWCNTs). The electrical conductivity of nanocomposites was about 60 times higher than that of PANI. The reason may be the
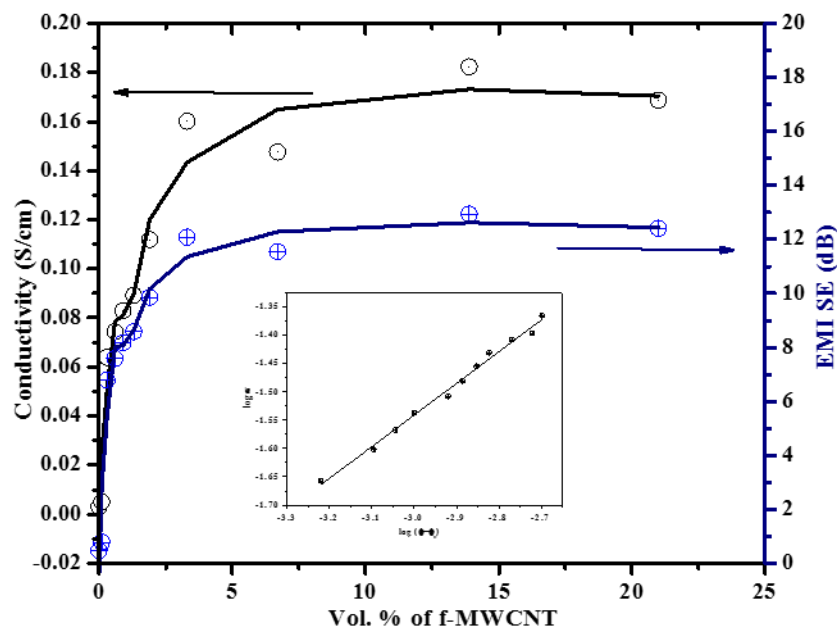
Figure 5.4a: The DC electrical conductivity and EMI SE of PANI and hybrid f-MWCNTs/PANI nanocomposites [the inset (enlarged view shown in figure 5.4b) showing the scaling law near percolation threshold]
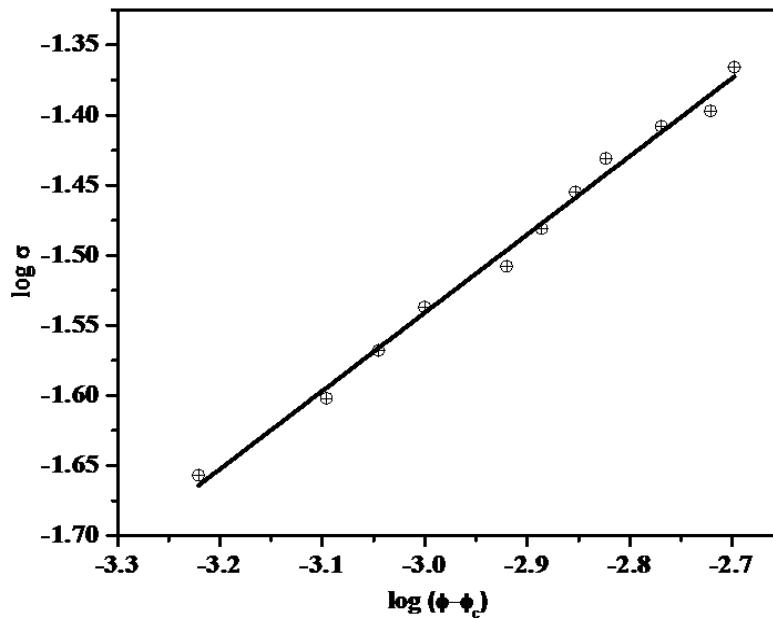
Figure 5.4b: scaling law near percolation threshold

Table 5.4. Comparison table of sample's electrical conductivity

Sr. No	Materials	conductivity	EMI SE = 20 log (1+1/2 σ. t. Zo)
1.	Pure PANI	0.3 x 10-2 S/cm	0.47 S/Ω
2.	f-MWCNTs(0.1 vol%)/PANI	0.5 x 10-2 S/cm	0.78 S/ Ω
3.	f-MWCNTs(0.3 vol%)/PANI	0.6 x 10-1 S/cm	6.78 S/ Ω
4.	f-MWCNTs(0.6 vol%)/PANI	0.7 x 10-1 S/cm	7.58 S/ Ω
5.	f-MWCNTs(0.9 vol%)/PANI	0.8 x 10-1 S/cm	8.17 S/ Ω
6.	f-MWCNTs(1.3 vol%)/PANI	0.1 S/cm	8.57 S/ Ω
7.	f-MWCNTs(1.9 vol%)/PANI	1.1 x 10-1 S/cm	9.85 S/ Ω
8.	f-MWCNTs(3.3 vol%)/PANI	1.6 x 10-1 S/cm	12.07 S/ Ω
9.	f-MWCNTs(6.7 vol%)/PANI	1.4 x 10-1 S/cm	11.54 S/ Ω
10.	f-MWCNTs(13.9 vol%)/PANI	1.8 x 10-1 S/cm	12.93 S/ Ω
11.	f-MWCNTs(21.0 vol%)/PANI	1.6 x 10-1 S/cm	12.40 S/ Ω

dispersion of f-MWCNTs in PANI mutually improve the continuity of the f-MWCNTs in the nanocomposites. The higher loading of f-MWCNTs generates more conducting bridges

which facilitate more charge to transfer between the quinoid ring of PANI and the f-MWCNTs (**see figure 5.5**).
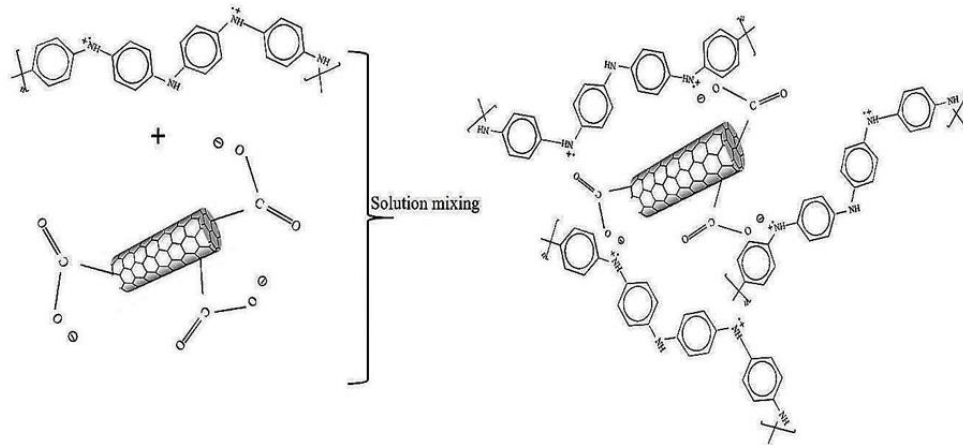
Figure 5.5: Schematic of the interaction between positively charged PANI and negatively charged f-MWCNTs

Bao *et al.* [210] reported the connection of MWCNTs with PANI at higher filler loading which leads to enhancing the electrical conductivity of nanocomposites. The plateau observed beyond 3.3 vol. % of f-MWCNTs indicate that the smearing region ranges from 0.1 vol. % to 3.3 vol. % of f-MWCNTs. According to classical percolation theory, the variation of electrical conductivity of nanocomposites beyond the percolation threshold can express by scaling law [112] (**equation 5.1**)

$$\sigma_c = A.(\Phi - \Phi_c)^t \qquad\qquad (5.1)$$

where σ_c is the electrical conductivity of the nanocomposite, A is a constant, Φ_c is the volumefraction of filler at the percolation threshold. The symbol Φ is the volume fraction of filler near the percolation threshold, and t is the critical exponent which governs the scaling behavior in the region of Φ_c. By **equation 5.1**, the inset in **figure 5.4** shows the best fit to the measured logarithm of direct current electrical conductivity as a function of the logarithm of $\Phi - \Phi_c$. From the scaling law plot, the value of t is found to be 0.565. Classical percolation theory predicts the value of t between 1.5 to 2.0 for a three-dimensional network, whereas it falls between 1.0 to 1.332 for a two-dimensional system. Accordingly, the value of t is

expected to be lower than 1.0 if the charge carriers flow in one dimension [104, 211]. In the present nanocomposite, the filler having aspect ratio nearly 1000 and hence the flow of charge inside may flow through a one-dimensional network of f-MWCNTs which resulted in the value of t less than 1.0. Another reason of improved electrical conductivity of nanocomposites may have the conversion of the granular structure of double morphology PANI to one-dimensional nanofibers. The electrical conductivities of the one-dimensional or two-dimensional structure are higher than that of three-dimensional counterparts.

5.6 Estimated EMI Shielding Efficiency

Figure 5.4 also represent the estimated EMI SE of hybrid f-MWCNTs/PANI nanocomposites. EMI SE depends on the electrical conductivity, thus with increasing the f-MWCNTs content, estimated EMI SE also improved. Based on the shielding theory (far-field shielding), the estimated value of shielding was calculated using **equation 3.7**.The EMI SE for pure PANIwas 0.47 dB and increased with f-MWCNTs content in PANI. The value of estimated EMI SE from 3.3 – 21 vol. % of f-MWCNTs in PANI was about 12 dB. The higher value of EMI shielding in hybrid nanocomposite compare to pure PANI is due to the increased value of electrical conductivity. The reason of electrical conductivity in the system may depend upon the morphology of the nanocomposites. It has reported in the literature that materials with high electrical conductivity are well suited for EMI shielding.

5.7 Morphological Analysis of MWCNTs

Figure 5.6 shows the TEM images of pristine MWCNTs and f-MWCNTs. The carbon nanotube has the weak van der Wall forces because of which it firmly agglomerated. The creation of additional functional groups on its surface diminishes these effects due to the existence of repulsive forces between the same charges of carbonyl groups. It could clearly see from TEM image of pristine MWCNTs (**figure 5.6a**) that the graphene sheet fragments of the outer shell, are relatively in order. The dark region (highlighted with a circle) in the microstructure of pristine MWCNTs can be the impurity content of Fe_2O_3 and Al_2O_3. The disturbed surface of f-MWCNTs (**figure 5.6b**) represents the surface treatment of pristine MWCNTs. Silva *et al.* [212] reported that Fe_2O_3 and Al_2O_3 impurity from CNT could remove via acid treatment. **Figure 5.7(a-c)** depicts the high-resolution TEM images of pristine

MWCNTs, f-MWCNTs and top view of MWCNTs. It seems that the sidewall of f-MWCNTs looks like leaves have been eaten by worms which indicate the creation of carboxylic acid groups on the side walls (**figure 5.7b**).
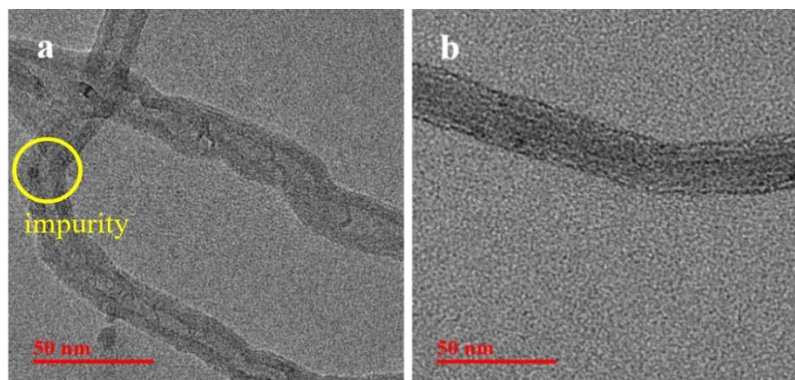
Figure 5.6: TEM images of pristine MWCNTs(a) and f-MWCNTs (b).
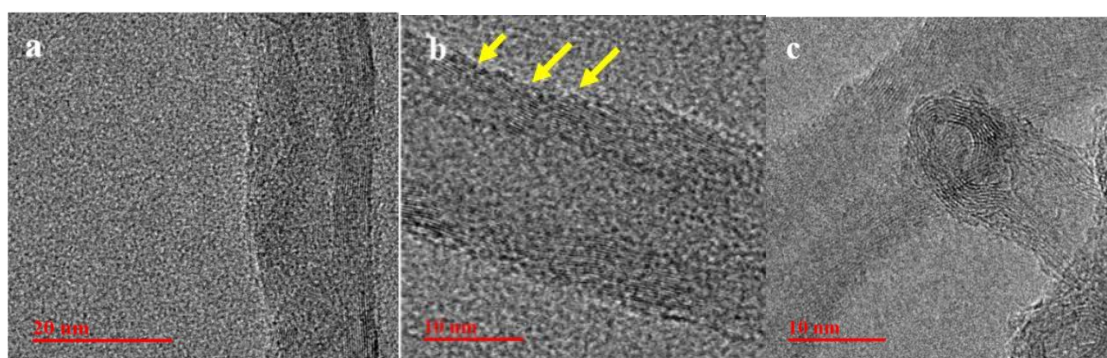
Figure 5.7: HRTEM images of pristine MWCNTs (a), f-MWCNTs (b) and top view to MWCNTs (c).

Figure 5.7c shows the top view of MWCNTs contained the numbers of cylinder which confirmed the identity of MWCNTs.

5.8 Structural Study of MWCNTs

Raman spectroscopy further confirmed the functionalization of pristine MWCNTs. **Figure 5.8** shows Raman spectra of pristine MWCNTs and f-MWCNTs. Three major characteristic bands observed in spectra of both samples: mode D (1337 cm^{-1}), mode G (1579 cm^{-1}), and mode G' (2678 cm^{-1}). The strong band observed at 1579 cm^{-1} ascribed to the in-

plane C–C stretching modes. MWCNTs have a number of concentric graphene layers, which result in a single symmetric band (G).
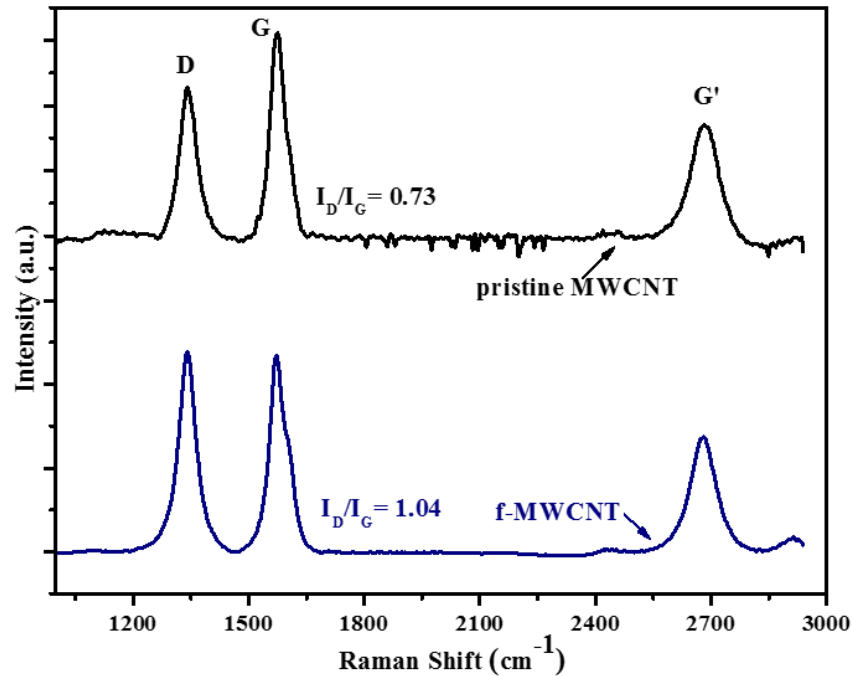
Figure 5.8: Raman spectra of pristine MWCNTs and f-MWCNTs

Due to many rolled graphene layers, their longitudinal and transverse components cannot distinguish at this vibration. An inactive in-plane mode (D-band) becomes active due to small imperfections produced by the particle size effect and the loss of translational symmetry in the disordered structure [105]. The significance of I_D/I_G is the ratio of sp^3 -hybridized carbon atoms (amorphous/disordered carbon) about sp^2-bonded carbon atoms (graphitic carbon) [181]. The variation in the relative intensity of the D and G lines (I_D/I_G) corresponds to the ordering of the graphitic structure, and this ratio is used to characterize the different sp^2 - based carbonaceous materials. The relative intensities between D and G modes are I_D/I_G = 1.04 (f-MWCNTs) and I_D/I_G = 0.73 (MWCNTs) (**see figure 5.8**). The intensity ratio I_D/I_G for f-MWCNTs was higher as compared to pristine MWCNTs, which reveals that mixture of concentrated H_2SO_4/HNO_3 increases the degree of disorders, greater disruption of the sp^2- bonded carbon atoms to sp^3-hybridised carbon atoms. It implies that greater extent of surface modification of pristine MWCNTs was carried out.

5.9 Morphological Analysis of Hybrid Nanocomposites

SEM images have examined the surface morphology, dispersion, and agglomeration of f-MWCNTs in the PANI matrix (**figure 5.9, 5.10 and 5.11**). **Figure 5.9 (a-c)** at different magnifications shows the SEM images of f-MWCNTs in f-MWCNTs (0.1vol%) /PANI nanocomposite. It also observed that f-MWCNTs dispersed in the PANI matrix, or somewhere it get agglomerated. The obtained morphology of PANI is in good agreement with the nanofibers produced by Huang *et al.* [102]. The clear view of morphology and dispersion of f-MWCNTs in f-MWCNTs (0.1 vol %)/PANI nanocomposite shown with TEM image in
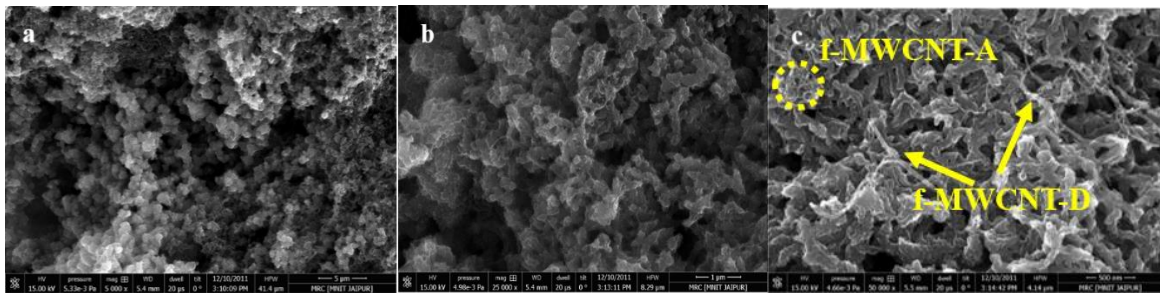
Figure 5.9: SEM images of f-MWCNTs (0.1 vol. %)/PANI nanocomposites at 5000X(a), 25000X(b) and 50000X (c) magnifications. [f-MWCNTs-D (dispersed) and f-MWCNTs-A (agglomerated)]
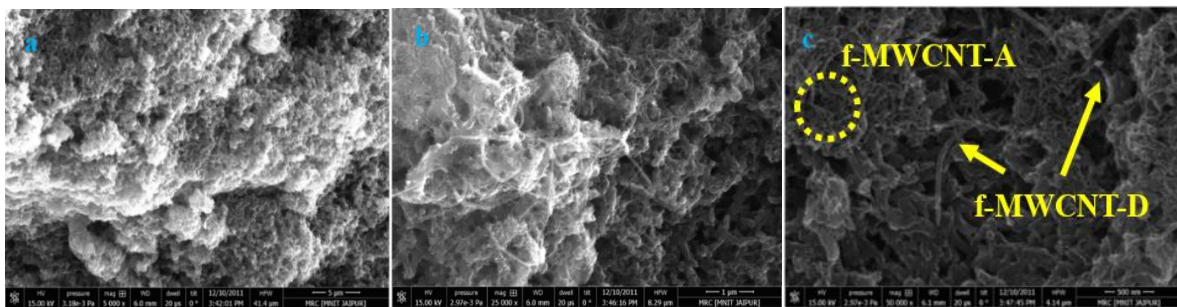
Figure 5.10: SEM images of f-MWCNTs (3.3 vol. %)/PANI nanocomposites at 5000X(a), 25000X (b) and 50000X (c) magnifications. [f-MWCNTs-D (dispersed) and f-MWCNTs-A (agglomerated)]

figure 5.12a. The obtained results from TEM were also in good agreement with the results available in the literature. It is able to understand that there is a synergistic action of PANI and f-MWCNTs and they can mutually improve the continuity and dispersion of the f-MWCNTs in the nanocomposites. The reason of the synergistic action is the interaction between f-MWCNTs and PANI, which can weaken the filler-filler or polymer-polymer

Intramolecular and Intermolecular interactions favorable to improve the dispersion of f-MWCNTs in PANI. **Figure 5.10 (a-c)** shows the SEM images of f-MWCNTs in f-MWCNTs (3.3vol %) /PANI nanocomposite at different magnifications. From these images, it illustrated that accumulation of f-MWCNTs on the surface of PANI nanofibers, or somewhere it gets through the polymer matrix. It was due to increase in concentration and different orientation of filler in PANI matrix. The segregation of carbon nanotube reduced the density of nanocomposites as explained above. The loading of f-MWCNTs in f-MWCNTs (13.9 vol %) /PANI nanocomposite at different magnifications [**figure 5.11 (a-b)**] shows that the fraction of
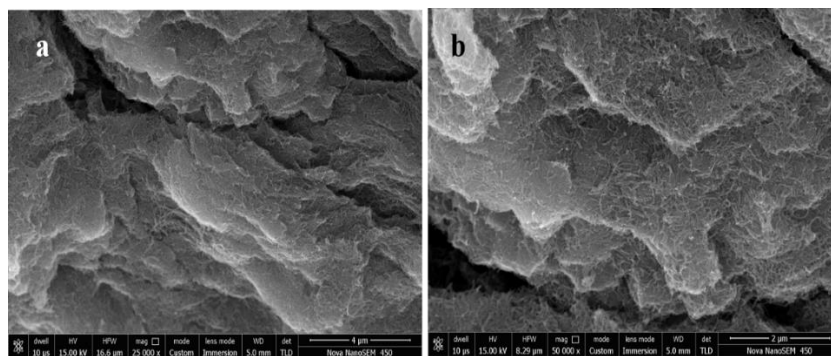
Figure 5.11: SEM images of f-MWCNTs (13.9 vol. %)/PANI nanocomposites at 25000X (a) and 50000X (b) magnifications
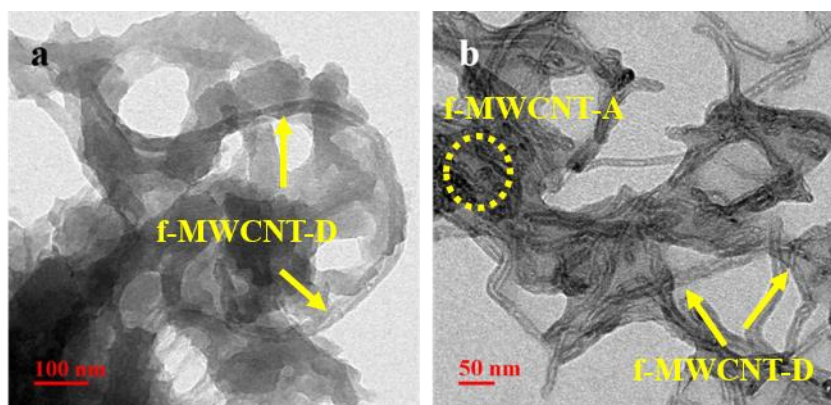
Figure 5.12: TEM images of f-MWCNTs (0.1 vol. %)/PANI(a) and f-MWCNTs (13.9 vol%)/PANI nanocomposites (b). [f-MWCNTs-D (dispersed) and f-MWCNTs-A (agglomerated)]

PANI reduced because of which f-MWCNTs can easily form the number of the connection between the conducting domains of PANI. The clear view of the connection of f-MWCNTs with PANI is depicted in TEM images **figure 5.12b**.The granular structure (obtained with

overgrowth) of dual morphology PANI transformed to the high yield fibrillar structure with the stirring process. This methodology is practically dissimilar from the prior efforts that focused on shaping PANI nanostructure. The literature shows this type of transformation (granular to fibrillar) via interfacial polymerization and rapidly mixed reaction. However, our study reveals a conversion of the granular structure of PANI into its fibrillar structure via solution mixing method. When the reaction carried out under stirring, the network of PANI nanofibers can saw with an irregular diameter which looks like the combination of many fibers **[see figure 5.12 (a, b)]**. Ghamdi *et al*. [213] reported the intermolecular hydrogen bonding between molecules of PANI and alcohol. They explained that such bonding made the polymeric chains enfolded by alcohol molecules, which inhibit the PANI nanofibers from aggregating together. The mechanical stirring breaks the intermolecular hydrogen bonding between polymeric chains and DMSO which leads to generating more embryonic nuclei on the surface of PANI fibers. The mechanical stirring boost the collision between embryonic nuclei and PANI fibers which may decline the activation energy of heterogeneous nucleation [214]. When nucleation takes place on the contact point of fibers, the nuclei at collision point will act as nanoscale glue to connect the fibers with each other. Qiu *et al.* [215]displayed the effect of stirring on the morphology of PANI and found the one-dimensional growth of PANI nanofibers.

5.10 Thermal Behaviour of Nanocomposites

The thermal stability of PANI, f-MWCNTs and hybrid f-MWCNTs/PANI nanocomposites examined under TGA shown in **figure 5.13.** In the case of f-MWCNTs, the first weight loss nearby 100 °C ascribed to the loss of water molecules. The steepest weight loss in the range of 200°C-300 °C represents the thermal degradation of carboxylic acid groups which were found on the side wall of MWCNTs [216]. The initial weight loss in PANI and f-MWCNTs/PANI nanocomposites up to 150 °C was due to loss of small amount of absorbed moisture and unreacted monomer [162]. The second weight loss was detected near about 300 °C attributed to the loss of dopant and low molecular weight oligomer. The third weight loss observed from 470 °C to 600 °C ascribed to the degradation and decomposition of backbone unit of PANI. The extent of weight loss for nanocomposites loaded with f-MWCNTs in PANI matrix found to be lower than for the PANI. The improved

thermal stability of nanocomposites about PANI can be noted specifically by onset temperature (T_{onset}) and decomposition temperature (T_d).
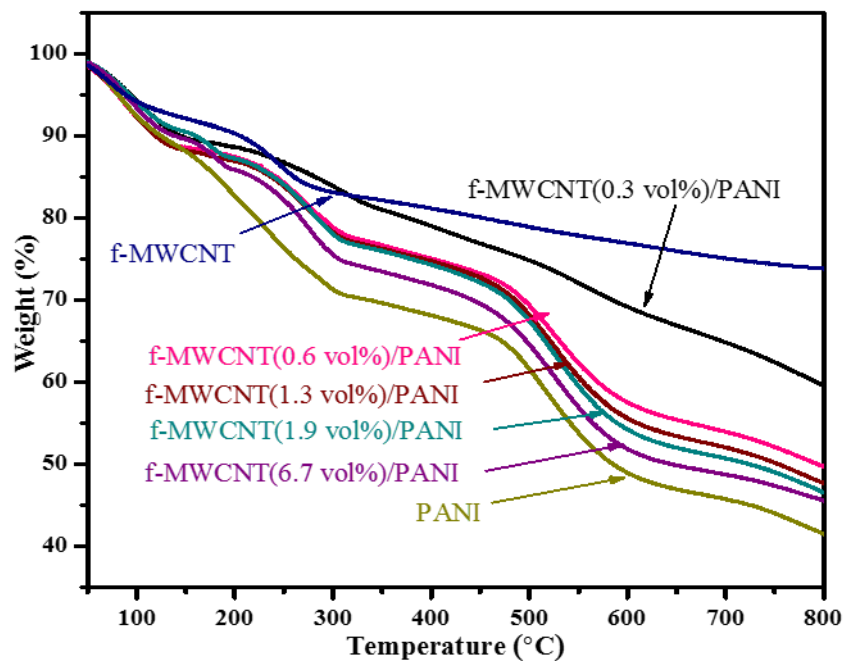
Figure 5.13: TGA of PANI, f-MWCNTs and hybrid f-MWCNTs/PANI nanocomposites

The onset temperature for f-MWCNTs and PANI were 215 °C and 478 °C respectively. For f-MWCNTs/PANI the onset temperature was observed to be at 535 °C (for 0.3 vol.% f-MWCNTs), 489 °C (for 0.6 vol.% f-MWCNTs), 487 °C (for 1.3 vol.% & 1.9 vol.% f-MWCNTs), and 480 °C (6.7 vol.% f-MWCNTs). The residual weight value at 800 °C and main decomposition temperature were 73.68% and 245 °C (for f-MWCNTs), 41.74% and 527 °C (PANI), 60.73% and 570 °C (0.3 vol.% f-MWCNTs), 49.95% and 538 °C (0.6 vol.% f-MWCNTs), 47.64% and 535 °C (1.3 vol.% f-MWCNTs), 46.61% and 535 °C (1.9 vol.% f-MWCNTs), and 45.58% and 536 °C (6.7 vol.% f-MWCNTs). **Figure 5.14** shows the graphical representation of TGA parameters (T_{onset}, T_d, and Char %).

From the above results; it was found that T_{onset} and T_d are much higher up to 0.3 vol. % of f-MWCNTs/PANI nanocomposites and not improved extensively beyond it. In this case, the temperature shift was found to be 57 °C (T_{onset}) and 43 °C. Moniruzzaman *et al.* [68] reported that MWCNTs (5 wt %)/PAN composite fibers show 24 °C shift in T_{onset} than those of pure PAN. The reason for higher thermal stability upto 0.3 vol. % f-MWCNTs could

ascribe to the obstruction of the flux of degradation product due to the interaction of f-MWCNTs with polymeric chains which results in delayed onset of degradation.
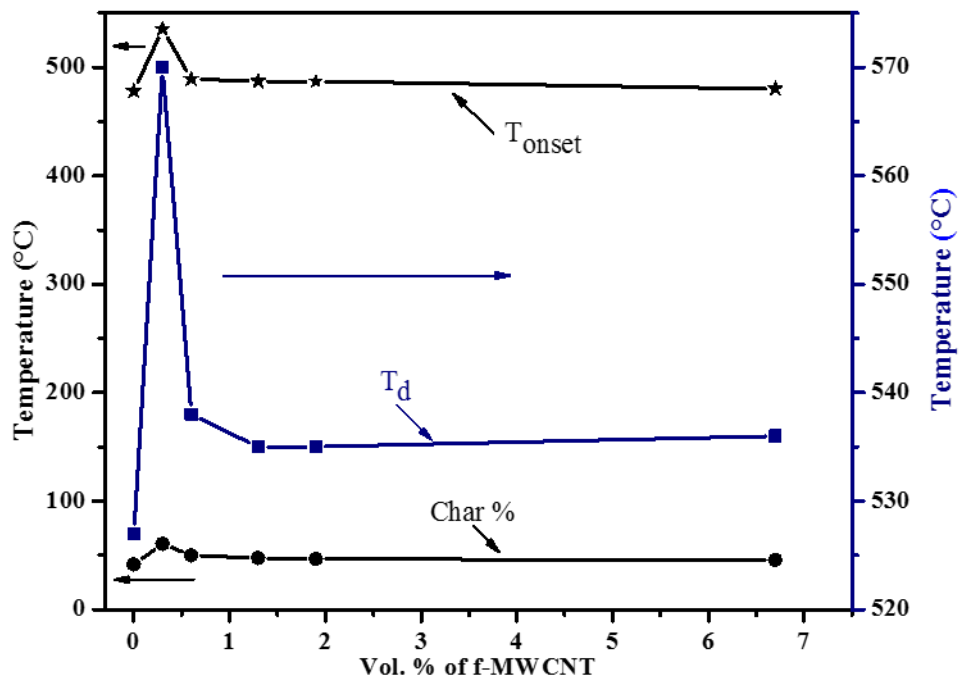
Figure 5.14: Graphical representation of TGA parameter (T_{onset}, T_d, and Char %) of PANI and hybrid f-MWCNTs/PANI nanocomposites

The slow degradation of polymer near the f-MWCNTs would shift T_{peak} toward higher temperature side. On the other hand, the higher content of f-MWCNTs started an adverse effect on the dispersion of f-MWCNTs. This effect occurred due to spatial hindrance enforced on f-MWCNTs by the nearby tubes. This worsening in the dispersion of f-MWCNTs would give rise to the dominance of undesirable effects like reducing the secondary bonding between polymeric chains. Therefore, there is no much difference in the thermal stability of f-MWCNTs/PANI nanocomposites at higher vol. % of f-MWCNTs compare to pure PANI.

The morphology and structure process-property correlation in case of PANI-based nanocomposites using f-MWCNTs as a filler in PANI matrix schematically shown in **figure 5.15.** Both, the electrical conductivity and estimated EMI shielding efficiency of the nanocomposites gradually increased irrespective of non-uniformly dispersed f-MWCNTs content due to the formation of more number of conducting bridge which generates path for

charge carrier to move. Based on present study it can be concluded that the prepared nanocomposite may be utilized as an EMI shielding plate and also in ESD applications.
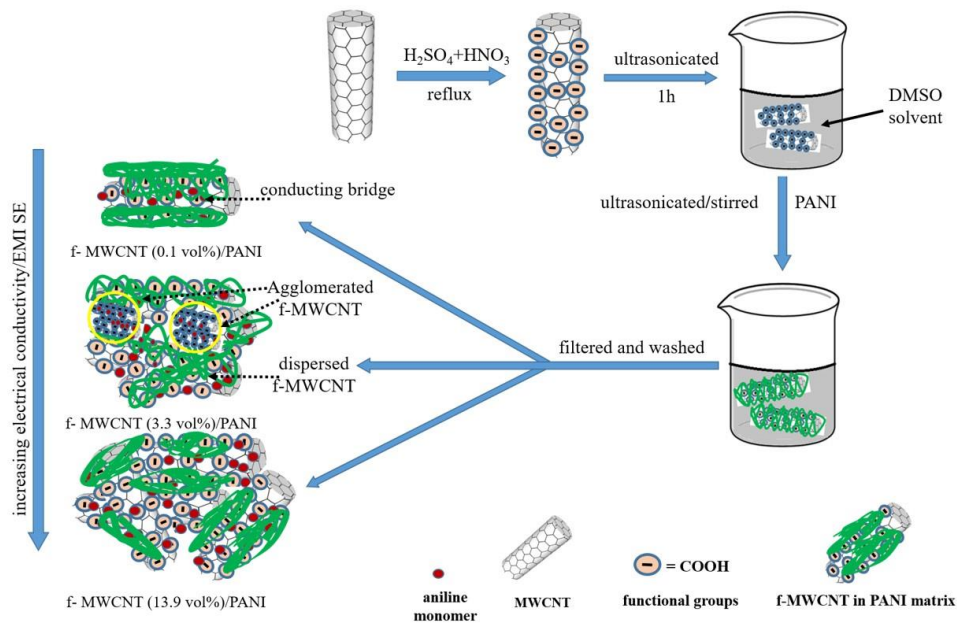
Figure 5.15: Schematic of preparation, morphological, structural and electrical property correlation of hybrid f-MWCNTs/PANI nanocomposites

An advance study is going on to explore the possibility of PANI-based nanocomposite as a potential EMI shielding material.

CHAPTER SIX

Self-Standing PANI Films

In this chapter, the structural, electrical and thermal analysis of two types of PANI films [PANI A (non-protonated) and PANI B (protonated)] discussed in detail. PANI B film has more crystallinity as compared to PANI A film. The electrical conductivity of PANI B film is slightly higher than that of PANI A. The morphological analysis of films reveals that PANI A has short fibers, however, PANI B has long fibers/bunch of fibers along with short fibers. The further study of these film is still going on.

===

The solution casting method was used to prepare self-standing films of PANI. The film dried in vacuum, after that treated with water. The obtained film was labeled as PANI A (non-protonated). The film treated with concentrated HCl labeled as PANI B (protonated). The prepared samples were characterized using XRD, FTIR, SEM, TGA techniques. Direct current electrical conductivity also measured with an electrometer.

6.1 Structural Study and Crystallinity Determination

XRD was carried out to confirm the effect of doping process on PANI crystallinity. **Figure 6.1** shows the XRD patterns of PANI A and PANI B film. A broad peak at 22.4° observed in the XRD pattern shows the amorphous nature of PANI A. The amorphous nature of PANI A was due to the non-conducting region consisting of disordered or folded polymeric chains. Zheng *et al.* [217] reported amorphous PANI film with NMP solvent without stretch or orientation of polymeric chains. The reason of non-ordering of polymeric chains in PANI A might be the higher boiling point of DMPU solvent. As films dried at 110 °C, It is believed that solvent could not evaporate which restrict the orientation of polymeric chains. It was reported that the crystalline phase formed in PANI with complete solvent evaporation because at same time polymeric chains get proper time for ordering [186]. It clearly appears from XRD data that PANI B has some crystallinity. The reason of higher crystallinity of PANI B than that of PANI A is the protonation with HCl dopant. The percent of crystallinity increased in PANI B film was about 10. The sharpness of the peak and high intensity indicate the degree of orientation of the polymer chains and population of the crystalline domain in amorphous region. The structure of polymeric chains depend upon the type of dopant used, which can contribute to increase or decrease in the crystallinity character of PANI [218]. In doping process, the participation of acids in polymeric chains create more
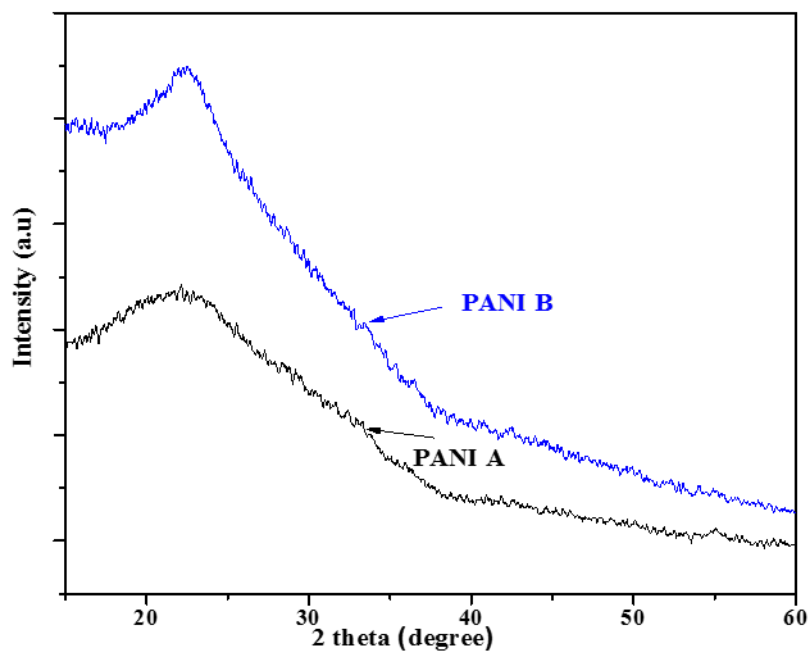
Figure 6.1: XRD patterns of PANI A and PANI B film

inter-chain space in bulk. When film dipped in concentrated hydrochloric acid, the dopant may get ordered in the polymeric chains which lead to increase the crystallinity of PANI film. FTIR spectra can confirm the presence of dopant which affects the crystallinity of PANI B.

6.2 Structural Study

The FTIR spectra was carried out to know the effect of dopant on the PANI films (**figure 6.2**). The band observed at 1590 and 1487 cm^{-1} assigned to the C=C stretching of quinoid and benzenoid rings of PANI, respectively [219]. The band observed at 1295 cm^{-1} confirmed the presence of C-N bending vibration in aromatic amines. The characteristic peaks at 1157 cm^{-1} attributed to the stretching mode of N=Q=N where Q represents the quinoid ring. The band at 1245 correspond to the C-N$^{+\cdot}$ stretching vibration in the polaron structure shows the existence of the conducting PANI. The vibrational bands typically of polymeric backbone in PANI A at 1590, 1487, 1295, 1157 and 830 cm^{-1} shifted to 1567, 1480, 1290, 1122 and 806 cm^{-1} after doping with HCl represents longer effective conjugation length. It also seems that the intensity of all peaks in PANI B are higher than that of PANI A. The reason of these combined effects are the increase of oscillator strengths to the backbone-

related vibrations owing to vibronic coupling with the pi electron charge oscillation along the chain [220]. For instant, the intensity of the peak at 1157 cm^{-1} rises significantly after doping which measures the degree of doping of the polymer backbone. MacDiarmid *et al.* [221] reported that the strong band at 1150 cm^{-1} ascribed as "electron-like band" measure the degree of electron delocalization and it considered as a characteristic peak of PANI conductivity.
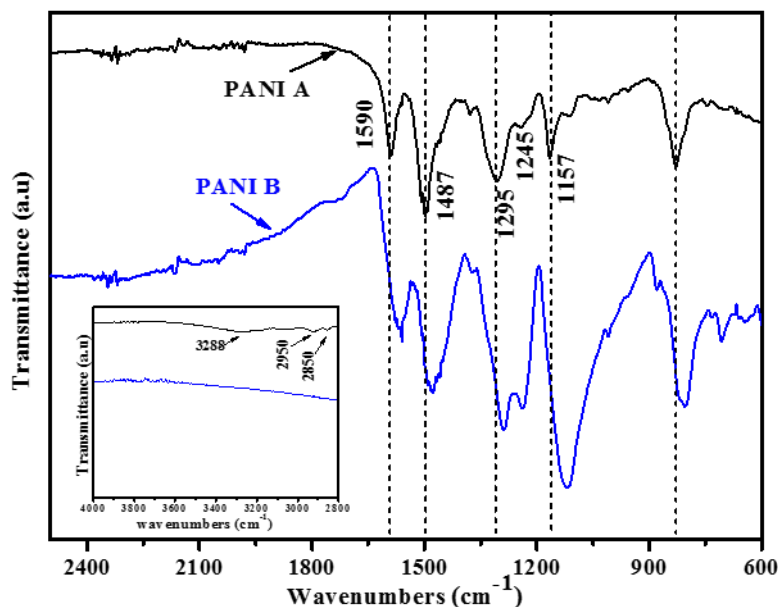
Figure 6.2. FTIR spectra of PANI A and PANI B film

It was interesting to note that in case of PANI A, the peak observed at 2850-2950 cm^{-1} and 3288 cm^{-1} (shown in the inset of **figure 6.2**) represents to sp^3 C-H stretch (in CH$_3$ and CH$_2$) of HPMI [222]. These newly appeared peaks were attributed to sp^2 and sp^3 originate from the reduced quinoid and the attached HPMI molecule.

6.3 Thermal Analysis

The thermograms of PANI A and PANI B films depicted in **figure 6.3**. The three-step weight loss found in TGA curve of the PANI films. The initial weight loss about 100°C could be assign to the loss of small amount of moisture and HPMI trapped in the PANI films. In case of PANI A, the second weight loss observed near about 260°C was attributed to the removal of DMPU because the boiling point of DMPU solvent is 246 °C. Whereas, PANI B shows second weight loss about 200 °C represents the loss of acid dopant bound to the polyaniline chain. XRD results also confirmed the presence of a dopant in polymeric chains.

It seems that third weight loss started close to 400°C is due to the degradation of the skeletal polyaniline chain structure after elimination of the dopant.The thermal stability of both PANI film can calculated from onset temperature (T_{onset}) and decomposition temperature (T_d). The onset temperature for PANI A and PANI B films were 448°C and 463°C, respectively. The
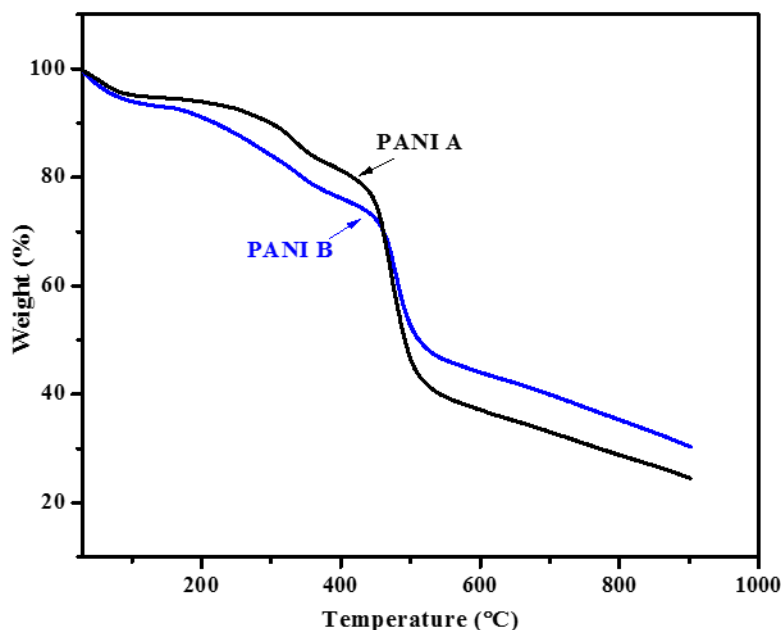
Figure 6.3. TGA curve of PANI A and PANI B film

main decomposition temperature and the residual weight value for PANI A and PANI B were 473°C and 38%, 486°C and 48% respectively. It has reported that higher the T_{onset} and T_d value higher will be the stability of the material. **Table 6.1** shows the T_{onset}, T_d and Char % of PANI A and PANI B.

Table 6.1: Calculation of onset temperature, decomposition temperature, and char percentage of the PANI A and PANI B

Material	Onset temperature (°C)	Decomposition temperature (°C)	Char%
PANI A	448	473	38%
PANI B	463	486	48%

It appears from TGA curve that PANI B has greater T_{onset}, T_d and Char % which indicates the higher stability of the film. The higher stability of PANI B was due to the

benzene segment of PANI. When films dipped into the dopant, this segment was condensed with HCl to produce chloride ion, as the –NH- bond is one of the weakest bonds and N atoms in benzene fragment is the more reactive atom in PANI chains. Palaniappan *et al.* [223] has reported that thermal stability of polyaniline in conducting form depends on the counter anion used during preparation.

6.4 Electrical Conductivity

The current-voltage characteristic of PANI A and PANI B films depicted in **figure 6.4**. The ohmic behavior of films may ascribe to the weak protonation of PANI when it was in powder form. However, the non-ohmic behavior of films can be explained with the conduction mechanism of PANI. In general, the electric current is not merely voted by electrons and holes as in semiconductor but also by the creation of polarons and bipolarons. As the applied voltage increase beyond 4 volts, it generates the polarons and bipolarons rapidly in the polymeric chains because of which electric current was increased sharply (**as shown in figure 6.4**). Bhadra *et al.* [224] reported that in heterogeneous system of PANI
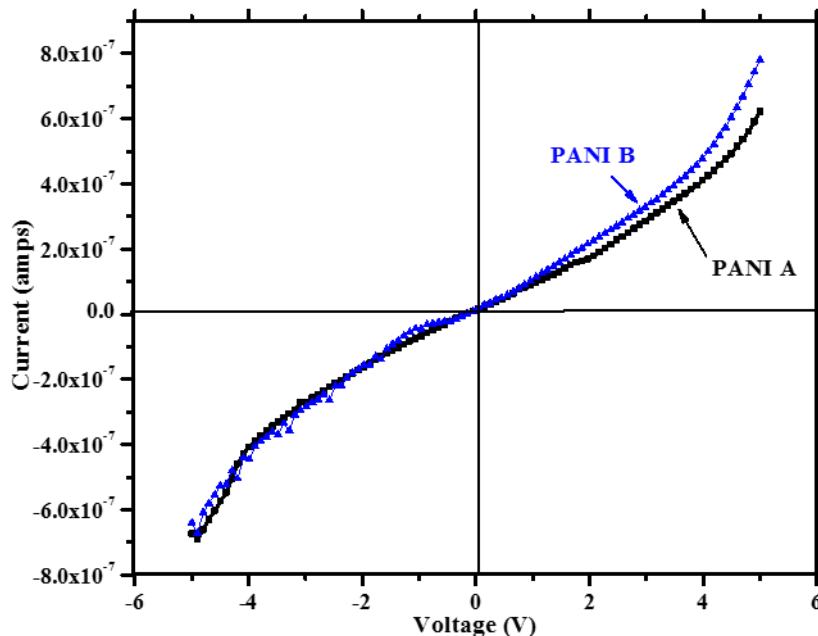
Figure 6.4: Current –voltage characteristic of PANI A and PANI B films

crystalline (ordered) region dispersed in an amorphous (disordered) region, the electrical conduction occurs through the electron delocalization or hopping of charge carrier due to an

ordered structure. The electrical conductivity of PANI A and PANI B up to 4 volts is 5.95 x 10^{-6} S/cm and 6.735 x 10^{-6} S/cm, respectively and beyond that, it is 7.29 x 10^{-6} S/cm and 8.45 x 10^{-6} S/cm. The high electrical conductivity of PANI B was due to its higher crystallinity compare to PANI A. The results are in good agreement with the crystallinity of PANIs (prepared with and without solvent). The low difference in conductivity after protonation of the film might be due to the tight coil conformation of PANI molecule when it mixed with DMPU solvent. In general, tight coil conformation takes place in the solid state, so the film is difficult to protonate completely.

The lower conductivity of PANI A compared to PANI B was due to the presence of secondary amine,i.e., HPMI in polymeric chains. HPMI is a nucleophilic agent with strong basicity (pKa= 11.2) have strong reactivity toward the PANI. The use of HPMI provide mechanical strength to the polymer but destroy the conjugated chains in the emeraldine base by quinoid ring substitution which reduce the chance of formation of polaron in polymeric chains. It has reported that the quinoid ring substitution in PANI leads to decrease its electrical conductivity. The mechanism of the reaction which shows the quinoid ring substitution depicted in **figure 6.5.** Another reason of very low electrical conductivity is the hydrolysis of the film which breaks the polymeric chain at –N=C bond as reported by Yang *et al.* [222].
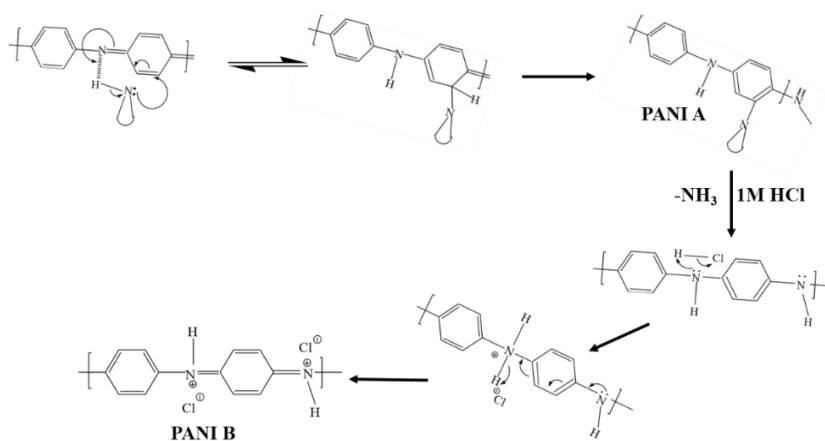
Figure 6.5: Mechanism of the reaction of PANI film formation.

It clearly seen from **figure 6.4** that the electrical conductivity of PANI B is higher than PANI A. The reason may have been the conduction in crystalline domains take place by the hopping of charge carrier through the polaron structure that made after the protonation of

PANI B with HCl. It has reported that conduction on the crystalline region or metallic region of PANI occurred though the hopping of charge carries [162]. On the other hand, the crystalline domains enclosed by an amorphous region or folded chains. Thus, the total electrical conductivity of the PANI B is subject to the bridging among the conductive regions.MacDiarmid *et al.*described in their report that degree of electron delocalization measured the higher electrical conductivity in PANI [221]. Higher crystallinity of PANI B as confirmed by XRD results also affect the electrical conductivity of polymer; higher crystallinity has the fewer number of defects in the polymer which lead to enhance in the electrical conductivity.

6.5 Morphological Analysis

A scanning electron microphotography of PANI A and PANI B films exposed in **figure 6.6, 6.7 and 6.8. Figure 6.6 (a, b)** shows the SEM images of PANI A at different magnifications. Its features are dense and hardly reported previously. However, the film with voids reported by many research groups [225]. The cross-sectional view of the PANI A shows that nanofibers of the polymer are broken and appeared like short fibers as indicated in **figure (6.6a and 6.6b)**. The reason of formation of short nanofibers might be due to attack of
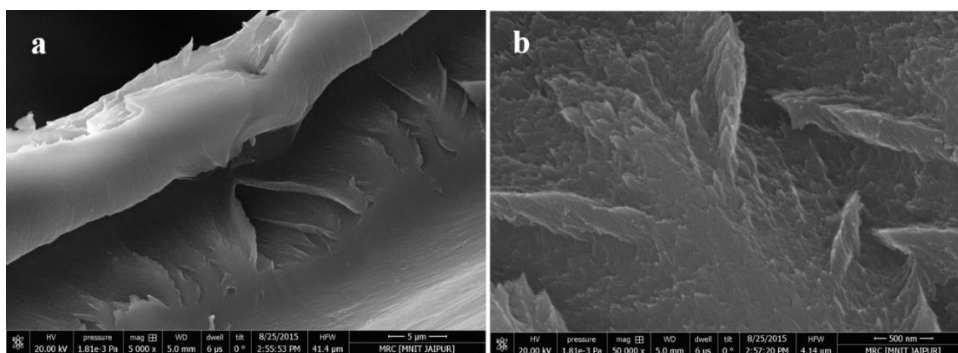
Figure 6.6: Cross-sectional SEM images of PANI A films at 5000X (a) and50000X (b) magnifications

HPMI on the quinoid ring of PANI A which destroy the conjugation system of bond in the polymeric chains. The structural integrity in PANI A may lead to forming the short fibers. Rather the observed morphology of films do not have any micro-void so it could have high electrical conductivity but due to loss of conjugation in PANI, its electrical conductivity may lose or decreased. In case of PANI B (**figure 6.7a and 6.7b**), it seems to be very interesting

from SEM image that along with short fibers the bunch of long fibers was also formed. The bunch of these fibers leads to a "lamellar-like" structure having no crossed linked network of fibers (**figure 6.7b**). The reason of getting a lamellar-like arrangement of fibers was the protonation of the film with concentrated hydrochloric acid. Abdiryim *et al.* and Sniechowski *et al.* reported that the doping of PANI with acid forms the fibers of polymer with lamellar
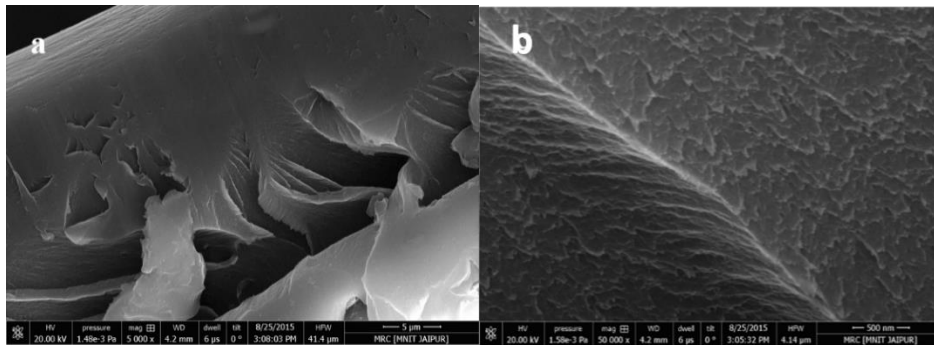
Figure 6.7: Cross-sectional SEM images of PANI B films at 5000X(a), and50000X (b)magnifications
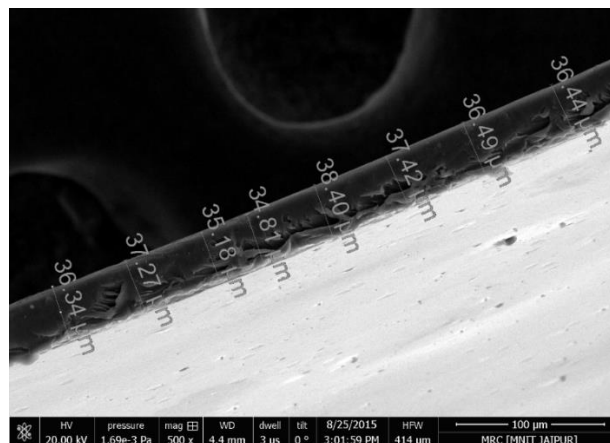
Figure 6.8: Cross-sectional SEM image of PANI B film

structure [226, 227]. The formation of long range bunched fibers after acid treatment increase the electrical conductivity of PANI B film. The average thickness of PANI A and PANI B films was approximately 35 micron. **Figure 6.8** shows the cross-sectional view of SEM image of PANIB film.

CHAPTER SEVEN

Conclusions and Future Work

This chapter concludes the synthesis and characterizations of PANIs powder (i.e., PANI 1, PANI 1VD, PANI 2 and PANI 2 VD), f-MWCNTs, hybrid f-MWCNTs/PANI nanocomposites and self-standing film of PANI (i.e., PANI A and PANI B). The overall outcomes of the materials after characterizations discussed in this section.

CHAPTER SEVEN   *Conclusions and Future Work*

===

The research work on synthesis and structure-electrical properties correlation of PANI and hybrid PANI/CNT nanocomposite has been successfully carried out. Based on the findings from density measurements, XRD analysis, FTIR spectroscopy, Raman spectroscopy electrical measurements, microscopic studies, TGA analysis and UV-Vis spectroscopy the following conclusions can be made.

- PANIs powder with (PANI 1) and without (PANI 2) solvent have successfully synthesized via chemical oxidative polymerization and solid state oxidative polymerization, respectively. The prepared PANIsfurther dried under vacuum named as PANI 1VD and PANI 2VD.

- The mixed (fibrillar and granular) morphology of PANI (with solvent) obtained via chemical oxidative polymerization. However, granular morphology obtained via solid state oxidative polymerization (without solvent).

- Functionalization of pristine MWCNTs done with covalent functionalization through which –COOH group attached on the surface of MWCNTs.

- The electrical conductivity of PANI (fibrillar and granular morphology) prepared with solvent was greater than that prepared without solvent due to high crystallinity and presence of nanofibers. The resistance experienced by the charge carriers in fibrillar morphology would be lesser than that experience in the granular morphology,i.e., in PANI prepared without solvent.

- Among all synthesized PANIs, PANI 1VD selected for further preparing hybrid MWCNTs/PANI nanocomposites with different filler loading via solution mixing method. PANI 1VD was also processed by solution casting method to prepare a self-standing film of pure PANI.
- The experimental densities of hybrid MWCNTs/PANI nanocomposites were very close to theoretical densities up to 3.3 vol% of f-MWCNTs loading. However, at high

loadings beyond 3.3 vol%, the experimental density was found to be lower than the theoretical densities which might be due to the agglomeration of CNT which hinders the infiltration of the polymer during processing.

- XRD study confirmed that pure PANIs, prepared with solvent, has a higher percent of crystallinity. It was due to the orientation of polymeric chains during solution evaporation. With increasing the loading of fillers in PANI matrix, the crystallinity of nanocomposites further increased. The study also confirmed that PANI B film has more crystallinity than that of PANI A film.

- TGA confirmed that vacuum dried PANIs have a lower content of moisture than that of air dried PANIs. In case of hybrid nanocomposites, it seems that the thermal stability of PANI was increased up to 0.3 vol. % of f-MWCNTs loading. However, there was no much difference in thermal stability at high filler loading.

- In hybrid nanocomposites, percolation threshold obtained at 0.1 vol. % f-MWCNTs and the maximum achieved electrical conductivity was 10^{-1}S/cm. By electrical conductivity, the estimated EMI shielding of nanocomposites at 3.3 vol. % of f-MWCNTs and beyond it was found to be 12 dB.

- The prepared hybrid MWCNTs/PANI nanocomposites have a maximum electrical conductivity of 0.1 S/cm, which is a good level of electrical conductivity for electromagnetic interference (EMI) shielding. Hence, the prepared hybrid nanocomposites could be suggested for electromagnetic interference (EMI) shielding/electrostatic dissipation (ESD) applications.

Future Work

Based on the present study, the following work on PANI and hybrid f-MWCNTs/PANI nanocomposites could be done in the future

- ➕ The dielectric study (dielectric constant, dissipation factor and their variation with frequency and temperature) of f-MWCNTs/PANI nanocomposites can be done in future.

- ➕ Based on f-MWCNTs/PANI nanocomposites, more nanocomposites system can be prepared using other suitable filler materials such as graphite flakes, graphene/graphene oxide for further study.

- ➕ Experimental study for EMI shielding for f-MWCNTs/PANI nanocomposites can be done.

- ➕ More suitable gel-inhibitors can be used for the preparation of the self-standing film of pure PANI which can provide mechanical strength without destroying the conjugated system of PANI.

- ➕ More detailed study on the self-standing film of PANI based nanocomposite can be done in future.

References

[1] Kumar A, Kumar V, Awasthi K. Polyaniline-Carbon Nanotube Composites: Preparation Methods, Properties and Applications. Polymer-Plastics Technology and Engineering. 2017:null-null.

[2] Yang D, Zuccarello G, Mattes BR. Physical Stabilization or Chemical Degradation of Concentrated Solutions of Polyaniline Emeraldine Base Containing Secondary Amine Additives. Macromolecules. 2002;35:5304-13.

[3] Saini P, Arora M, Gupta G, Gupta BK, Singh VN, Choudhary V. High permittivity polyaniline–barium titanate nanocomposites with excellent electromagnetic interference shielding response. Nanoscale. 2013;5:4330-6.

[4] Baker CO, Huang X, Nelson W, Kaner RB. Polyaniline nanofibers: broadening applications for conducting polymers. Chemical Society Reviews. 2017;46:1510-25.

[5] Chauhan AK, Gupta SK, Taguchi D, Manaka T, Jha P, Veerender P, et al. Enhancement of the carrier mobility of conducting polymers by formation of their graphene composites. RSC Advances. 2017;7:11913-20.

[6] Zhang Q, Esrafilzadeh D, Crook JM, Kapsa R, Stewart EM, Tomaskovic-Crook E, et al. Electrical Stimulation Using Conductive Polymer Polypyrrole Counters Reduced Neurite Outgrowth of Primary Prefrontal Cortical Neurons from NRG1-KO and DISC1-LI Mice. Scientific Reports. 2017;7:42525.

[7] Lu X, Zhang W, Wang C, Wen T-C, Wei Y. One-dimensional conducting polymer nanocomposites: Synthesis, properties and applications. Progress in Polymer Science. 2011;36:671-712.

[8] Schoch KF. Update on electrically conductive polymers and their applications. IEEE Electrical Insulation Magazine. 1994;10:29-32.

[9] Angelopoulos M. Conducting polymers in microelectronics. IBM J Res Dev. 2001;45:57-75.

[10] Bhadra S, Chattopadhyay S, Singha NK, Khastgir D. Improvement of conductivity of electrochemically synthesized polyaniline. Journal of Applied Polymer Science. 2008;108:57-64.

[11] Bhadra S, Singha NK, Khastgir D. Polyaniline by new miniemulsion polymerization and the effect of reducing agent on conductivity. Synthetic Metals. 2006;156:1148-54.

[12] Wei Y, Jang G-W, Hsueh KF, Scherr EM, MacDiarmid AG, Epstein AJ. Thermal transitions and mechanical properties of films of chemically prepared polyaniline. Polymer. 1992;33:314-22.

[13] Lu W-K, Elsenbaumer RL, Wessling B. Proceedings of the International Conference on Science and Technology of Synthetic Metals (ICSM '94)Corrosion protection of mild steel by coatings containing polyaniline. Synthetic Metals. 1995;71:2163-6.

[14] Fahlman M, Jasty S, Epstein AJ. Corrosion protection of iron/steel by emeraldine base polyaniline: an X-ray photoelectron spectroscopy study. Synthetic Metals. 1997;85:1323-6.

[15] Joo J, Epstein AJ. Electromagnetic radiation shielding by intrinsically conducting polymers. Applied Physics Letters. 1994;65:2278-80.

[16] Desilvestro J, Scheifele W, Haas O. In situ determination of gravimetric and volumetric charge densities of battery electrodes polyaniline in aqueous and nonaqueous electrolytes. Journal of the electrochemical society. 1992;139:2727-36.

[17] Palaniappan S, John A. Polyaniline materials by emulsion polymerization pathway. Progress in Polymer Science. 2008;33:732-58.

[18] Chaudhari HK, Kelkar DS. Investigation of Structure and Electrical Conductivity in Doped Polyaniline. Polymer International. 1997;42:380-4.

[19] Anderson MR, Mattes BR, Reiss H, Kaner RB. Conjugated polymer films for gas separations. Science. 1991;252:1412-5.

[20] Mehwish N, Kausar A, Siddiq M. Polyvinylidenefluoride/Poly(styrene-butadiene-styrene)/Silver Nanoparticle-grafted-Acid Chloride Functional MWCNTs-Based Nanocomposites: Preparation and Properties. Polymer-Plastics Technology and Engineering. 2015;54:474-83.

[21] Baughman RH, Zakhidov AA, de Heer WA. Carbon Nanotubes--the Route Toward Applications. Science. 2002;297:787-92.

[22] Thostenson ET, Ren Z, Chou T-W. Advances in the science and technology of carbon nanotubes and their composites: a review. Composites Science and Technology. 2001;61:1899-912.

[23] Dai L, Mau AWH. Controlled Synthesis and Modification of Carbon Nanotubes and C60: Carbon Nanostructures for Advanced Polymeric Composite Materials. Advanced Materials. 2001;13:899-913.

[24] Hirsch A. Functionalization of Single-Walled Carbon Nanotubes. Angewandte Chemie International Edition. 2002;41:1853-9.

[25] Bahr JL, Tour JM. Covalent chemistry of single-wall carbon nanotubes. Journal of Materials Chemistry. 2002;12:1952-8.

[26] Andrews R, Jacques D, Qian D, Rantell T. Multiwall Carbon Nanotubes: Synthesis and Application. Accounts of Chemical Research. 2002;35:1008-17.

[27] Fischer JE. Chemical Doping of Single-Wall Carbon Nanotubes. Accounts of Chemical Research. 2002;35:1079-86.

[28] Niyogi S, Hamon MA, Hu H, Zhao B, Bhowmik P, Sen R, et al. Chemistry of Single-Walled Carbon Nanotubes. Accounts of Chemical Research. 2002;35:1105-13.

[29] Spinks GM, Mottaghitalab V, Bahrami-Samani M, Whitten PG, Wallace GG. Carbon-Nanotube-Reinforced Polyaniline Fibers for High-Strength Artificial Muscles. Advanced Materials. 2006;18:637-40.

[30] Sariciftci NS, Smilowitz L, Heeger AJ, Wudl F. Photoinduced Electron Transfer from a Conducting Polymer to Buckminsterfullerene. Science. 1992;258:1474-6.

[31] Diaz AF, Logan JA. Electroactive polyaniline films. Journal of Electroanalytical Chemistry and Interfacial Electrochemistry. 1980;111:111-4.

[32] Genies EM, Syed AA, Tsintavis C. Electrochemical Study Of Polyaniline In Aqueous And Organic Medium. Redox And Kinetic Properties. Molecular Crystals and Liquid Crystals. 1985;121:181-6.

[33] Gupta V, Miura N. High performance electrochemical supercapacitor from electrochemically synthesized nanostructured polyaniline. Materials Letters. 2006;60:1466-9.

[34] Karami H, Asadi MG, Mansoori M. Pulse electropolymerization and the characterization of polyaniline nanofibers. Electrochimica Acta. 2012;61:154-64.

[35] Kobayashi N, Teshima K, Hirohashi R. Conducting polymer image formation with photoinduced electron transfer reaction. Journal of Materials Chemistry. 1998;8:497-506.

[36] Teshima K, Yamada K, Kobayashi N, Hirohashi R. Photopolymerization of aniline with a tris(2,2[prime or minute]-bipyridyl)ruthenium complex-methylviologen polymer bilayer electrode system. Chemical Communications. 1996:829-30.

[37] de Barros RA, de Azevedo WM, de Aguiar FM. Photo-induced polymerization of polyaniline. Materials Characterization. 2003;50:131-4.

[38] Xie A, Tao F, Sun W, Li Y, Jiang C, Hu L, et al. Design and Synthesis of Graphene/Porous Polyaniline Nanocomposite Using Attapulgite as Template for High-Performance Supercapacitors. Journal of The Electrochemical Society. 2017;164:H70-H7.

[39] Nguyen DN, Yoon H. Recent advances in nanostructured conducting polymers: from synthesis to practical applications. Polymers. 2016;8:118.

[40] Martin CR. Template Synthesis of Electronically Conductive Polymer Nanostructures. Accounts of Chemical Research. 1995;28:61-8.

[41] Choi J, Kim SJ, Lee J, Lim JH, Lee SC, Kim KJ. Controlled self-assembly of nanoporous alumina for the self-templating synthesis of polyaniline nanowires. Electrochemistry Communications. 2007;9:971-5.

[42] Wang C, Wang Z, Li M, Li H. Well-aligned polyaniline nano-fibril array membrane and its field emission property. Chemical Physics Letters. 2001;341:431-4.

[43] Wu C-G, Bein T. Conducting Polyaniline Filaments in a Mesoporous Channel Host. Science. 1994;264:1757-9.

[44] X. Zheng Z, Y. Xi Y, Dong P, G. Huang H, Z. Zhou J, L. Wu L, et al. The enhanced photoluminescence of zinc oxide and polyaniline coaxial nanowire arrays in anodic oxide aluminium membranes. PhysChemComm. 2002;5:63-5.

[45] Nabid MR, Asadi S, Sedghi R, Bayandori Moghaddam A. Chemical and Enzymatic Polymerization of Polyaniline/Ag Nanocomposites. Chemical Engineering & Technology. 2013;36:1411-6.

[46] Kojima K, Yamauchi T, Shimomura M, Miyauchi S. Covalent immobilization of glucose oxidase on poly[1-(2-carboxyethyl)pyrrole] film for glucose sensing. Polymer. 1998;39:2079-82.

[47] Sharma AL, Singhal R, Kumar A, Rajesh, Pande KK, Malhotra BD. Immobilization of glucose oxidase onto electrochemically prepared poly(aniline-co-fluoroaniline) films. Journal of Applied Polymer Science. 2004;91:3999-4006.

[48] Lakard B, Herlem G, Lakard S, Antoniou A, Fahys B. Urea potentiometric biosensor based on modified electrodes with urease immobilized on polyethylenimine films. Biosensors and Bioelectronics. 2004;19:1641-7.

[49] Nakaminami T, Ito S-i, Kuwabata S, Yoneyama H. Uricase-catalyzed oxidation of uric acid using an artificial electron acceptor and fabrication of amperometric uric acid sensors with use of a redox ladder polymer. Analytical chemistry. 1999;71:1928-34.

[50] Rajesh, Kaneto K. A new tyrosinase biosensor based on covalent immobilization of enzyme on N-(3-aminopropyl) pyrrole polymer film. Current Applied Physics. 2005;5:178-83.

[51] Kobayashi S, Uyama H, Kimura S. Enzymatic polymerization. Chem Rev. 2001;101:3793-818.

[52] Mejias L, Reihmann MH, Sepulveda-Boza S, Ritter H. New Polymers from Natural Phenols Using Horseradish or Soybean Peroxidase. Macromolecular Bioscience. 2002;2:24-32.

[53] McEldoon JP, Dordick JS. Unusual Thermal Stability of Soybean Peroxidase. Biotechnology Progress. 1996;12:555-8.

[54] Nagarajan R, Tripathy S, Kumar J, Bruno FF, Samuelson L. An Enzymatically Synthesized Conducting Molecular Complex of Polyaniline and Poly(vinylphosphonic acid). Macromolecules. 2000;33:9542-7.

[55] Liu W, Cholli AL, Nagarajan R, Kumar J, Tripathy S, Bruno FF, et al. The role of template in the enzymatic synthesis of conducting polyaniline. Journal of the American Chemical Society. 1999;121:11345-55.

[56] Nagarajan R, Liu W, Kumar J, Tripathy SK, Bruno FF, Samuelson LA. Manipulating DNA conformation using intertwined conducting polymer chains. Macromolecules. 2001;34:3921-7.

[57] Stejskal J, Spirkova M, Riede A, Helmstedt M, Mokreva P, Prokes J. Polyaniline dispersions 8. The control of particle morphology. Polymer. 1999;40:2487-92.

[58] Park C-S, Kim DY, Kim DH, Lee H-K, Shin BJ, Tae H-S. Humidity-independent conducting polyaniline films synthesized using advanced atmospheric pressure plasma polymerization with in-situ iodine doping. Applied Physics Letters. 2017;110:033502.

[59] Cruz GJ, Morales J, Castillo-Ortega MM, Olayo R. Synthesis of polyaniline films by plasma polymerization. Synthetic Metals. 1997;88:213-8.

[60] Nastase C, Nastase F, Dumitru A, Ionescu M, Stamatin I. Thin film composites of nanocarbons-polyaniline obtained by plasma polymerization technique. Composites Part A: Applied Science and Manufacturing. 2005;36:481-5.

[61] Nastase F, Stamatin I, Nastase C, Mihaiescu D, Moldovan A. Synthesis and characterization of PAni–SiO2 and PTh–SiO2 nanocomposites' thin films by plasma polymerization. Progress in Solid State Chemistry. 2006;34:191-9.

[62] Abu-Thabit NY. Chemical Oxidative Polymerization of Polyaniline: A Practical Approach for Preparation of Smart Conductive Textiles. Journal of Chemical Education. 2016;93:1606-11.

[63] Sapurina IY, Stejskal J. Oxidation of aniline with strong and weak oxidants. Russian Journal of General Chemistry. 2012;82:256-75.

[64] Liu D, Wang X, Deng J, Zhou C, Guo J, Liu P. Crosslinked Carbon Nanotubes/Polyaniline Composites as a Pseudocapacitive Material with High Cycling Stability. Nanomaterials. 2015;5:1034-47.

[65] Katoch A, Burkhart M, Hwang T, Kim SS. Synthesis of polyaniline/TiO 2 hybrid nanoplates via a sol–gel chemical method. Chemical engineering journal. 2012;192:262-8.

[66] Kumar A, Jangir LK, Kumari Y, Kumar M, Kumar V, Awasthi K. Electrical behavior of dual-morphology polyaniline. Journal of Applied Polymer Science. 2016;133:n/a-n/a.

[67] Zhang Q, Wang W, Li J, Zhu J, Wang L, Zhu M, et al. Preparation and thermoelectric properties of multi-walled carbon nanotube/polyaniline hybrid nanocomposites. Journal of Materials Chemistry A. 2013;1:12109-14.

[68] Moniruzzaman M, Winey KI. Polymer nanocomposites containing carbon nanotubes. Macromolecules. 2006;39:5194-205.

[69] Charrier G, Desrues A, Barchasz C, Leroy J, Cornut R, Jousselme B, et al. Covalently functionalized carbon nanotubes as stable cathode materials of lithium/organic batteries. Journal of Materials Chemistry A. 2016;4:15036-40.

[70] Park H, Zhao J, Lu JP. Effects of Sidewall Functionalization on Conducting Properties of Single Wall Carbon Nanotubes. Nano Letters. 2006;6:916-9.

[71] Cho JW, Kim JW, Jung YC, Goo NS. Electroactive Shape-Memory Polyurethane Composites Incorporating Carbon Nanotubes. Macromolecular Rapid Communications. 2005;26:412-6.

[72] Georgakilas V, Kordatos K, Prato M, Guldi DM, Holzinger M, Hirsch A. Organic Functionalization of Carbon Nanotubes. Journal of the American Chemical Society. 2002;124:760-1.

[73] Chen J, Rao AM, Lyuksyutov S, Itkis ME, Hamon MA, Hu H, et al. Dissolution of Full-Length Single-Walled Carbon Nanotubes. The Journal of Physical Chemistry B. 2001;105:2525-8.

[74] Vasiliev I, Curran SA. Cross linking of thiolated carbon nanotubes: An ab initio study. Journal of Applied Physics. 2007;102:024317.

[75] Mickelson ET, Huffman CB, Rinzler AG, Smalley RE, Hauge RH, Margrave JL. Fluorination of single-wall carbon nanotubes. Chemical Physics Letters. 1998;296:188-94.

[76] Tasis D, Tagmatarchis N, Bianco A, Prato M. Chemistry of Carbon Nanotubes. Chemical Reviews. 2006;106:1105-36.

[77] Bahr JL, Mickelson ET, Bronikowski MJ, Smalley RE, Tour JM. Dissolution of small diameter single-wall carbon nanotubes in organic solvents? Chemical Communications. 2001:193-4.

[78] Holzinger M, Vostrowsky O, Hirsch A, Hennrich F, Kappes M, Weiss R, et al. Sidewall Functionalization of Carbon Nanotubes. Angewandte Chemie International Edition. 2001;40:4002-5.

[79] Kim B-H, Lee K-R, Chung Y-C, Park M. Functionalization effect on a Pt/carbon nanotube composite catalyst: a first-principles study. Physical Chemistry Chemical Physics. 2016;18:22687-92.

[80] Mawhinney DB, Naumenko V, Kuznetsova A, Yates Jr JT, Liu J, Smalley RE. Surface defect site density on single walled carbon nanotubes by titration. Chemical Physics Letters. 2000;324:213-6.

[81] Hu H, Bhowmik P, Zhao B, Hamon MA, Itkis ME, Haddon RC. Determination of the acidic sites of purified single-walled carbon nanotubes by acid–base titration. Chemical Physics Letters. 2001;345:25-8.

[82] Xie X-L, Mai Y-W, Zhou X-P. Dispersion and alignment of carbon nanotubes in polymer matrix: A review. Materials Science and Engineering: R: Reports. 2005;49:89-112.

[83] Mallakpour S, Soltanian S. Surface functionalization of carbon nanotubes: fabrication and applications. RSC Advances. 2016;6:109916-35.

[84] S. Duesberg G, Burghard M, Muster J, Philipp G. Separation of carbon nanotubes by size exclusion chromatography. Chemical Communications. 1998:435-6.

[85] Richard C, Balavoine F, Schultz P, Ebbesen TW, Mioskowski C. Supramolecular Self-Assembly of Lipid Derivatives on Carbon Nanotubes. Science. 2003;300:775.

[86] Guo Z, Sadler PJ, Tsang SC. Immobilization and Visualization of DNA and Proteins on Carbon Nanotubes. Advanced Materials. 1998;10:701-3.

[87] Chen RJ, Zhang Y, Wang D, Dai H. Noncovalent Sidewall Functionalization of Single-Walled Carbon Nanotubes for Protein Immobilization. Journal of the American Chemical Society. 2001;123:3838-9.

[88] Cheng F, Imin P, Maunders C, Botton G, Adronov A. Soluble, Discrete Supramolecular Complexes of Single-Walled Carbon Nanotubes with Fluorene-Based Conjugated Polymers. Macromolecules. 2008;41:2304-8.

[89] Curran SA, Ajayan PM, Blau WJ, Carroll DL, Coleman JN, Dalton AB, et al. A Composite from Poly(m-phenylenevinylene-co-2,5-dioctoxy-p-phenylenevinylene) and Carbon Nanotubes: A Novel Material for Molecular Optoelectronics. Advanced Materials. 1998;10:1091-3.

[90] Coleman JN, Dalton AB, Curran S, Rubio A, Davey AP, Drury A, et al. Phase Separation of Carbon Nanotubes and Turbostratic Graphite Using a Functional Organic Polymer. Advanced Materials. 2000;12:213-6.

[91] Shvartzman-Cohen R, Nativ-Roth E, Baskaran E, Levi-Kalisman Y, Szleifer I, Yerushalmi-Rozen R. Selective Dispersion of Single-Walled Carbon Nanotubes in the Presence of Polymers: the Role of Molecular and Colloidal Length Scales. Journal of the American Chemical Society. 2004;126:14850-7.

[92] Dhand C, Arya SK, Singh SP, Singh BP, Datta M, Malhotra BD. Preparation of polyaniline/multiwalled carbon nanotube composite by novel electrophoretic route. Carbon. 2008;46:1727-35.

[93] Dhand C, Solanki PR, Datta M, Malhotra BD. Polyaniline/Single-Walled Carbon Nanotubes Composite Based Triglyceride Biosensor. Electroanalysis. 2010;22:2683-93.

[94] Bachhav S, Patil D. Synthesis and characterization of polyaniline-multiwalled carbon nanotube nanocomposites and its electrical percolation behavior. American Journal of Materials Science. 2015;5:90-5.

[95] Konyushenko EN, Stejskal J, Trchová M, Hradil J, Kovářová J, Prokeš J, et al. Multi-wall carbon nanotubes coated with polyaniline. Polymer. 2006;47:5715-23.

[96] Choudhury A, Kar P. Doping effect of carboxylic acid group functionalized multi-walled carbon nanotube on polyaniline. Composites Part B: Engineering. 2011;42:1641-7.

[97] Philip B, Xie J, Abraham JK, Varadan VK. Polyaniline / carbon nanotube composites: starting with phenylamino functionalized carbon nanotubes. Polymer Bulletin. 2005;53:127-38.

[98] Wei Z, Wan M, Lin T, Dai L. Polyaniline Nanotubes Doped with Sulfonated Carbon Nanotubes Made Via a Self-Assembly Process. Advanced Materials. 2003;15:136-9.

[99] Bhattacharya M. Polymer nanocomposites—a comparison between carbon nanotubes, graphene, and clay as nanofillers. Materials. 2016;9:262.

[100] Huang J, Kaner RB. Nanofiber Formation in the Chemical Polymerization of Aniline: A Mechanistic Study. Angewandte Chemie International Edition. 2004;43:5817-21.

[101] Huang J, Virji S, Weiller BH, Kaner RB. Polyaniline Nanofibers: Facile Synthesis and Chemical Sensors. Journal of the American Chemical Society. 2003;125:314-5.

[102] Huang J, Kaner RB. A General Chemical Route to Polyaniline Nanofibers. Journal of the American Chemical Society. 2004;126:851-5.

[103] Jeon I-Y, Tan L-S, Baek J-B. Synthesis and electrical properties of polyaniline/polyaniline grafted multiwalled carbon nanotube mixture via in situ static interfacial polymerization. Journal of Polymer Science Part A: Polymer Chemistry. 2010;48:1962-72.

[104] Mariano LC, Salvatierra RV, Cava CE, Koehler M, Zarbin AJG, Roman LS. Electrical Properties of Self-Assembled Films of Polyaniline/Carbon Nanotubes Composites. The Journal of Physical Chemistry C. 2014;118:24811-8.

[105] Salvatierra RV, Moura LG, Oliveira MM, Pimenta MA, Zarbin AJG. Resonant Raman spectroscopy and spectroelectrochemistry characterization of carbon nanotubes/polyaniline thin film obtained through interfacial polymerization. Journal of Raman Spectroscopy. 2012;43:1094-100.

[106] Sen T, Mishra S, Shimpi NG. Synthesis and sensing applications of polyaniline nanocomposites: a review. RSC Advances. 2016;6:42196-222.

[107] Chen L, Pang X-J, Qu M-Z, Zhang Q-t, Wang B, Zhang B-L, et al. Fabrication and characterization of polycarbonate/carbon nanotubes composites. Composites Part A: Applied Science and Manufacturing. 2006;37:1485-9.

[108] Li Y, Wang Y, Wu D, Jing X. Effects of ultrasonic irradiation on the morphology of chemically prepared polyaniline nanofibers. Journal of Applied Polymer Science. 2009;113:868-75.

[109] Husin MR, Arsad A, Hassan A, Hassan O. Influence of Different Ultrasonic Wave on Polymerization of Polyaniline Nanofiber. Applied Mechanics and Materials: Trans Tech Publ; 2014. p. 50-4.

[110] Gajendran P, Saraswathi R. Polyaniline-carbon nanotube composites. Pure and Applied Chemistry. 2008;80:2377-95.

[111] Wang Q, Yao Q, Chang J, Chen L. Enhanced thermoelectric properties of CNT/PANI composite nanofibers by highly orienting the arrangement of polymer chains. Journal of Materials Chemistry. 2012;22:17612-8.

[112] Oyharçabal M, Olinga T, Foulc M-P, Lacomme S, Gontier E, Vigneras V. Influence of the morphology of polyaniline on the microwave absorption properties of epoxy polyaniline composites. Composites Science and Technology. 2013;74:107-12.

[113] Sandler JKW, Kirk JE, Kinloch IA, Shaffer MSP, Windle AH. Ultra-low electrical percolation threshold in carbon-nanotube-epoxy composites. Polymer. 2003;44:5893-9.

[114] Li H-C, Lu S-Y, Syue S-H, Hsu W-K, Chang S-C. Conductivity enhancement of carbon nanotube composites by electrolyte addition. Applied Physics Letters. 2008;93:033104.

[115] Li J, Ma PC, Chow WS, To CK, Tang BZ, Kim JK. Correlations between Percolation Threshold, Dispersion State, and Aspect Ratio of Carbon Nanotubes. Advanced Functional Materials. 2007;17:3207-15.

[116] Choi ES, Brooks JS, Eaton DL, Al-Haik MS, Hussaini MY, Garmestani H, et al. Enhancement of thermal and electrical properties of carbon nanotube polymer composites by magnetic field processing. Journal of Applied Physics. 2003;94:6034-9.

[117] Li S, Qin Y, Shi J, Guo Z-X, Li Y, Zhu D. Electrical Properties of Soluble Carbon Nanotube/Polymer Composite Films. Chemistry of Materials. 2005;17:130-5.

[118] Tamburri E, Orlanducci S, Terranova ML, Valentini F, Palleschi G, Curulli A, et al. Modulation of electrical properties in single-walled carbon nanotube/conducting polymer composites. Carbon. 2005;43:1213-21.

[119] Bauhofer W, Kovacs JZ. A review and analysis of electrical percolation in carbon nanotube polymer composites. Composites Science and Technology. 2009;69:1486-98.

[120] Boudenne A, Ibos L, Fois M, Majesté JC, Géhin E. Electrical and thermal behavior of polypropylene filled with copper particles. Composites Part A: Applied Science and Manufacturing. 2005;36:1545-54.

[121] Grossiord N, Loos J, van Laake L, Maugey M, Zakri C, Koning CE, et al. High-Conductivity Polymer Nanocomposites Obtained by Tailoring the Characteristics of Carbon Nanotube Fillers. Advanced Functional Materials. 2008;18:3226-34.

[122] Sarvi A, Sundararaj U. Rheological percolation in polystyrene composites filled with polyaniline-coated multiwall carbon nanotubes. Synthetic Metals. 2014;194:109-17.

[123] Yao S-H, Dang Z-M, Jiang M-J, Xu H-P, Bai J. Influence of aspect ratio of carbon nanotube on percolation threshold in ferroelectric polymer nanocomposite. Applied Physics Letters. 2007;91:212901.

[124] Eken AE, Tozzi EJ, Klingenberg DJ, Bauhofer W. A simulation study on the combined effects of nanotube shape and shear flow on the electrical percolation thresholds of carbon nanotube/polymer composites. Journal of Applied Physics. 2011;109:084342.

[125] George S, Sebastian MT. Three-phase polymer–ceramic–metal composite for embedded capacitor applications. Composites Science and Technology. 2009;69:1298-302.

[126] Wessling B. New Insight into Organic Metal Polyaniline Morphology and Structure. Polymers. 2010;2:786.

[127] Green AA, Hersam MC. Processing and properties of highly enriched double-wall carbon nanotubes. Nat Nano. 2009;4:64-70.

[128] Ghatak S, Chakraborty G, Meikap AK, Woods T, Babu R, Blau WJ. Synthesis and characterization of polyaniline/carbon nanotube composites. Journal of Applied Polymer Science. 2011;119:1016-25.

[129] Jeon I-Y, Kang S-W, Tan L-S, Baek J-B. Grafting of polyaniline onto the surface of 4-aminobenzoyl-functionalized multiwalled carbon nanotube and its electrochemical properties. Journal of Polymer Science Part A: Polymer Chemistry. 2010;48:3103-12.

[130] Morávková Z, Trchová M, Tomšík E, Čechvala J, Stejskal J. Enhanced thermal stability of multi-walled carbon nanotubes after coating with polyaniline salt. Polymer Degradation and Stability. 2012;97:1405-14.

[131] Roth S, Graupner W. Conductive polymers: Evaluation of industrial applications. Synthetic Metals. 1993;57:3623-31.

[132] Hino T, Taniguchi S, Kuramoto N. Syntheses of conductive adhesives based on epoxy resin and polyanilines by using N-tert-butyl-5-methylisoxazolium perchlorate as a thermally

latent curing reagent. Journal of Polymer Science Part A: Polymer Chemistry. 2006;44:718-26.

[133] Hosoda M, Hino T, Kuramoto N. Facile preparation of conductive paint made with polyaniline/dodecylbenzenesulfonic acid dispersion and poly(methyl methacrylate). Polymer International. 2007;56:1448-55.

[134] Bhadra S, Singha NK, Khastgir D. Semiconductive composites from ethylene 1-octene copolymer and polyaniline coated nylon 6: Studies on mechanical, thermal, processability, electrical, and EMI shielding properties. Polymer Engineering & Science. 2008;48:995-1006.

[135] Kausar A, Rafique I, Muhammad B. Review of Applications of Polymer/Carbon Nanotubes and Epoxy/CNT Composites. Polymer-Plastics Technology and Engineering. 2016;55:1167-91.

[136] Landi BJ, Raffaelle RP, Heben MJ, Alleman JL, VanDerveer W, Gennett T. Single wall carbon nanotube-Nafion composite actuators. Nano Letters. 2002;2:1329-32.

[137] Mottaghitalab V, Xi B, Spinks GM, Wallace GG. Polyaniline fibres containing single walled carbon nanotubes: Enhanced performance artificial muscles. Synthetic Metals. 2006;156:796-803.

[138] Hyder MN, Lee SW, Cebeci FÇ, Schmidt DJ, Shao-Horn Y, Hammond PT. Layer-by-layer assembled polyaniline nanofiber/multiwall carbon nanotube thin film electrodes for high-power and high-energy storage applications. ACS nano. 2011;5:8552-61.

[139] Yun S, Kim J. Sonication time effect on MWNT/PANI-EB composite for hybrid electro-active paper actuator. Synthetic Metals. 2007;157:523-8.

[140] Rajesh, Ahuja T, Kumar D. Recent progress in the development of nano-structured conducting polymers/nanocomposites for sensor applications. Sensors and Actuators B: Chemical. 2009;136:275-86.

[141] Bai H, Chen Q, Li C, Lu C, Shi G. Electrosynthesis of polypyrrole/sulfonated polyaniline composite films and their applications for ammonia gas sensing. Polymer. 2007;48:4015-20.

[142] Irimia-Vladu M, Fergus JW. Suitability of emeraldine base polyaniline-PVA composite film for carbon dioxide sensing. Synthetic Metals. 2006;156:1401-7.

[143] Ferrer-Anglada N, Kaempgen M, Roth S. Transparent and flexible carbon nanotube/polypyrrole and carbon nanotube/polyaniline pH sensors. physica status solidi (b). 2006;243:3519-23.

[144] Sadek AZ, Wlodarski W, Shin K, Kaner RB, Kalantar-zadeh K. A layered surface acoustic wave gas sensor based on a polyaniline/In 2 O 3 nanofibre composite. Nanotechnology. 2006;17:4488.

[145] Sadek AZ, Wlodarski W, Shin K, Kaner RB, Kalantar-zadeh K. A polyaniline/WO3 nanofiber composite-based ZnO/64° YX LiNbO3 SAW hydrogen gas sensor. Synthetic Metals. 2008;158:29-32.

[146] Ali SR, Ma Y, Parajuli RR, Balogun Y, Lai WYC, He H. A Nonoxidative Sensor Based on a Self-Doped Polyaniline/Carbon Nanotube Composite for Sensitive and Selective Detection of the Neurotransmitter Dopamine. Analytical Chemistry. 2007;79:2583-7.

[147] Sudha JD, Sivakala S, Patel K, Radhakrishnan Nair P. Development of electromagnetic shielding materials from the conductive blends of polystyrene polyaniline-clay nanocomposite. Composites Part A: Applied Science and Manufacturing. 2010;41:1647-52.

[148] Geetha S, Satheesh Kumar KK, Rao CRK, Vijayan M, Trivedi DC. EMI shielding: Methods and materials—A review. Journal of Applied Polymer Science. 2009;112:2073-86.

[149] Wang Y, Jing X. Intrinsically conducting polymers for electromagnetic interference shielding. Polymers for Advanced Technologies. 2005;16:344-51.

[150] Grimes CA, Mungle C, Kouzoudis D, Fang S, Eklund PC. The 500 MHz to 5.50 GHz complex permittivity spectra of single-wall carbon nanotube-loaded polymer composites. Chemical Physics Letters. 2000;319:460-4.

[151] Lee CY, Song HG, Jang KS, Oh EJ, Epstein AJ, Joo J. Electromagnetic interference shielding efficiency of polyaniline mixtures and multilayer films. Synthetic Metals. 1999;102:1346-9.

[152] Koul S, Chandra R, Dhawan SK. Conducting polyaniline composite for ESD and EMI at 101 GHz. Polymer. 2000;41:9305-10.

[153] Saini P, Choudhary V, Singh BP, Mathur RB, Dhawan SK. Polyaniline–MWCNT nanocomposites for microwave absorption and EMI shielding. Materials Chemistry and Physics. 2009;113:919-26.

[154] Makeiff DA, Huber T. Microwave absorption by polyaniline–carbon nanotube composites. Synthetic Metals. 2006;156:497-505.

[155] Han MS, Lee YK, Kim WN, Lee HS, Joo JS, Park M, et al. Effect of multi-walled carbon nanotube dispersion on the electrical, morphological and rheological properties of polycarbonate/multi-walled carbon nanotube composites. Macromolecular Research. 2009;17:863-9.

[156] Ghasemi H, Sundararaj U. Electrical properties of in situ polymerized polystyrene/polyaniline composites: The effect of feeding ratio. Synthetic Metals. 2012;162:1177-83.

[157] Pérez R, Pinto NJ, Johnson Jr AT. Influence of temperature on charge transport and device parameters in an electrospun hybrid organic/inorganic semiconductor Schottky diode. Synthetic Metals. 2007;157:231-4.

[158] Rivera R, Pinto NJ. Schottky diodes based on electrospun polyaniline nanofibers: Effects of varying fiber diameter and doping level on device performance. Physica E: Low-dimensional Systems and Nanostructures. 2009;41:423-6.

[159] Pinto NJ, Johnson AT, MacDiarmid AG, Mueller CH, Theofylaktos N, Robinson DC, et al. Electrospun polyaniline/polyethylene oxide nanofiber field-effect transistor. Applied Physics Letters. 2003;83:4244-6.

[160] Tseng RJ, Huang J, Ouyang J, Kaner RB, Yang. Polyaniline Nanofiber/Gold Nanoparticle Nonvolatile Memory. Nano Letters. 2005;5:1077-80.

[161] Thomas SC, Ren X, Gottesfeld S, Zelenay P. Direct methanol fuel cells: progress in cell performance and cathode research. Electrochimica Acta. 2002;47:3741-8.

[162] Kumar A, Mishra A, Awasthi K, Kumar V. Thermal Stability and Electrical Properties of Polyaniline Synthesized by Oxidative Polymerization Method. Macromolecular Symposia. 2015;357:168-72.

[163] Kumar A, Jangir LK, Kumari Y, Kumar M, Kumar V, Awasthi K. Optical and Structural Study of Polyaniline/Polystyrene Composite Films. Macromolecular Symposia. 2015;357:229-34.

[164] Wang Z, Zhu Z-Z, Shi J, Li H-L. Electrocatalytic oxidation of formaldehyde on platinum well-dispersed into single-wall carbon nanotube/polyaniline composite film. Applied Surface Science. 2007;253:8811-7.

[165] Shi J, Wang Z, Li H-l. Electrochemical fabrication of polyaniline/multi-walled carbon nanotube composite films for electrooxidation of methanol. Journal of Materials Science. 2007;42:539-44.

[166] Shi J, Zhang Z-Y, Hu Y-Q, Hua Y-X. Incorporation of 4-aminobenzene functionalized multi-walled carbon nanotubes in polyaniline for application in formic acid electrooxidation. Journal of Applied Polymer Science. 2010;118:1815-20.

[167] Manesh KM, Santhosh P, Gopalan AI, Lee K-P. Electrocatalytic Dioxygen Reduction at Glassy Carbon Electrode Modified with Polyaniline Grafted Multiwall Carbon Nanotube Film. Electroanalysis. 2006;18:1564-71.

[168] Chaudhuri SK, Lovley DR. Electricity generation by direct oxidation of glucose in mediatorless microbial fuel cells. Nat Biotech. 2003;21:1229-32.

[169] Qiao Y, Li CM, Bao S-J, Bao Q-L. Carbon nanotube/polyaniline composite as anode material for microbial fuel cells. Journal of Power Sources. 2007;170:79-84.

[170] Akbari E, Buntat Z. Benefits of using carbon nanotubes in fuel cells: a review. International Journal of Energy Research. 2017;41:92-102.

[171] Tang L, Duan F, Chen M. Silver nanoparticle decorated polyaniline/multiwalled super-short carbon nanotube nanocomposites for supercapacitor applications. RSC Advances. 2016;6:65012-9.

[172] Oueiny C, Berlioz S, Perrin F-X. Carbon nanotube–polyaniline composites. Progress in Polymer Science. 2014;39:707-48.

[173] Singu BS, Male U, Srinivasan P, Yoon KR. Preparation and performance of polyaniline–multiwall carbon nanotubes–titanium dioxide ternary composite electrode material for supercapacitors. Journal of Industrial and Engineering Chemistry.

[174] Yuksel R, Durucan C, Unalan HE. Ternary nanocomposite SWNT/WO3/PANI thin film electrodes for supercapacitors. Journal of Alloys and Compounds. 2016;658:183-9.

[175] Yu T, Zhu P, Xiong Y, Chen H, Kang S, Luo H, et al. Synthesis of microspherical polyaniline/graphene composites and their application in supercapacitors. Electrochimica Acta. 2016;222:12-9.

[176] Lin H, Li L, Ren J, Cai Z, Qiu L, Yang Z, et al. Conducting polymer composite film incorporated with aligned carbon nanotubes for transparent, flexible and efficient supercapacitor. Scientific Reports. 2013;3:1353.

[177] Liu H, Wang Y, Gou X, Qi T, Yang J, Ding Y. Three-dimensional graphene/polyaniline composite material for high-performance supercapacitor applications. Materials Science and Engineering: B. 2013;178:293-8.

[178] Singh V, Mohan S, Singh G, Pandey PC, Prakash R. Synthesis and characterization of polyaniline–carboxylated PVC composites: Application in development of ammonia sensor. Sensors and Actuators B: Chemical. 2008;132:99-106.

[179] Fu Y, Elsenbaumer RL. Thermochemistry and Kinetics of Chemical Polymerization of Aniline Determined by Solution Calorimetry. Chemistry of Materials. 1994;6:671-7.

[180] Tantawy HR, Aston DE, Smith JR, Young JL. Comparison of Electromagnetic Shielding with Polyaniline Nanopowders Produced in Solvent-Limited Conditions. ACS Applied Materials & Interfaces. 2013;5:4648-58.

[181] Zhao Z, Yang Z, Hu Y, Li J, Fan X. Multiple functionalization of multi-walled carbon nanotubes with carboxyl and amino groups. Applied Surface Science. 2013;276:476-81.

[182] Wu M, Wang L, Zhao F, Zeng B. Ionic liquid polymer functionalized carbon nanotubes-coated polyaniline for the solid-phase microextraction of benzene derivatives. RSC Advances. 2015;5:99483-90.

[183] Sain PK, Goyal RK, Bhargava AK, Prasad YVSS. Thermal and dielectric behavior of flexible polycarbonate/lead zirconate titanate composite system. Journal of Applied Polymer Science. 2014;131:n/a-n/a.

[184] Sain PK, Goyal RK, Bhargava AK, Prasad YVSS. Thermal and electronic behaviour of polycarbonate–copper nanocomposite system. Journal of Physics D: Applied Physics. 2013;46:455501.

[185] Stejskal J, Hlavata D, Holler P, Trchová M, Prokeš J, Sapurina I. Polyaniline prepared in the presence of various acids: a conductivity study. Polymer international. 2004;53:294-300.

[186] Sain PK, Goyal RK, Prasad YVSS, Jyoti, Sharma KB, Bhargava AK. Few-layer-graphene/polycarbonate nanocomposites as dielectric and conducting material. Journal of Applied Polymer Science. 2015;132:n/a-n/a.

[187] Mirghani MES, Kabbashi NA, Alam MZ, Qudsieh IY, Alkatib MaFR. Rapid Method for the Determination of Moisture Content in Biodiesel Using FTIR Spectroscopy. Journal of the American Oil Chemists' Society. 2011;88:1897-904.

[188] Hongxia J, Qiaoling L, Yun Y, Zhiwu G, Xiaofeng Y. Preparation and microwave adsorption properties of core–shell structured barium titanate/polyaniline composite. Journal of Magnetism and Magnetic Materials. 2013;332:10-4.

[189] Wang J, Wang J, Yang Z, Wang Z, Zhang F, Wang S. A novel strategy for the synthesis of polyaniline nanostructures with controlled morphology. Reactive and Functional Polymers. 2008;68:1435-40.

[190] John H, Biju Kumar S, Mathew KT, Joseph R. Effect of drying conditions on microwave conductivity of polyaniline. Journal of Applied Polymer Science. 2002;83:2008-12.

[191] Wang Y, Chen K, Li T, Li H, Zeng R, Zhang R, et al. Soluble polyaniline nanofibers prepared via surfactant-free emulsion polymerization. Synthetic Metals. 2014;198:293-9.

[192] Su B, Tong Y, Bai J, Lei Z, Wang K, Mu H, et al. Acid doped polyaniline nanofibers synthesized by interfacial polymerization.

[193] Riaz U, Ahmad S, Ashraf SM. Effect of Dopant on the Nanostructured Morphology of Poly (1-naphthylamine) Synthesized by Template Free Method. Nanoscale Research Letters. 2007;3:45.

[194] Wang Y, Jing X. Formation of Polyaniline Nanofibers: A Morphological Study. The Journal of Physical Chemistry B. 2008;112:1157-62.

[195] Wolter A, Rannou P, Travers JP, Gilles B, Djurado D. Model for aging in HCl-protonated polyaniline: Structure, conductivity, and composition studies. Physical Review B. 1998;58:7637-47.

[196] Yue J, Epstein AJ, Zhong Z, Gallagher PK, Macdiarmid AG. Thermal stabilities of polyanilines. Synthetic Metals. 1991;41:765-8.

[197] Neoh KG, Kang ET, Tan KL. Thermal degradation of leucoemeraldine, emeraldine base and their complexes. Thermochimica Acta. 1990;171:279-91.

[198] Wei Y, Hsueh KF. Thermal analysis of chemically synthesized polyaniline and effects of thermal aging on conductivity. Journal of Polymer Science Part A: Polymer Chemistry. 1989;27:4351-63.

[199] Bellucci F, Khamis I, Senturia S, Latanision R. Moisture effects on the electrical conductivity of kapton polyimide. Journal of the Electrochemical Society. 1990;137:1778-84.

[200] Babu VJ, Vempati S, Ramakrishna S. Conducting polyaniline-electrical charge transportation. 2013.

[201] Zhang D. On the conductivity measurement of polyaniline pellets. Polymer Testing. 2007;26:9-13.

[202] Borah R, Banerjee S, Kumar A. Surface functionalization effects on structural, conformational, and optical properties of polyaniline nanofibers. Synthetic Metals. 2014;197:225-32.

[203] Reda SM, Al-Ghannam SM. Synthesis and Electrical Properties of Polyaniline Composite with Silver Nanoparticles. Advances in Materials Physics and Chemistry. 2012;Vol.02No.02:7.

[204] Sain PK, Goyal RK, Bhargava AK, Prasad YVSS. Thermal and electronic behaviour of polycarbonate–copper nanocomposite system. Journal of Physics D: Applied Physics. 2013;46:455501-8.

[205] Wu T-M, Lin Y-W. Doped polyaniline/multi-walled carbon nanotube composites: Preparation, characterization and properties. Polymer. 2006;47:3576-82.

[206] Peng C, Zhang S, Jewell D, Chen GZ. Carbon nanotube and conducting polymer composites for supercapacitors. Progress in Natural Science. 2008;18:777-88.

[207] Saini P, Arora M, Gupta G, Gupta BK, Singh VN, Choudhary V. High permittivity polyaniline-barium titanate nanocomposites with excellent electromagnetic interference shielding response. Nanoscale. 2013;5:4330-6.

[208] Park O-K, Jeevananda T, Kim NH, Kim S-i, Lee JH. Effects of surface modification on the dispersion and electrical conductivity of carbon nanotube/polyaniline composites. Scripta Materialia. 2009;60:551-4.

[209] Yılmaz F, Küçükyavuz Z. Conducting polymer composites of multiwalled carbon nanotube filled doped polyaniline. Journal of applied polymer science. 2009;111:680-4.

[210] Bao J, Tie C, Xu Z, Suo Z, Zhou Q, Hong J. A Facile Method for Creating an Array of Metal-Filled Carbon Nanotubes. Advanced Materials. 2002;14:1483-6.

[211] Samukhin AN, Prigodin VN, Jastrabík L. Critical Percolation and Transport in Nearly One Dimension. Physical Review Letters. 1997;78:326-9.

[212] Silva WM, Ribeiro H, Seara LM, Calado HDR, Ferlauto AS, Paniago RM, et al. Surface properties of oxidized and aminated multi-walled carbon nanotubes. Journal of the Brazilian Chemical Society. 2012;23:1078-86.

[213] Al-Ghamdi A, Al-Saigh ZY. Surface and thermodynamic characterization of conducting polymers by inverse gas chromatography: I. Polyaniline. Journal of Chromatography A. 2002;969:229-43.

[214] Li D, Kaner RB. Shape and Aggregation Control of Nanoparticles: Not Shaken, Not Stirred. Journal of the American Chemical Society. 2006;128:968-75.

[215] Qiu W, Ma L, Gan M, Bai Y, Fu D, Li Z, et al. Preparation and characterization of polyaniline nanofiber colloids. Polymer Engineering & Science. 2013;53:1631-6.

[216] Trchová M, Šeděnková I, Tobolková E, Stejskal J. FTIR spectroscopic and conductivity study of the thermal degradation of polyaniline films. Polymer Degradation and Stability. 2004;86:179-85.

[217] Zheng W, Angelopoulos M, Epstein AJ, MacDiarmid AG. Concentration Dependence of Aggregation of Polyaniline in NMP Solution and Properties of Resulting Cast Films. Macromolecules. 1997;30:7634-7.

[218] Biscaro RS, Rezende MC, Faez R. Reactive doping of PAni–CSA and its use in microwave absorbing materials. Polymers for Advanced Technologies. 2009;20:28-34.

[219] Sharma BK, Khare N, Sharma R, Dhawan SK, Vankar VD, Gupta HC. Dielectric behavior of polyaniline–CNTs composite in microwave region. Composites Science and Technology. 2009;69:1932-5.

[220] Wang Y, Rubner MF. An investigation of the conductivity stability of acid-doped polyanilines. Synthetic Metals. 1992;47:255-66.

[221] Quillard S, Louarn G, Lefrant S, Macdiarmid AG. Vibrational analysis of polyaniline: A comparative study of leucoemeraldine, emeraldine, and pernigraniline bases. Physical Review B. 1994;50:12496-508.

[222] Yang D, Mattes BR. Polyaniline emeraldine base in N-methyl-2-pyrrolidinone containing secondary amine additives: B. Characterization of solutions and thin films. Synthetic Metals. 2002;129:249-60.

[223] Palaniappan S, Narayana BH. Temperature effect on conducting polyaniline salts: Thermal and spectral studies. Journal of Polymer Science Part A: Polymer Chemistry. 1994;32:2431-6.

[224] Bhadra S, Khastgir D, Singha NK, Lee JH. Progress in preparation, processing and applications of polyaniline. Progress in Polymer Science. 2009;34:783-810.

[225] Chapman P, Loh XX, Livingston AG, Li K, Oliveira TAC. Polyaniline membranes for the dehydration of tetrahydrofuran by pervaporation. Journal of Membrane Science. 2008;309:102-11.

[226] Abdiryim T, Jamal R, Nurulla I. Doping effect of organic sulphonic acids on the solid-state synthesized polyaniline. Journal of Applied Polymer Science. 2007;105:576-84.

[227] Sniechowski M, Djurado D, Dufour B, Rannou P, Pron A, Luzny W. Direct analysis of lamellar structure in polyaniline protonated with plasticizing dopants. Synthetic Metals. 2004;143:163-9.

List of publications from this research work

- Anil Kumar, Lokesh Kumar Jangir, Yogita Kumari, Manoj Kumar, Vinod Kumar, Kamlendra Awasthi,"Electrical behavior of dual-morphology polyaniline", Journal of Applied Polymer Science 133 (2016) 44091 **DOI**: 10.1002/app.44091

- Anil Kumar, Vinod Kumar, Kamlendra Awasthi, "Polyaniline-carbon nanotube composites: Preparation Methods, Properties and Applications", Polymer-Plastics Technology and Engineering, (2017), **DOI:** 10.1080/03602559.2017.1300817

- Anil Kumar, Vinod Kumar, Manoj Kumar, Kamlendra Awasthi, "Synthesis and characterization of hybrid PANI/MWCNT nanocomposites for EMI applications", Polymer Composites (2017) **DOI:** 10.1002/pc.24418

- Anil Kumar, Vinod Kumar, Manoj Kumar, Kamlendra Awasthi, "Polyaniline in N, N'-dimethyl propylene urea containing secondary amine additive and properties of resulting cast films" (2017) (Journal of Polymer Science Part A: Polymer Chemistry) (submitted)

Other publications

- Anil Kumar, Lokesh Kumar Jangir, Yogita Kumari, Manoj Kumar, Vinod Kumar, Kamlendra Awasthi, "Optical and Structural Study of Polyaniline/Polystyrene Composite Films", Macromolecular Symposia 357 (2015) 229-234 **DOI**: 10.1002/masy.201500039

- Anil Kumar, Amit Mishra, Kamlendra Awasthi,Vinod Kumar "Thermal Stability and Electrical Properties of Polyaniline Synthesized by Oxidative Polymerization Method", Macromolecular Symposia 357 (2015) 168-172 **DOI**:10.1002/masy.201400218

- Lokesh Kumar Jangir, Yogita Kumari, Anil Kumar, Manoj Kumar, Kamlendra Awasthi, "Investigation of luminescence and structural properties of ZnO nanoparticles, synthesized with different precursors", Materials Chemistry Frontiers (2017), (accepted), **DOI**: 10.1039/C7QM00058H

- Yogita Kumari, Lokesh Kumar Jangir, Anil Kumar, Manoj Kumar, Kamlendra Awasthi, "Investigation of thermal stability of TiO_2 nanoparticles using 1-thioglycerol as capping agent", Solid State Communications 263 (2017) 1-5